NTNU
Norwegian University of
Science and Technology

Estimating Net Erosion in the Western Barents Sea

Richard Anthony Elks

Petroleum Geosciences
Submission date: June 2016
Supervisor: Ståle Emil Johansen, IPT
Co-supervisor: Kenneth Duffaut, IPT

Norwegian University of Science and Technology
Department of Petroleum Engineering and Applied Geophysics

Abstract

Quantification of uplift and erosion in the western Barents Sea has been a relevant and challenging problem for geoscientists for several decades. Uplift and erosion processes have implications for petroleum prospectivity, such as effects on source rock maturation, reservoir properties and migration of hydrocarbons. Thus, demand for new data and interpretation techniques is ongoing. Net erosion has been estimated in previous studies using various techniques such as vitrinite reflectance, opal A – opal CT, seismic shot gathers and sonic logs. The purpose of this project is to estimate net erosion in the western Barents Sea using sonic logs, compare these results with seismic data and interpret the mechanisms causing both local and regional uplift and erosion in various parts of the western Barents Sea.

11 wells from the western Barents Sea have been used to estimate net erosion in various areas. In an attempt to increase reliability and comparability to a reference trend, sonic logs have been filtered to process only shale lithologies in the Kolmule formation. Several wells in the western part of the study area produced net erosion estimates of approximately 1000 – 1500 m, with some areas in the north and north east estimated to have been eroded approximately 1500 – 2000 m. The higher estimates are less reliable, with uncertainties ranging from ± 500 – 800 m. More reliable estimates were calculated in the west and south west, with uncertainties ranging from ± 150 – 300 m. Greater uncertainties are attributed to poor gamma ray and sonic logs, short Kolmule intervals, sparse data and/or variations in thermal histories that have not been accounted for.

The western Barents Sea has been divided into several structural provinces for interpretation using net erosion estimates and seismic data. Net erosion estimates from sonic logs were found to correlate well with seismic data. Where velocity data has been poor or absent in structural provinces, a combination of seismic data and previous studies have been used to estimate net erosion.

The results herein suggest the occurrence of one or more significant regional Cenozoic uplift and erosion events in the western Barents Sea, which agrees with several previous studies. The cause of this erosion is attributed to several phases of tectonic uplift during Cenozoic time, followed by severe glacial erosion and isostatic rebound.

Acknowledgements

I would like to thank my supervisor, Professor Ståle Emil Johansen, for the ongoing motivation and knowledge he has offered during this process. He has consistently encouraged me to use my own ideas, but also steered me in the right direction when he has felt necessary.

Secondly, I would like to thank my co-supervisor, Associate Professor Kenneth Duffaut, for his ideas and motivation. His focus and technical knowledge have been invaluable.

Thirdly, I would like to thank research assistant Dicky Harishidayat and Dr. Kamaldeen Olakunle Omosanya for their technical skills and willingness to help.

Finally, I would like to thank the friends I have made at NTNU for making this a great experience.

Table of contents

List of figures

List of tables

Chapter 1: Introduction

Uplift and erosion are ongoing and intimately linked geological processes. These processes occur worldwide and play a large part in shaping the Earth. The processes of uplift and erosion have implications for petroleum prospectivity such as effects on source rock maturation, reservoir properties and migration of hydrocarbons. Therefore estimating the magnitude, timing and nature of uplift and erosion plays an important role in geological studies and petroleum exploration. The western Barents Sea, illustrated in Figure 1.1, has undergone several significant uplift events leading to severe erosion in much of the study area. Due to the implications for petroleum prospectivity, quantification of uplift and erosion effects has been an ongoing relevant topic and challenging problem for geoscientists for several decades.

Several geophysical and geological techniques have been utilised in previous studies to estimate the magnitude of uplift and erosion. In this study, sonic logs will be used to analyse the compaction trends of shales in order to estimate net erosion. A main focus will be on sonic log processing and developing a systematic workflow based on published methodology. Uncertainty plays an important role in estimating net erosion as it can be the difference between approving and denying the continued exploration of an area. Therefore it will be calculated and discussed for each of the net erosion estimates.

Trends of increasing net erosion to the north and north east of the study area have been suggested in previous studies, as well as little to no net erosion to the south west, such as the Tromsø Basin and Sørvestnaget Basin. The results from this study will be plotted on a map, and the study area will be divided into several structural provinces in order to investigate the effects of uplift and erosion both on a regional and local scale. To comment on the validity of net erosion estimates, the results will be compared to seismic data. Possible mechanisms responsible for several examples of local uplift will be explored by interpretation of seismic data, and the causes of the regional uplift and erosion observed in most of the western Barents Sea will be discussed.

Reliability in estimating uplift and erosion in a petroleum prospective area is of great value for risk assessment in exploration. Understanding the magnitude and trends of these effects has been challenging and results from previous studies have varied significantly. The purpose

of this project is to estimate regional net erosion in various areas of the Barents Sea by analysis of sonic logs, compare results with seismic data and investigate the mechanisms causing both regional and local uplift and erosion.

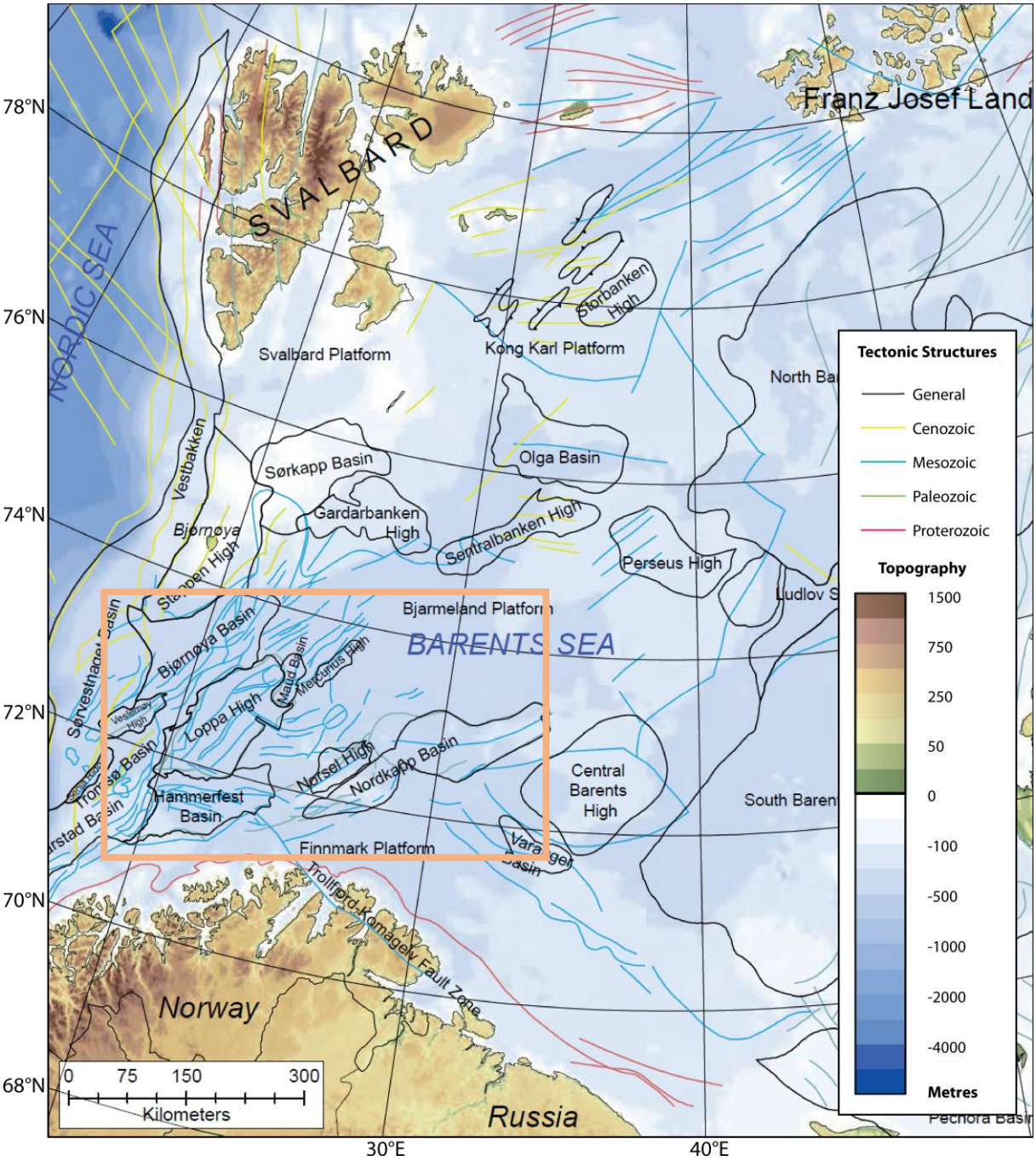

Figure 1.1. Regional setting of the Barents Sea. The Barents Sea is bound by young passive margins to the north and west, the Svalbard and Franz Josef Land archipelagos to the north, Novaya Zemlya to the east, and the Kola Peninsula and Norwegian coast in the south. Approximate location of the study area indicated by the orange rectangle. Modified from Smelror et al. (2009).

Chapter 2: Theoretical background

2.1. Geology

2.1.1. Regional setting

The Barents Sea is a marginal sea in the Arctic Ocean, located off the northern shores of Norway and Russia, Figure 1.1. It is a large epicontinental sea bound by young passive margins to the west and north. The archipelagos of Svalbard and Franz Josef Land lie to the north, and Novaya Zemlya lies to the east. The boundary extends south to the Kola Peninsula and Norwegian coast (Faleide et al., 1984).

2.1.2. Structure and evolution

The Barents Sea, along with the North Sea and Norwegian Sea, was once a part of a larger epicontinental sea lying between the continents of Fennoscandia, Svalbard and Greenland. For this reason, many similarities as well as important differences exist between their stratigraphic and evolutionary aspects (Faleide et al., 2010).

The Norwegian continental margin runs north-south and lies to the west of mainland Norway, extending up to Svalbard and continuing further north, Figure 2.1. It exists as a mainly rifted volcanic margin along offshore mid-Norway (62 – 70°N) and a mainly sheared margin along the western Barents Sea and Svalbard (70 – 82°N). The whole area has been exposed to a long history of post-Caledonian extension until breakup in Early-Cenozoic time (Faleide et al., 2008).

The young passive margins to the west and north of the Barents Sea developed during the Cenozoic opening of the Norwegian-Greenland Sea and Eurasia basin, respectively (Dimakis et al., 1998). A reconstruction of the opening of the Greenland-Norwegian Sea and Eurasia basin is illustrated below, Figure 2.2.

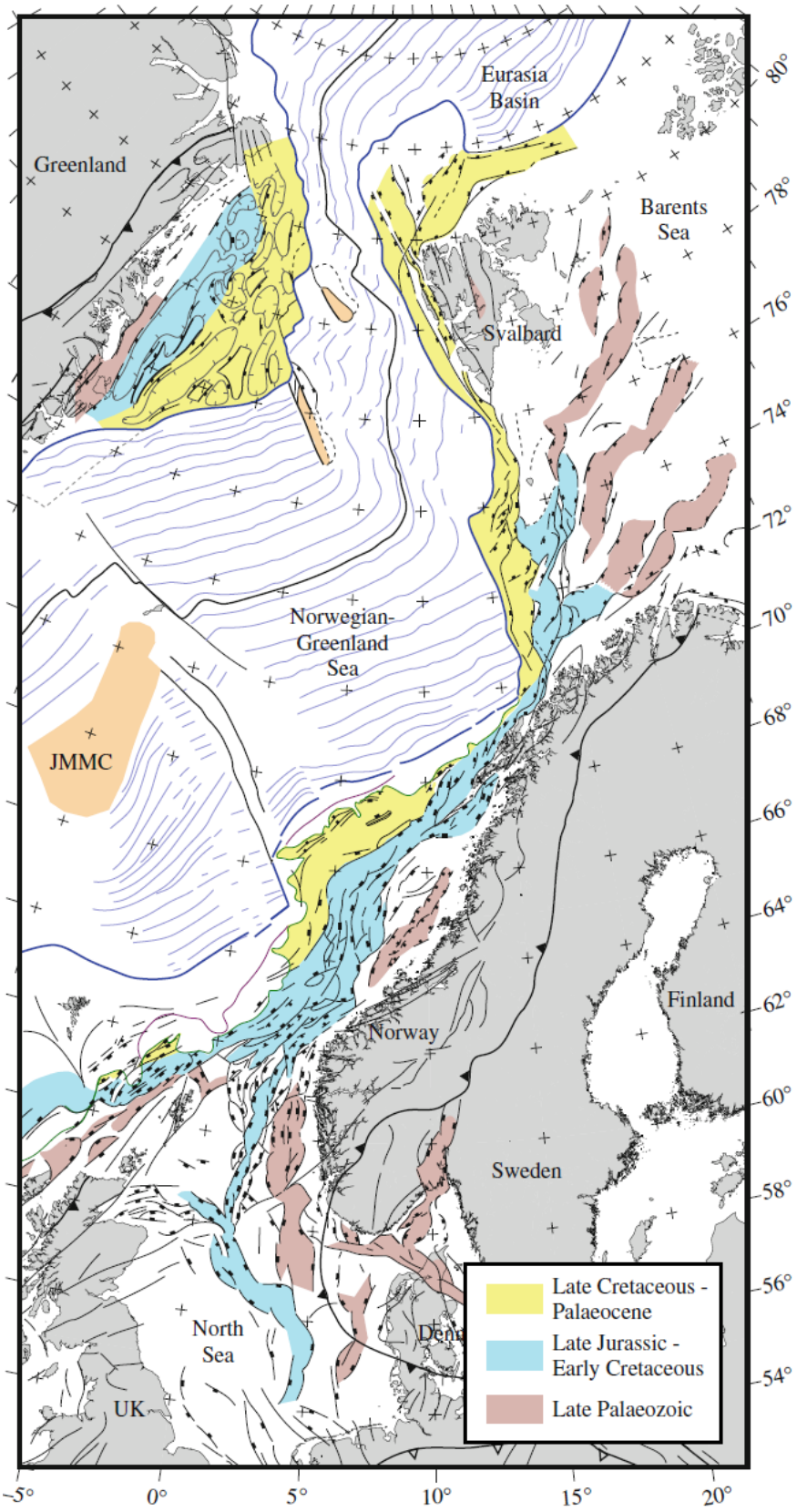

Figure 2.1. Regional map showing the Norwegian continental shelf extending from the North Sea to Svalbard and beyond. Modified from Faleide et al. (2010).

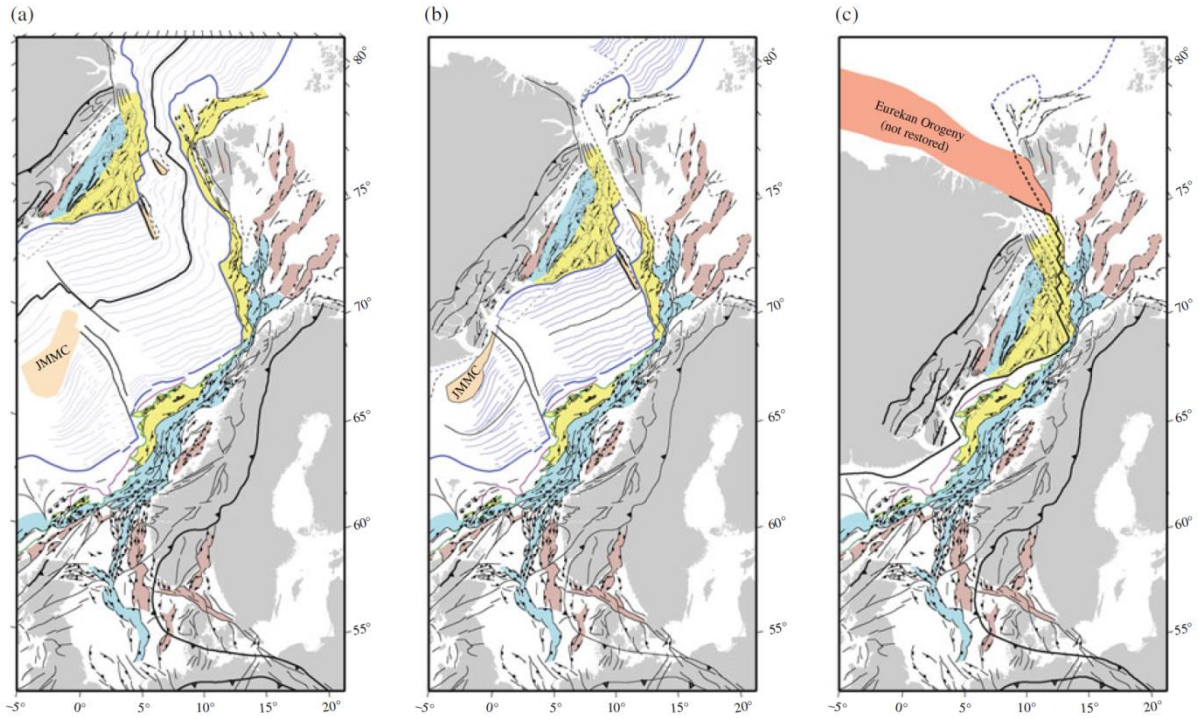

Figure 2.2. Tectonic reconstruction of the opening of the Norwegian-Greenland Sea, leading to the development of the North Sea, Norwegian Sea and Barents Sea at different geological times: (a) Present day, (b) ca. 33 Ma, (c) ca. 55 Ma. Modified from Faleide et al. (2010).

The study area for this report and its structural features are illustrated in Figure 2.3. This area is underlain by thick stratigraphic layers of Upper Palaeozoic to Cenozoic rocks. The western Barents Sea consists of three distinct geological provinces, as described by Faleide et al., 2010. These are:

i. The Svalbard Platform, lying between Svalbard and Bjørnøya, bound to the west by the continental margin. This platform is characterized by flat-lying Upper Palaeozoic and Mesozoic, mainly Triassic, sediments.
ii. A basin province, located between the Svalbard Platform and the northern Norwegian coastline, bound to the west by the continental margin. This province is characterized by several sub-basins and highs, consisting of Jurassic-Cretaceous sediments in the east, and Palaeocene-Eocene sediments in the west. The structural relief of the basin province is increasingly accentuated to the west.
iii. The continental margin, which runs north-south along the western boundary of the Barents Sea. This margin consists of three main sections:

a. The Senja Fracture Zone, a sheared margin located in the south (70 – 72°30'N), from the Norwegian coast to an area south west of Bjørnøya.
b. A central rifted complex, associated with volcanism, lying to the southwest of Bjørnøya (72°30' – 75°N).
c. A northern zone along the Hornsund Fault Zone (75 – 80°N). This is an initially sheared and later rifted margin.

The transition between continental and ocean zones occurs on a narrow region which follows the line of Early Tertiary break-up. The margin is covered by a thick Upper Cenozoic sedimentary wedge (Faleide et al., 2010).

The metamorphic basement of the western Barents Sea is most likely due to the Caledonides, which were consolidated during the Late Silurian to Early Devonian Caledonian orogeny. This gave rise to the fusing of the North America-Greenland and Fennoscandian-Russian plates, followed by strong post-orogenic uplift and erosion (Faleide et al., 1984).

The Caledonian compressional regime changed during the Late Devonian time to a left-lateral shear regime. This was characterized by large-scale strike-slip movements (Harland, 1973). During this phase, folding and formation of grabens occurred due to transpression and transtension, as well as the formation of rift basins from Tromsø to Nordkapp (Faleide et al., 1984). Extensional faults during the Late Devonian-Early Carboniferous have a northeasterly trend, similar to that of the pre-existing Caledonian structures (Rønnevik et al., 1982).

The geological history of the western Barents Sea, following Caledonian time, consists of three major rift phases – Late Devonian-Carboniferous, Middle Jurassic-Early Cretaceous, and Early Tertiary. Several tectonic pulses occurred during each of these phases. Crustal extension dominated during Late Palaeozoic times, which was followed by the migration of rifting towards the west during later phases of extension. During this time, well-defined rifts and pull-apart basins formed in the southwest, as well as a belt of strike-slip faults in the north. The Svalbard Platform and eastern areas of the regional basin have been reasonably geologically stable since these extensional forces (Faleide et al., 2010).

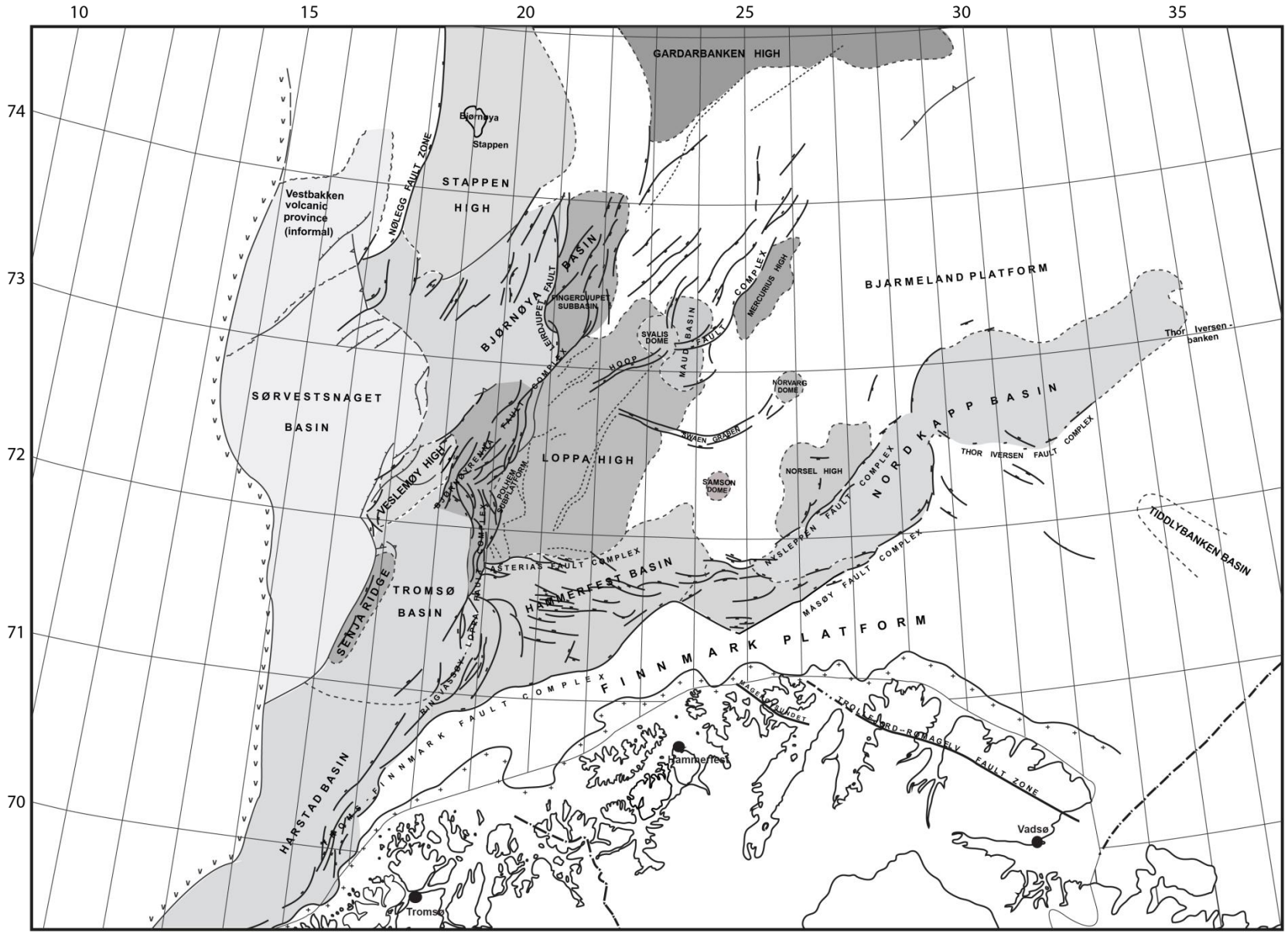

Figure 2.3. Main structural features of the Barents Sea. Basins, highs, platforms and domes are outlines and annotated. Modified from NPD (year unknown).

2.1.3. Stratigraphy

The Barents Sea geology consists of a thick succession of Palaeozoic to Cenozoic sediments. Lateral and vertical variations in thicknesses and facies are evident and characterised by Upper Palaeozoic mixed carbonates, evaporites and clastics, overlain by Mesozoic-Cenozoic classic sediments. Little information exists regarding the characteristics and state of the crystalline crust under the Barents Sea, however indirect evidence suggests it was metamorphosed during the Caledonian Orogeny (Faleide et al., 2010).

The majority of the Cenozoic sediments have been removed due to uplift and erosion during Late Cenozoic time. In some areas, these processes have removed even older strata. The erosion is greatest in the western Barents Sea, with some areas exhibiting erosion depths of more than 3,000 m in the northwest, and 1,000 – 1,500 m in the southeast. Estimates of net erosion in the eastern extent of the Barents Sea are lower at approximately 250 – 1000 m (Faleide et al., 2010).

A summary of the stratigraphy of the Barents Sea has been summarised in a lithostratigraphic chart, Figure 2.4. The gaps in this illustration in Paleogene and Neogene times are due to severe Cenozoic uplift and subsequent erosion.

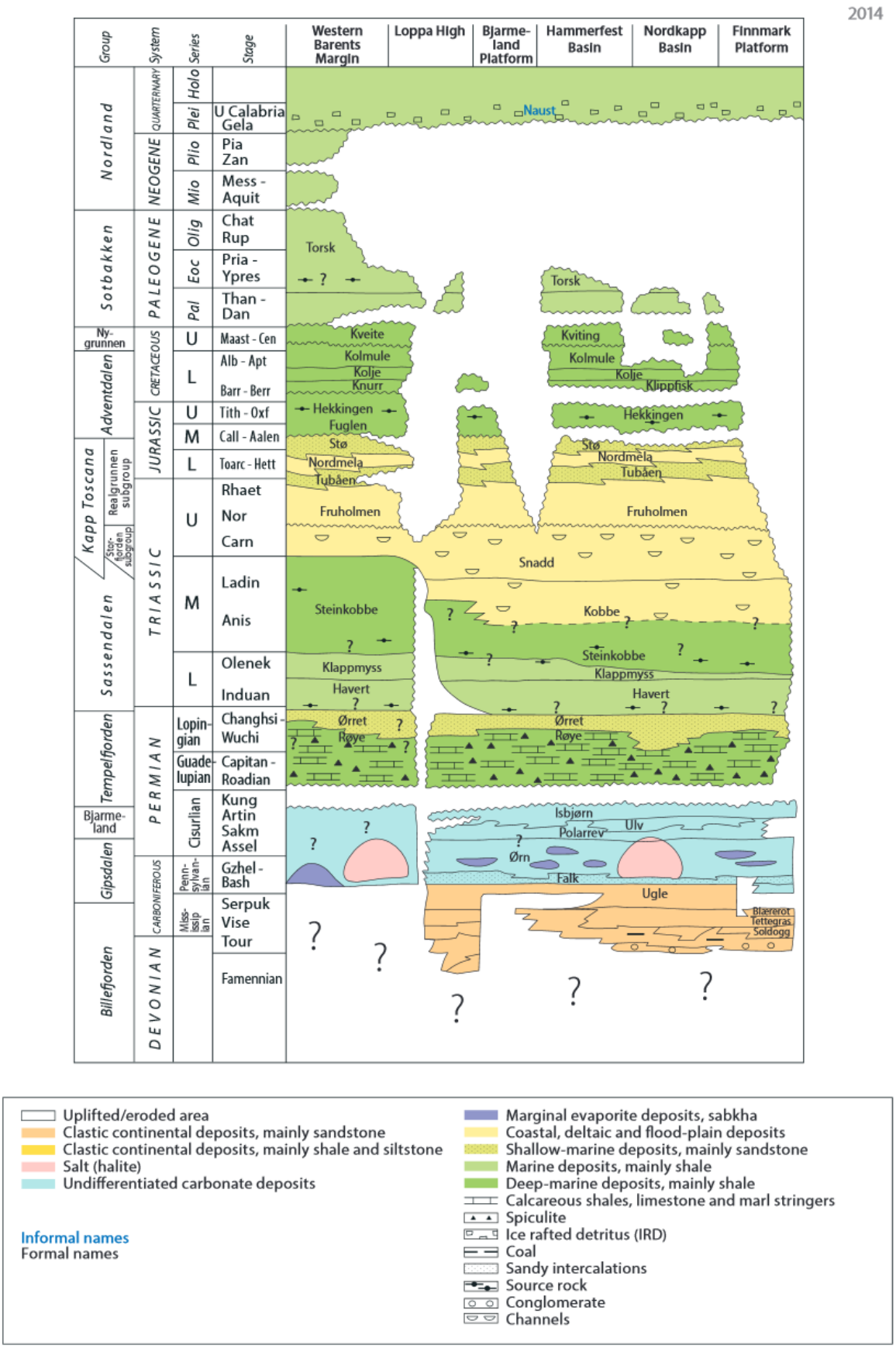

Figure 2.4. Lithostratigraphic chart of the Norwegian Barents Sea showing the formations relative to their age and location. Formation names annotated. From NPD (2014).

2.2. Uplift and erosion

2.2.1. Uplift and erosion terminology

To avoid confusion it is important to clarify the differences between the different terms relating to uplift and erosion. England and Molnar (1990) and Riis and Jensen (1992) have written about these differences and provided definitions for the terms.

The word 'uplift' refers to vertical movement in a direction opposite to the gravity vector. To determine if uplift has occurred, one needs to define the object which has moved and a frame of reference to which the object is moving in relation to. This has often been where confusion has arisen in geological and tectonic literature – that an object, frame of reference, or both have not been specified. When speaking in geological terms, the objects are often rocks and the frame of reference is either the Earth's surface or a geoid (England and Molnar, 1990).

Two terms for uplift exist, according to Riis and Jensen (1992):

i. Uplift of rocks, which refers to the vertical movement of a rock body or marker horizon with respect to a given datum. Upward movement is positive, and downward movement is negative, which is referred to as subsidence.
ii. Surface uplift refers to the vertical movement of the Earth's surface, often the sea floor or land surface, with respect to a given datum.

Uplift of rocks can be due to various mechanisms, the main two being tectonic uplift and isostatic uplift. Tectonic uplift is the uplift of rocks due to a response to tectonic forces or temperature changes, whereas isostatic uplift is the result of loading or unloading of Earth's crust (Riis and Jensen, 1992).

Exhumation of rocks refers to the displacement of rocks with respect to the surface. The rate of exhumation is the rate of erosion or rate of overburden removal by tectonic processes (England and Molnar, 1990).

A simple relationship exists, as described by Gallagher (2012), which relates the uplift of rocks (U_r), surface uplift (U_s) and exhumation (U_e) to each other:

$$U_s = U_r - U_e$$

This infers that surface uplift and rock uplift are the same if exhumation is zero.

2.2.2. Net erosion

For the purposes of this report, calculations will be made on the term 'net erosion'. Net erosion is defined as the difference between the maximum burial depth and present day burial depth, with reference to a surface or marker horizon. The differences between uplift, erosion and net erosion are illustrated in Figure 2.5.

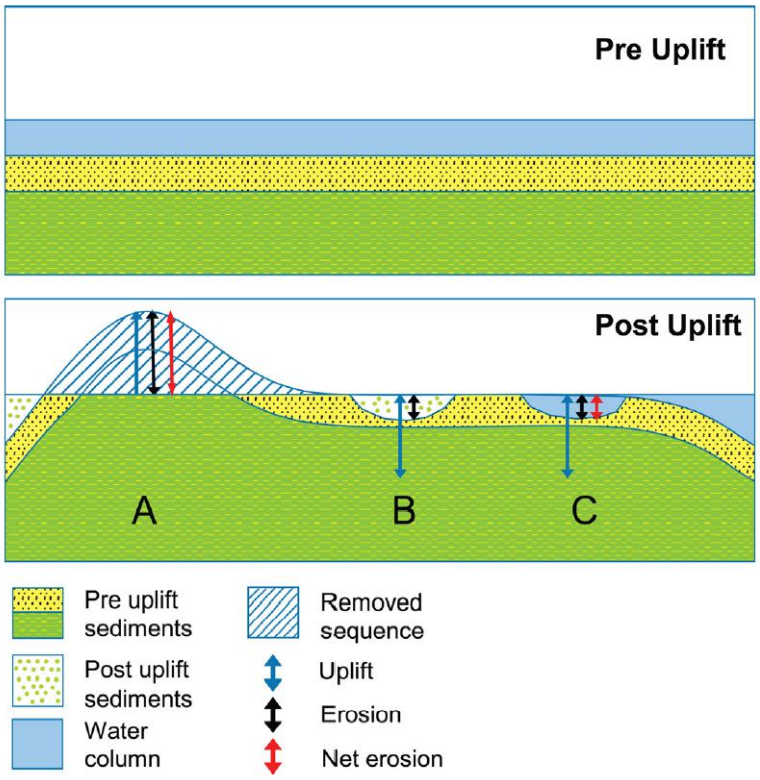

Figure 2.5. Differences between uplift, erosion and net erosion. Net erosion refers to the difference between maximum burial depth and present day burial depth. From Henriksen et al. (2011).

2.2.3. Uplift mechanisms

Uplift mechanisms have been categorised in different ways in various publications. For the purpose of this report, they are broken down into four categories – tectonic, thermal,

isostatic and stress mechanisms. The mechanism causing uplift is generally challenging to determine, and often a combination of two or more mechanisms are responsible. Determining the cause(s) of uplift is useful to geoscientists as it tells them about the geological history, the nature of uplift and can also provide useful information on the petroleum prospectivity of an area.

Typically, the four mentioned mechanisms lead to a change in density in the Earth's upper crust and mantle, which in turn leads to displacement of rocks or surfaces in the form of uplift or subsidence until isostatic equilibrium is achieved. Uplift (and subsidence) can occur both transiently and permanently. Transient uplift disappears once the driving force is removed, whereas permanent uplift remains after the driving force is removed (Gallagher, 2012).

2.2.3.1. Tectonic uplift

Plate tectonics is the large-scale part of tectonics that directly involves the movement and interaction of lithospheric plates (Fossen, 2010). Tectonic uplift occurs when the lithospheric plates behave in a way that causes uplift of rocks or surface uplift. This form of uplift is due to convergence of plates, thermal anomalies and in special cases divergence of plates.

The largest scale of uplift seen is in orogenic belts. Orogenic belts are typically 1000 km long and 100 – 500 km wide, however they can occur as strings of orogenic belts which can be over 20,000 km long and as wide as 100 – 1000 km (Roeder, 2012). When plate boundaries converge, the crust contracts and this can lead to high rates of surface uplift due to the isostatic compensation in response to the tectonically thickened crust. In turn, this leads to high rates of erosion as the relief increases (Willett et al., 2001). Examples of different types of folding due to orogeny are illustrated below, Figure 2.6.

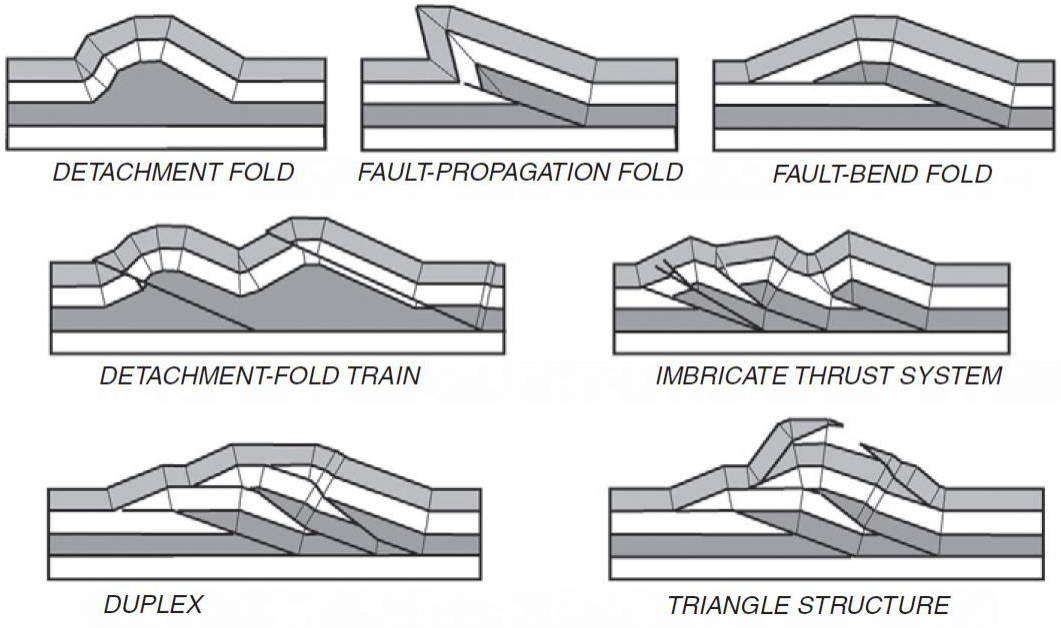

Figure 2.6. Several examples of uplift due to tectonic mechanisms. From Roeder (2012).

2.2.3.2. Thermal uplift

Thermally driven uplift occurs when the lithospheric mantle becomes hotter or when a hot material replaces a cooler material. Thermal uplift often occurs transiently and disappears after the thermal anomaly no longer exists (Gallagher, 2012).

Mantle convection is one driving force responsible for thermal uplift. This can cause magmatic underplating, where low density melt replaces the upper mantle of the lower crust, which produces long wavelength, permanent uplift (Gallagher, 2012). This is illustrated below, Figure 2.7.

Mantle convection can also produce dynamic uplift. In this case, a thermally driven mantle plume rises due to the lower density of the hotter mantle. As it rises, it pushes up on the crust, causing long wavelength uplift. Once the temperature anomaly disappears, the uplifted area subsides. Rohrman et al. (2002) has argued this to be the cause of uplift in parts of the North Atlantic margins, in particular southern Norway.

Thermal uplift can also occur in rift margins during rifting. Where rifting occurs, the hotter mantle is introduced closer to the surface resulting in a reduction in mean density, leading to surface uplift due to isostatic adjustments, Figure 2.8. As well as this, the hot mantle will cool

at the edges which tend to sink, causing secondary convection cells which in turn uplifts the rift flanks. Both of these types of uplift seen in a rift setting can lead to uplift of a few hundred metres (Gallagher, 2012).

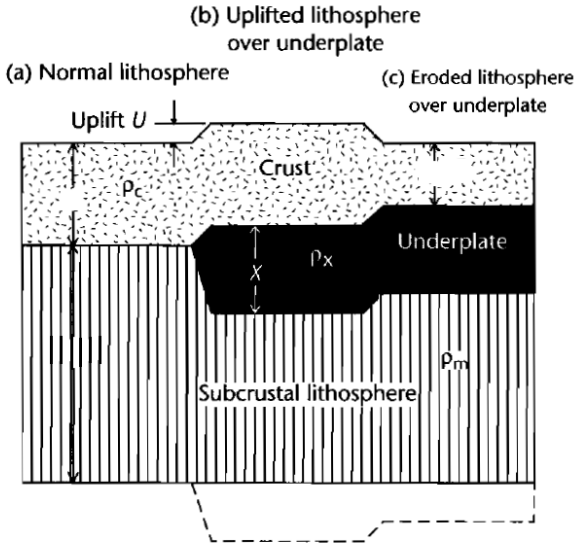

Figure 2.7. Uplift caused by magmatic underplating as a result of mantle plume activity. From Allen and Allen (1990).

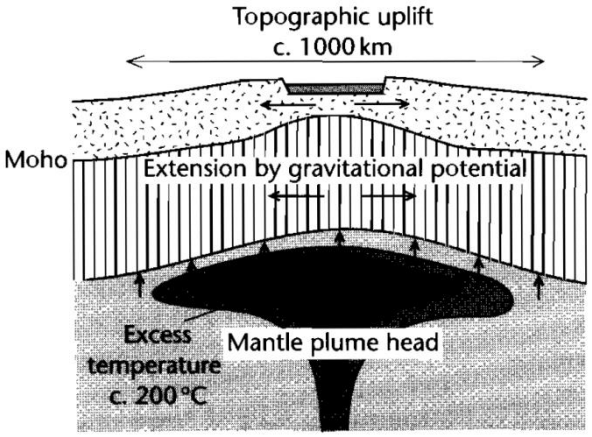

Figure 2.8. Active rifting above a mantle plume head. This upwelling of the mantle plume causes long wavelength topographic doming, as well as extension of the lithosphere. From Allen and Allen (1990).

2.2.3.3. Isostatic uplift

The constant-horizontal-stress reference state refers to the average stress in the lithosphere being equal everywhere to the same depth of isostatic compensation under the thickest lithosphere. This is maintained by isostatic equilibrium (Fossen, 2010). An example of isostatic uplift is illustrated below, Figure 2.9.

Isostatic adjustments are made in the Earth's surface and sub-surface until isostatic equilibrium is reached. Loading of the lithosphere tends to cause subsidence, however if regional isostasy operates, uplift can occur as peripheral bulges in response to surface loading.

The nature of movement is influenced by the necking depth in relation to the compensation depth, Figure 2.10. The necking depth is the reference level about which thinning occurs, and the compensation depth is depth over overlying sediments.

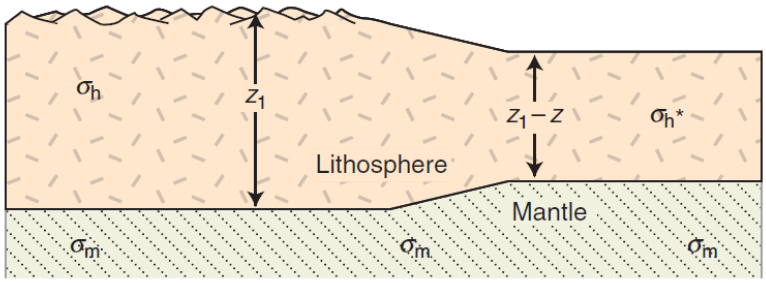

Figure 2.9. The relationship between erosion, isostasy and stress. Z1 = thickest lithosphere, and below the lithosphere the mantle is assumed to behave like a fluid. Modified from Fossen (2010).

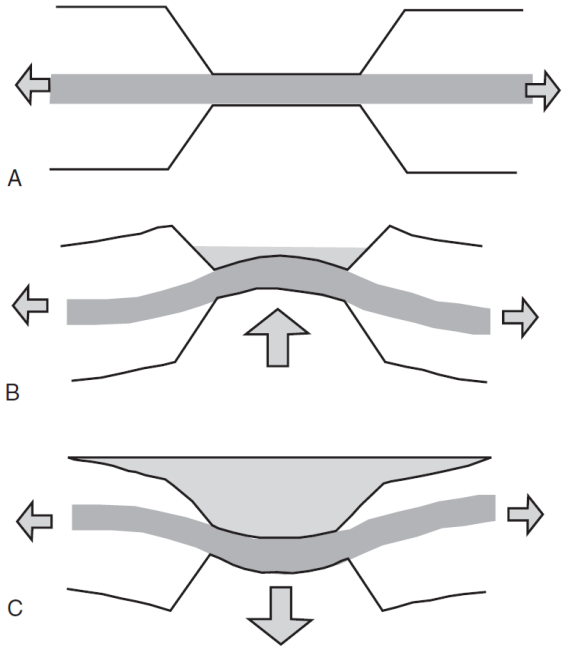

Figure 2.10. The influence of necking depth on the direction of movement. The setting in equilibrium (A), uplift resulting from necking depth being greater than compensation depth (B), and subsidence resulting from compensation depth being greater than necking depth (C). From Gallagher (2012).

2.2.3.4. Stress uplift

Crustal and whole lithosphere thickening from stress conditions that produce compression can produce uplift. Under appropriate circumstances, extension can also produce uplift. Both compression and extension can also produce subsidence. The nature of movement is dependent on the initial and final density distributions in the lithosphere. Crustal thickening alone tends to reduce the average density of the lithosphere, resulting in uplift, whereas thickening of the sub-crustal lithosphere tends to produce subsidence (Gallagher, 2012). The effects of crustal and lithospheric thickening are illustrated below, Figure 2.11.

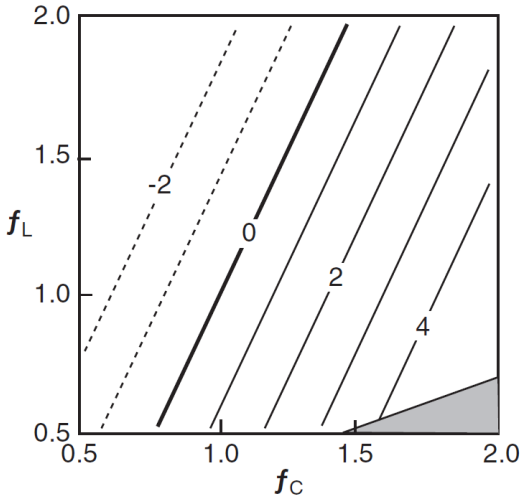

Figure 2.11. The result (uplift or subsidence) from different crustal thickening/thinning (fC) and lithospheric thickening/thinning (fL) regimes. The values for fC and fL are thickening/thinning factors, and the uplift/subsidence values given in kilometres. From Gallagher (2012).

2.2.4. Implications of uplift and erosion for petroleum prospectivity

As mentioned, uplift and erosion have significant implications for petroleum prospectivity. These effects have been well documented (Dore and Jensen, 1996, Henriksen et al., 2011). Many negative effects are mentioned, however several positive effects also exist and are often overlooked.

The different effects of uplift and erosion on a petroleum prospective area mentioned by Henriksen et al. (2011) are illustrated below, Figure 2.12. This shows that net erosion effects source rock maturity and reservoir quality, whereas uplift effects on seal capacity, hydrocarbon migration and trap volume.

More detailed descriptions of both positive and negative implications have been discussed by Dore and Jensen (1996). These are summarised below in Table 2.1 and Table 2.2.

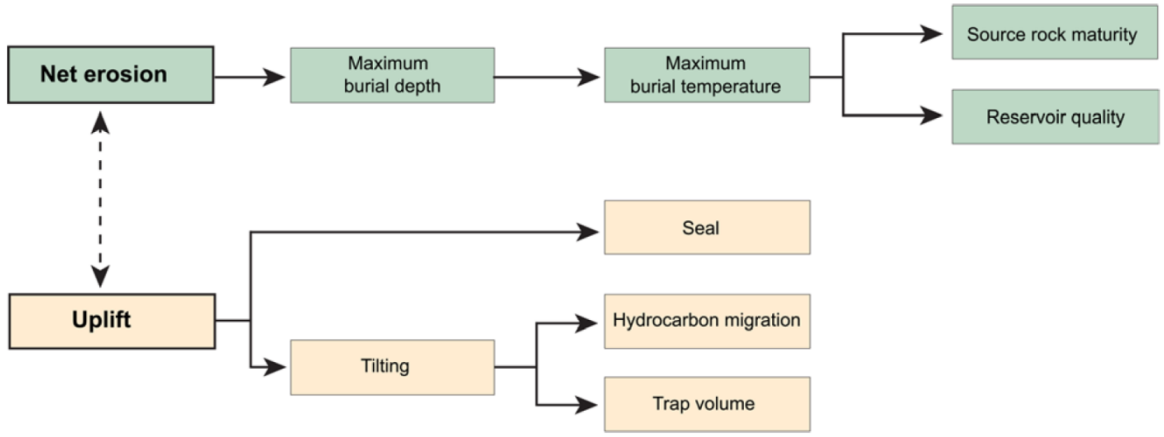

Figure 2.12. Effects of uplift and net erosion on the elements that govern petroleum prospectivity. From Henriksen et al. (2011).

Table 2.1. Negative implications of uplift and erosion for petroleum prospectivity (Dore and Jensen, 1996).

Effect	Description
Reservoir quality	Increasing burial depths and reservoir temperatures lead to changes in reservoir properties, especially porosity. These changes occur due to the compaction of the rocks, both mechanical and chemical, as they are buried more deeply.
Seal capacity	Preservation of oil and gas in a reservoir requires an effective seal. Basin inversion can greatly affect the sealing capacity of a top seal, as catastrophic failure can occur, causing oil and gas spillage. Traps which are not bounded by faults, but instead by stratigraphic or anticline traps, have a higher survival rate when uplifted and eroded.
Petroleum generation, migration and biodegradation	Source rocks can only mature positively – the process cannot be reversed. Therefore the measured maturity of a source rock reflects the maximum temperature at which it has experienced. In the Barents Sea, mature source rocks occur at much shallower depths than expected, indicating that they have ceased to generate hydrocarbons due to uplift.
Changes in structural attitude	Tilting of structures with pre-existing hydrocarbon accumulations will encourage spillage. The Barents Sea has been uplifted and eroded more severely to the north and east, which could have led to spillage of hydrocarbons as the structural traps are tilted.
Gas expansion and exsolution from oil	Decrease in pressure from uplift and erosion causes the gas in a gas accumulation or gas cap to expand. This leads to the expulsion of hydrocarbons from the closure. Also, an oil accumulation lying close to its bubble point will expel gas when pressure is reduced.

Table 2.2. Positive implications of uplift and erosion for petroleum prospectivity (Dore and Jensen, 1996).

Effect	Description
Local redeposition	Adjacent areas of uplifted and eroded areas experience net subsidence. This leads to deposition of erosion products of the uplifted and eroded area and accelerates the maturation of source rocks.
More mature than expected source rocks	Rocks which have been uplifted will be more thermally mature than expected as they have been buried more deeply than they are today. This means that rocks at shallower depths than what is normally considered the oil window have possibly been within the oil window before they were uplifted.
Methane exsolution from formation water	Formation water has the potential to produce methane as a result of thermal maturation of organic matter in the section. Methane gas can be liberated from formation water when uplifted as a consequence of a decrease in pressure and temperature.
Fracture enhancement of reservoirs	The strain reservoir rocks are able to withstand before brittle fracturing occurs is often significantly less than that of which caprocks can withstand. This means that uplifted reservoir rocks can be fractured, while sealing caprocks retain their sealing capacity, bringing hydrocarbons closer to the surface and making the area more accessible for drilling.
Remigration	There is a possibility for spilled hydrocarbons to remigrate to shallower or adjacent structures. This means that deeply stored hydrocarbon reserves have the possibility to migrate upwards to a more accessible location.

2.2.5. Measuring uplift and net erosion

Several methods have been used to quantify uplift and erosion various publications (Dore and Jensen, 1996, Henriksen et al., 2011, Jensen et al., 1990). The methods have been categorised as either regional or local methods. A summary of these methods is shown below, Table 2.3.

Local methods are based on physical and chemical changes caused by burial, mostly influenced by changes in temperature and pressure (sediment compaction). This gives an estimate of the maximum palaeo-temperature and/or maximum burial depth. Often this method uses well data or kinetic modelling, in which a reference in an area with zero uplift and erosion must be established. Regional methods are based on analysis of maps, profiles and velocity data. Examples of these are mass balance and palaeogeographical reconstruction methods (Dore and Jensen, 1996).

Table 2.3. Various regional and local methods that can be used to estimate uplift and net erosion (Jensen et al., 1990).

Regional methods (analysis of map, profile and velocity data)
Subcrop maps
Extrapolation from seismic profiles
Geomorphology and palaeogeographical reconstructions
Seismic velocity analysis

Local methods (analysis of rock parameters and well data)
Shale compaction (sonic velocity, porosity)
Sandstone porosity and diagenesis
Clay mineral diagenesis
Vitrinite reflectance trends
Colour of microfossils (TAI)
Organic geochemistry (pyrolysis data, geochemical markers)
Fluid inclusion analysis
Fission track studies
Opal A – Opal CT – quartz transformations
PVT modelling of hydrocarbon accumulations
Drilling parameters (Dx component)
Kinetic modelling

2.2.6. Uplift and net erosion in the Barents Sea

The topography of the Barents Sea today is partly due to the underlying bedrock and structural trends, but also to the Late-Cenozoic glacial erosion. Shallow banks separated by deep troughs, running towards the continental margin, characterize the Barents Sea floor. Submarine fans are found at the mouths of these troughs, which vary in size. The Bjørnøya Fan is the largest and the fans located along the margin next to Svalbard are considerably smaller (Faleide et al., 1996).

Glaciation in the northern hemisphere maybe have started as early as 5.5 Ma or even earlier (Faleide et al., 1996). Evidence shows that extremely high rates of erosion have occurred in the southwestern Barents Sea during the last 2.7 Ma, which has given rise to the glacial morphology of the continental shelf and the development of a several-kilometer-thick sediment fan along the continental margin (Laberg et al., 2012).

For approximately the last 2.7 Ma, total glacial erosion of the deep troughs has been considerably high and is estimated at approximately 1000 – 1100 m. The rates of erosion are

found to peak between 1.5 and 0.7 Ma. These rates are among the highest estimated for areas at the same latitude (Laberg et al., 2012).

Attempts have been made to model the uplift and erosion history of the Barents Sea for a long time, the first model formulated by Nansen (1904). Later studies by Harland (1969) supported Nansen's theories and suggested a thermal mechanism as the cause of uplift. Bathymetric inversion based on isostatic equilibrium conducted by Vågnes and Amundsen (1993) has shown that the degree of uplift and erosion observed in the Barents Sea could not be due to erosion alone.

Previous studies regarding the mechanisms causing the uplift observed in the Barents Sea have not always agreed. Dore and Jensen (1996) mention differing theories regarding the cause of uplift in several publications. These are pre-opening Atlantic margin elevation (Ghazi, 1992, Torske, 1972), mantle phase changes (Riis and Fjeldskaar, 1992), intraplate stress (Cloetingh et al., 1990), isostatic response to sedimentary unloading (Riis and Fjeldskaar, 1992) or a combination of several of these phenomena (Dore, 1992, Jensen and Schmidt, 1993, Reemst et al., 1994). The more recent general consensus is that the initial uplift was tectonic and occurred in several phases during the Cenozoic, and the latest and most significant of these phases occurred in the Pliocene – Pleistocene and was associated to the severe glaciation during that period (Dore and Jensen, 1996).

The relatively disappointing results of oil and gas exploration in the Barents Sea have been largely attributed to Cenozoic uplift and erosion. For this reason, considerable resources have been expended on measuring this phenomenon, understanding the timing of the phases, mapping its distribution and investigating its effect on hydrocarbon generation, trapping, and preservation (Dore and Jensen, 1996).

Chapter 3: Methodology

For this research paper, well logs were analysed and seismic data were interpreted. The full dataset consisted of 21 seismic lines and 89 well logs from the Barents Sea. From these data, eight seismic lines and 11 well logs were selected for interpretation and analysis, approximate locations shown in Figure 3.1.

To get a broad overview of the uplift and net erosion patterns across the western Barents Sea, the 11 wells that were analysed were selected based on their location and the contents of the log. The 11 selected wells as well as their coordinates are shown below in Table 3.1.

Table 3.1. Well summary, including location, total depth and intersecting seismic line(s).

Well ID	x-coordinate (m)	y-coordinate (m)	Total depth (m)	Intersecting line(s)
7120/9-1	498125	7932343	2300	MCG1102-004
7121/5-2	523051	7952738	2543	MCG1102-005
7121/7-1	503105	7930306	2160	MCG1102-023
7124/3-1	632001	7966518	4730	MCG1102-022
7125/1-1	645188	7981934	2200	MCG1102-022 and MCG1102-007
7131/4-1	849533	7984178	1295	MCG1102-009
7219/8-1S	445743	8031654	4611	MCG1102-004
7223/5-1	578198	8050357	2549	MCG1102-007 and MCG1102-025
7226/2-1	683359	8097235	2992	MCG1102-025
7321/7-1	502403	8148910	3550	MCG1102-029
7324/10-1	607068	8121933	2919	MCG1102-009

Projection: ED50-UTM34

The seismic lines selected were part of a large dataset of super-tie lines in the Barents Sea, surveyed by MultiClient Geophysical ASA (MCG). Three composite seismic lines were created using seven of the original seismic lines to simplify the interpretation process. Composite lines were constructed based on well locations, so that all wells selected for analysis were intersected by seismic lines. This resulted in one line, CL1, to be bending back on itself. Another seismic line crossing the three composite lines was used to tie the composite lines together. The selected seismic lines are summarised below, Table 3.2.

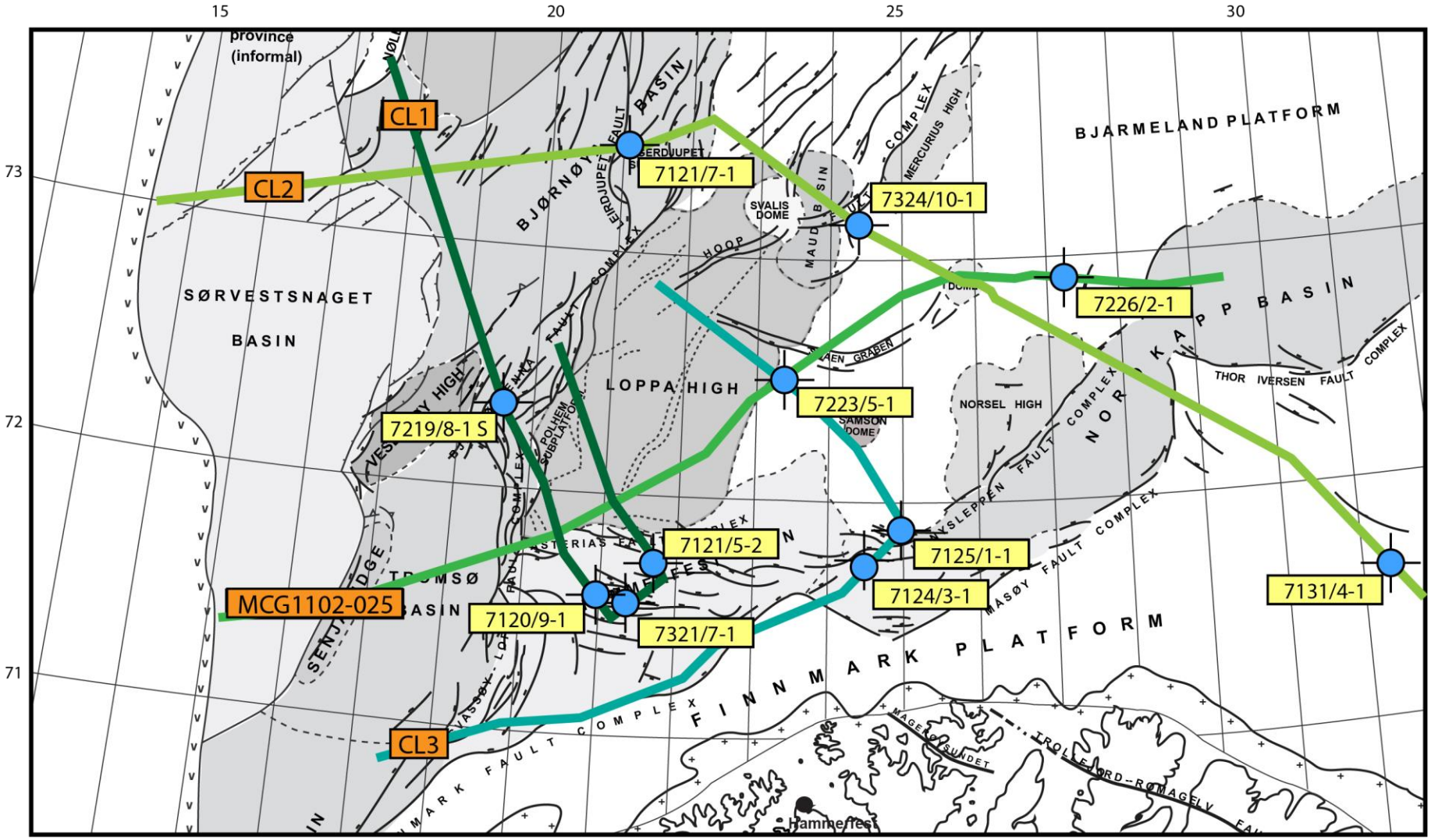

Figure 3.1. Study area overview with approximate locations of wells and seismic lines. Composite seismic lines (CL1 – CL3) have been constructed to intersect all wells, hence the unusual paths. Structural elements are annotated. Modified from NPD (year unknown).

Table 3.2. Line summary for the eight seismic lines used for seismic interpretation.

Composite/tie line	Lines used
Composite line 1	MCG1102-004 MCG1102-005 MCG1102-023
Composite line 2	MCG1102-009 MCG1102-029
Composite line 3	MCG1102-007 MCG1102-022
Tie line	MCG1102-025

3.1. Estimating net erosion from P-wave velocity variations

For the well log analysis, wireline logs of 11 wells were analysed, processed and displayed in order to estimate uplift from P-wave velocity variations. The data that were analysed were mainly sonic logs and gamma ray logs, however density, neutron porosity and deep resistivity were also considered when selecting wells and intervals.

Figure 3.2 is a schematic diagram illustrating the process of net erosion estimations. The x-axis shows P-wave velocity and the y-axis shows depth. A normal compaction or reference (no uplift and erosion) velocity-depth trend is shown in red. Above this line is a velocity-depth trend of an area which has undergone uplift and erosion, shown in blue. The uplifted and eroded rocks are still compacted to the same degree as they were at their deepest burial point, and therefore the blue line plots higher than the red reference trend.

The difference in depth between the reference trend and uplifted and eroded rock trend corresponds to the vertical difference between present day burial depth and maximum burial depth, or net erosion. This process has been carried out on 11 wells in the Barents Sea.

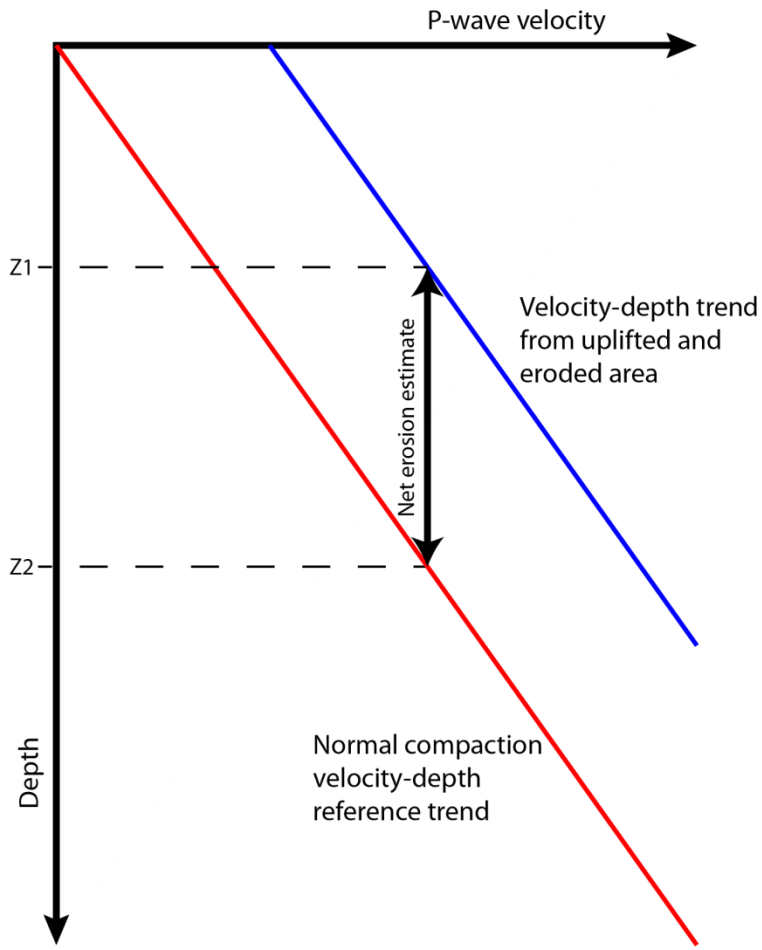

Figure 3.2. Schematic diagram illustrating velocity-depth trends for an area with normal compaction (red) and in an uplifted and eroded area (blue).

3.1.1. Reference trend

Storvoll et al. (2005) has developed a reference trend which will be used herein to calculate net erosion. This was constructed using 60 wells along the Norwegian Shelf. All wells were subject to thorough quality control and most of the wells were chosen as they were dry wildcat wells, which minimises the effect of varying pore-fluid saturation on sonic velocity. The sonic logs have not been corrected for overpressure. Entire log data sets were used, as opposed to averaged values (Storvoll et al., 2005).

Of the 60 wells that were selected for studying, 22 were from the northern North Sea, 24 from the Haltenbanken area and 14 from the Barents Sea. The results were then compared to several published velocity trends (Hansen, 1996, Hermanrud et al., 1998, Hjelstuen et al., 1996, Japsen, 2000, Teige et al., 1999). The velocity-depth trend is agreed to approach zero

at infinite depth between sources, however a simplified linear velocity-depth trend is expressed in the following way (Storvoll et al., 2005):

$$Z = 1.76V_p - 2600$$

Where Z is depth in metres and V_p is the P-wave velocity in metres per second. This trend is illustrated in Figure 3.3, along with previous studies results. For the purposes of this paper, the trend calculated by Storvoll et al. (2005) is considered to be a sound reference. No uncertainty value or specifics in methodology have been provided, so the reference trend has been allocated an arbitrary uncertainty value of ± 100 m. This reference trend will be used in conjunction with P-wave velocity data sets from the western Barents Sea to estimate uplifts.

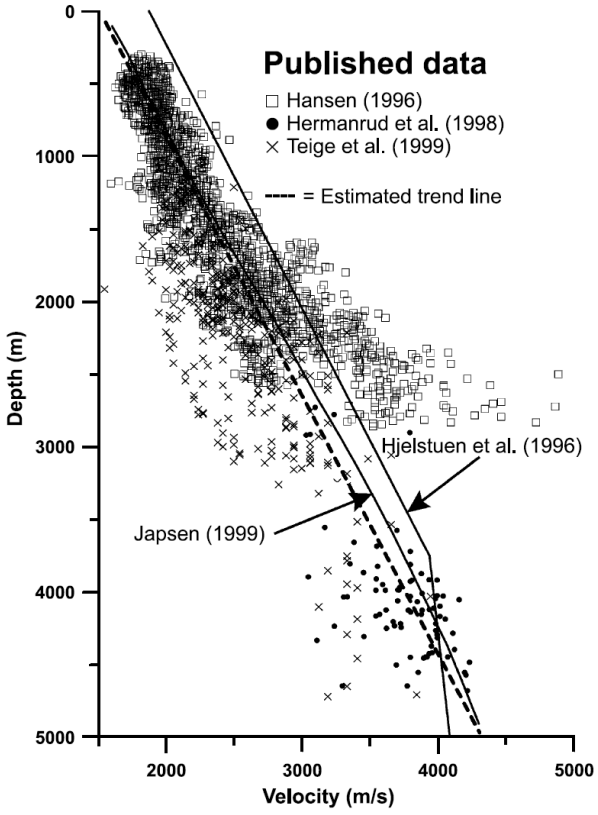

Figure 3.3. Velocity-depth trend used in this report (stippled line) compared with previously published data. The trend is first-order linear and estimated at $Z=1.76V_p - 2600$. From Storvoll et al. (2005).

3.1.2. Data processing

All data were imported and quality checked using Petrel and then exported as ASCII files. The ASCII files were read and processed using MATLAB. Kelly bushing height, water depth, and formation interval depth data were sourced from the completion logs on the Wellbore Statistics web page provided by NPD (2016). The P-wave velocities were calculated from compressional sonic data, and converted from slowness (µs/ft) to velocity (m/s).

To improve consistency of results, all data points selected for analysis were from the Kolmule formation. Formation interval depths were found in the Wellbore Statistics web page provided by NPD (2016). The Kolmule formation was chosen due to its widespread coverage, high clay content and due to it being penetrated by many wells in the western Barents Sea. It is also relatively young, and therefore more likely to have been effected only by the more recent uplift and erosion events.

The velocity-depth analyses were restricted to shale lithologies to improve consistency and comparability to the reference trend. Lithologies with a clay volume greater than 80% were considered clean shales and included in the data analysis. The clay volumes were calculated by analysing gamma ray logs using the following formula as described by (Cannon, 2016):

$$V_{clay} = \frac{GR_{max} - GR_{min}}{GR_{log} - GR_{min}}$$

Where GR_{max} is the 100% clay limit or clay line, GR_{min} is the 100% sand limit or sand line, and GR_{log} is the value of the log for a particular data point. Sand and shale lines were selected by the user based on gamma ray logs. See Figure 3.4 for a schematic diagram of the sand and shale line picking process. The result is V_{clay}, or volume of clay. The sand and shale lines varied well to well, and in some cases varied within a well. Therefore each well was individually processed and studied to calculate clay volumes.

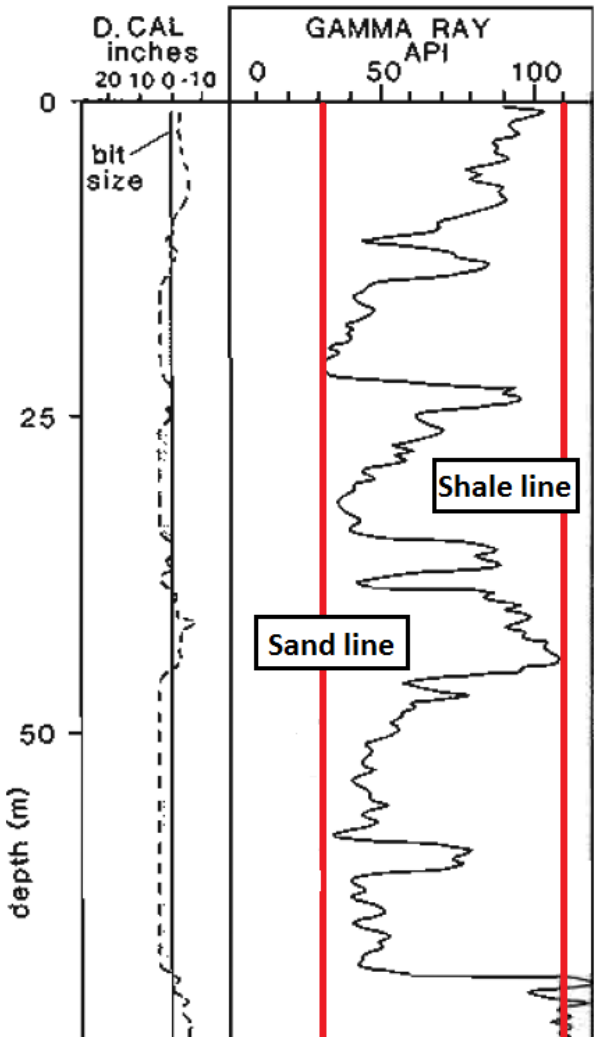

Figure 3.4. Processing of gamma ray logs to calculate clay volume. Sand and shale lines are manually selected from the local minimum and local maximum gamma ray log values. Modified from Rider (2000).

Minimum and maximum gamma ray values were manually selected for each well log. Often the gamma ray log changed dramatically due to a change in casing size, indicated by a change in caliper log. Where this occurred, multiple intervals were taken from the gamma ray log to adjust the minimum and maximum values selected. An example of selecting minimum and maximum gamma ray values over an interval with varying casing size and subsequent gamma ray log values is illustrated below, Figure 3.5.

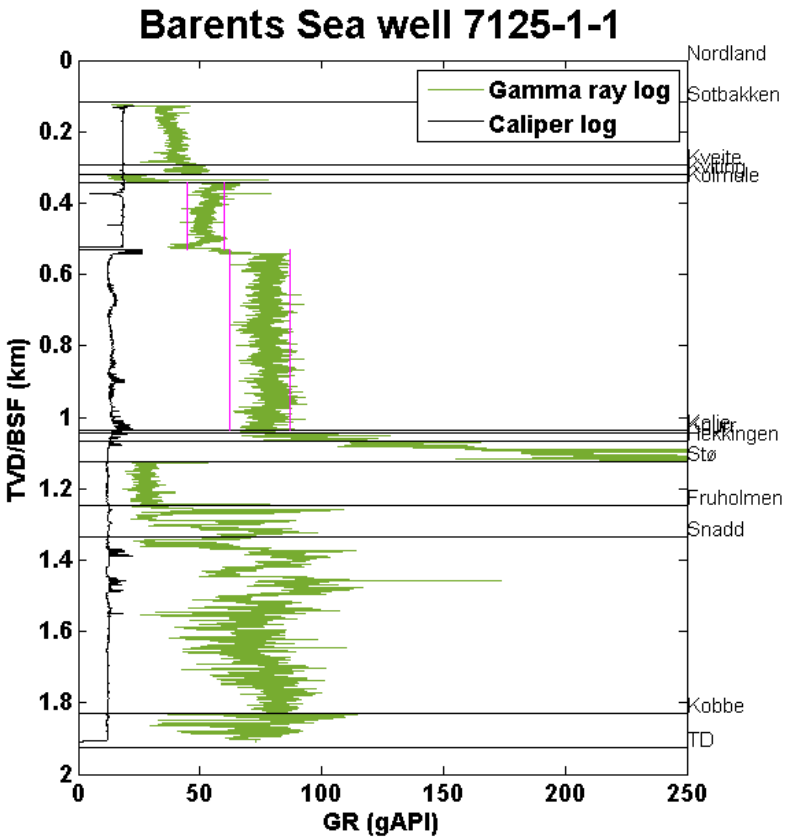

Figure 3.5. Gamma ray log for well 7125/1-1. Selected minimum and maximum gamma ray values shown in pink. The change in caliper log marks a change in gamma ray log, and different minimum and maximum values are chosen.

Using only Kolmule formation and restricting the data points to only greater than 80% clay constrained the values so that the faster sandy lithologies were excluded. Using shaly lithologies also meant that thin cracks in formations wouldn't affect the velocities as much as in sandy lithologies (Storvoll et al., 2005). As the reference trend is calculated using all lithologies and clay contents, this could give some absolute uncertainty, however the relative uplift estimates will be more reliable. All data points were then adjusted to be calculated from sea bottom by subtracting the water depth and kelly bushing height.

The accepted data points and subsequent regression trend were then plotted against the reference trend, Figure 3.6. The uplift was calculated as the difference between regression trend for each well and the reference trend. Minimum and maximum uplift values were extracted from the plots for the start and end of each accepted interval, respectively, and an average value was calculated from these, illustrated in Figure 3.7.

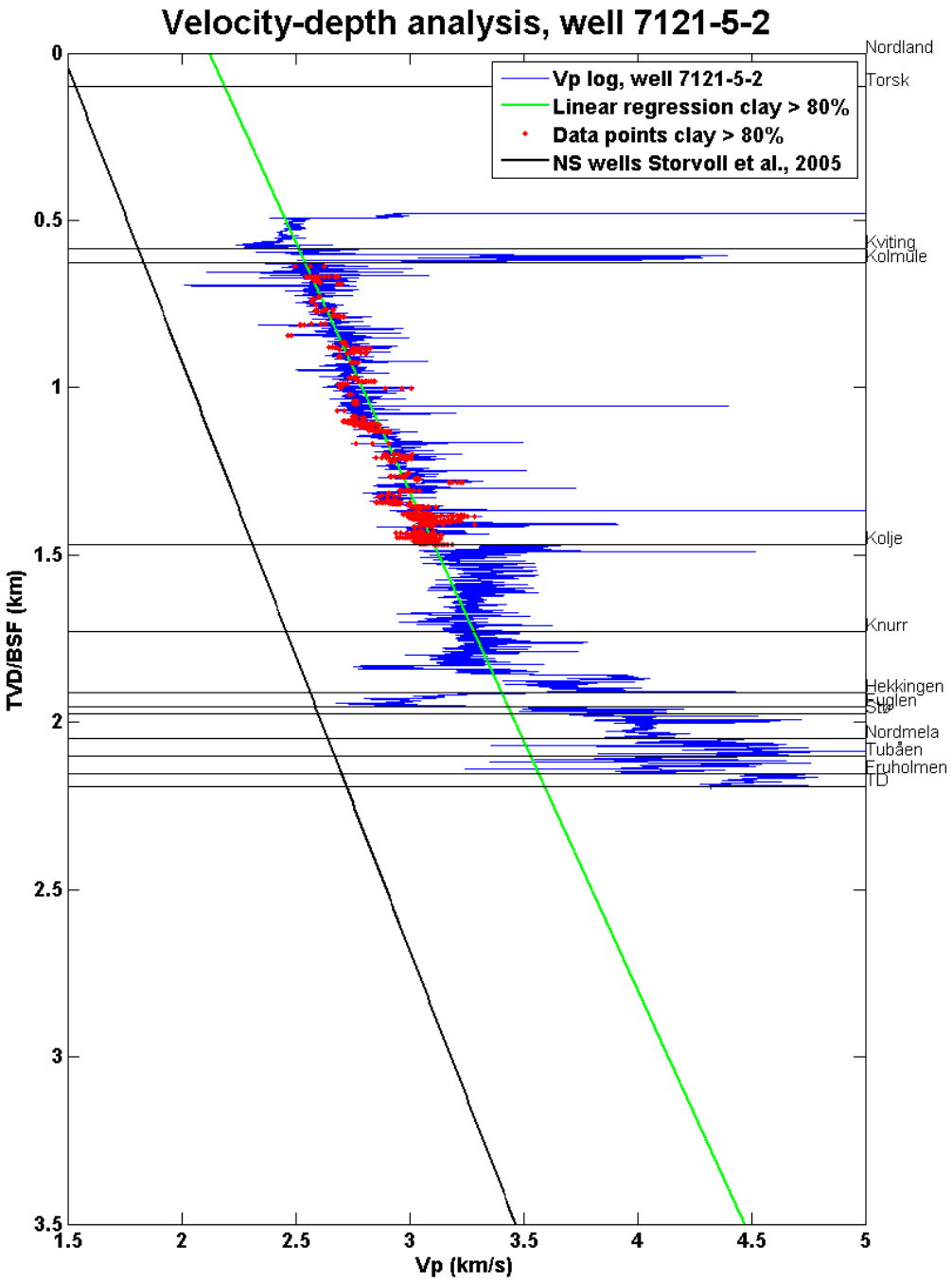

Figure 3.6. Velocity-depth analysis for well 7121/5-2. Sonic log (blue), data points with clay content >80% (red), Storvoll et al., (2005) reference trend (black) and calculated regression trend (green).

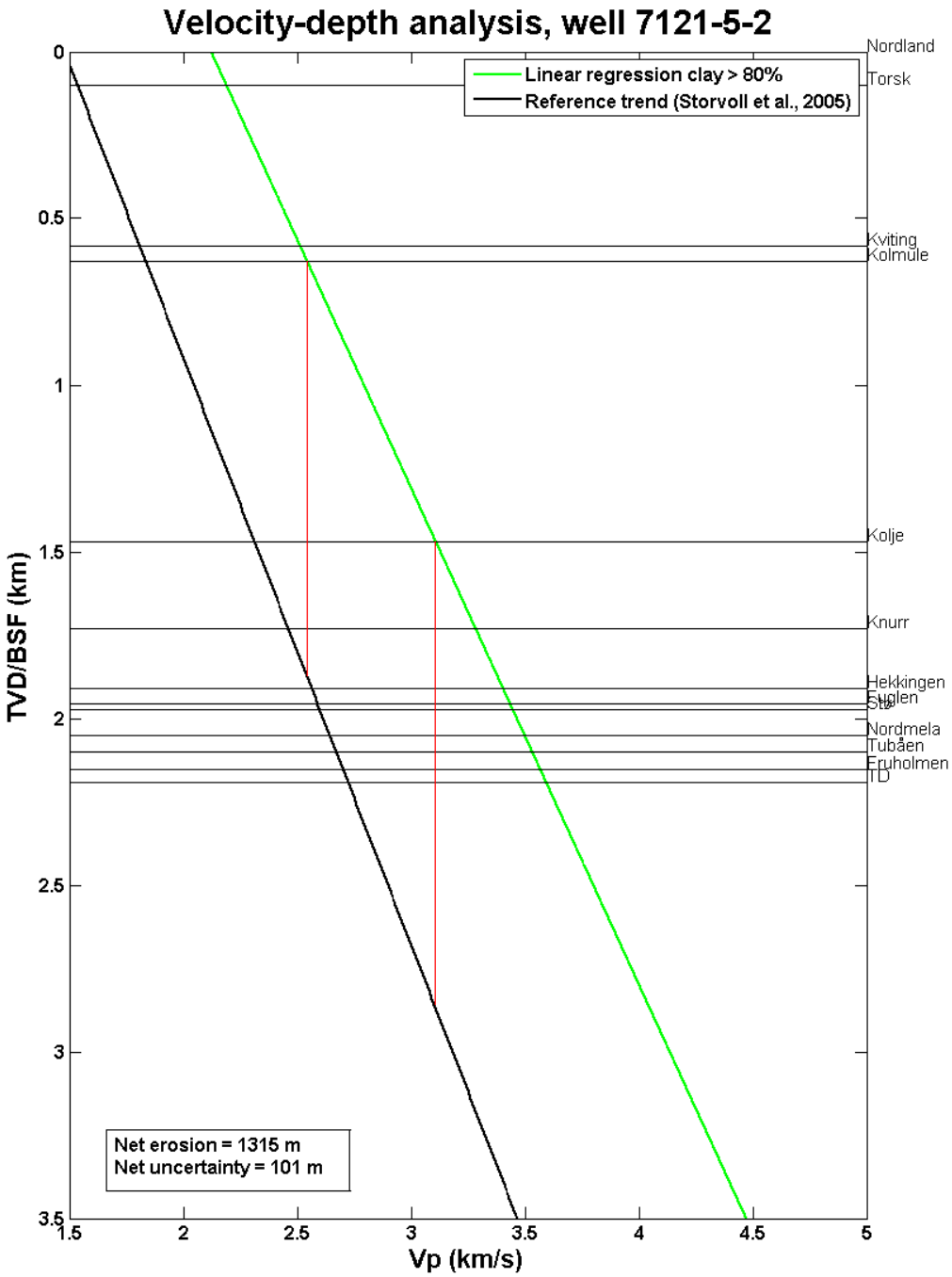

Figure 3.7. Velocity-depth analysis for well 7121/5-2. Regression trend (green), Storvoll et al., (2005) reference trend (black) and maximum and minimum net erosion values for the Kolmule formation (red).

3.1.3. Uncertainties in estimating net erosion from sonic logs

Several sources for error exist when estimating net erosion from P-wave velocity variations. These are uncertainties related to either systematic or measurement errors. Systematic errors are naturally occurring changes in data, such as lateral variations in facies and

different temperature and pressure conditions than the reference area. Measurement errors are the errors which are derived from measurement methodology, such as the quality of the data set and statistical errors (Baig et al., 2016).

Another factor contributing to uncertainty is introduced when picking minimum and maximum gamma ray log values in order to calculate the volume of clay. This was more prominent in some wells than others. An example of a poor gamma ray log is illustrated in Figure 3.8, where the gamma ray log for the Kolmule interval is very varied, which makes it challenging to assign maximum and minimum values for the gamma ray log, even if the log is broken down into smaller intervals.

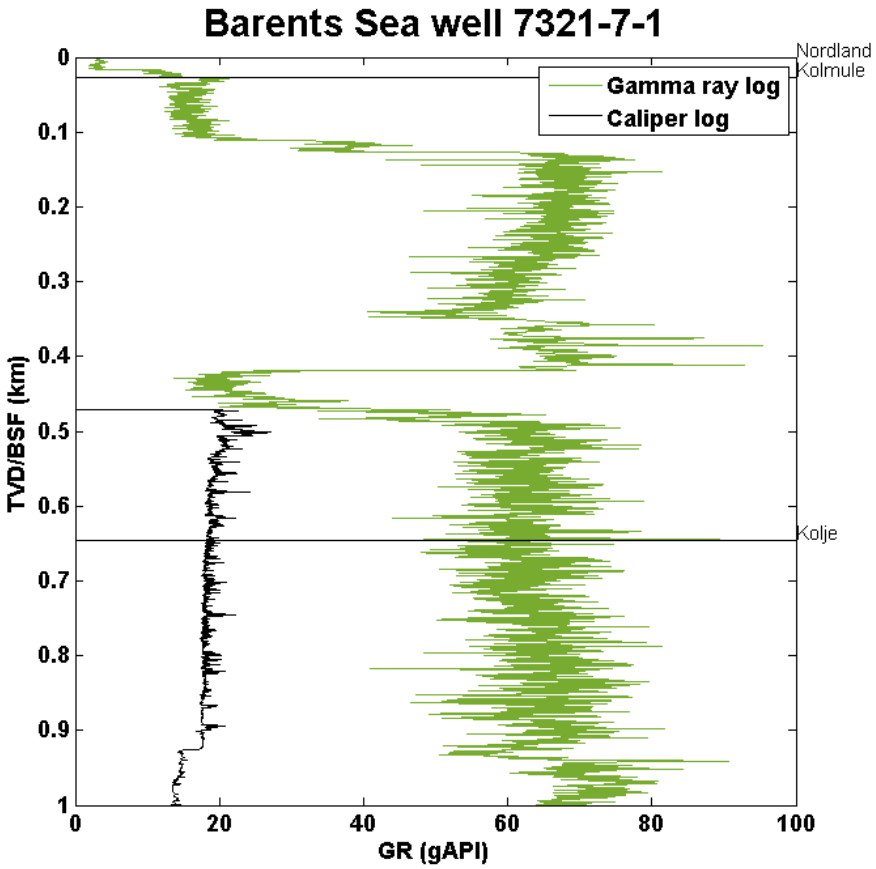

Figure 3.8. Poor gamma ray log with missing caliper log data. This resulted in poorly defined minimum and maximum gamma ray values and therefore inaccurate V_{clay} calculations.

The slopes (m-values) of the calculated regression trends were observed to differ in varying degrees to the slope of the reference trend. A strong correlation was observed to exist between the trend slope and factors such as the length of the interval, density of accepted data points and quality of the gamma ray log. For this reason, uncertainty was calculated based on the variation of slope between each of the calculated trends and the reference trend in the following way:

$$uncertainty = \frac{|calculated\ trend\ m - reference\ trend\ m|}{reference\ trend\ m} \times uplift\ estimate$$

This value was then added to the reference trend uncertainty of ± 100 m.

3.1.4. Assumptions

Several assumptions have been made during the net erosion estimation process:

- **Velocity-depth trends are linear**. This is not true across longer intervals (Allen and Allen, 1990), however a linear relationship has been assumed for the shorter intervals used in this study.
- **Shales in Barents Sea wells and reference trend wells are homogeneous**. It is clear that across such a large study area, variations in lithologies are likely to occur, affecting the properties of these rocks. In order to compare velocity-depth trends, shales in the Barents Sea wells and reference trend wells are assumed homogeneous.
- **Common thermal history across entire Barents Sea**. The transition from mechanical to chemical compaction occurs at around 70°C and has shown to significantly affect the velocity-depth trends (Storvoll et al., 2005). In order to simplify this study, the thermal history across the entire Barents Sea is assumed to be uniform.

3.1.5. Workflow

A workflow has been created to illustrate how net erosion has been estimated using sonic logs, Figure 3.9. This summarises the processing steps and analysis of the wells, from importing of data to calculating a net erosion estimate.

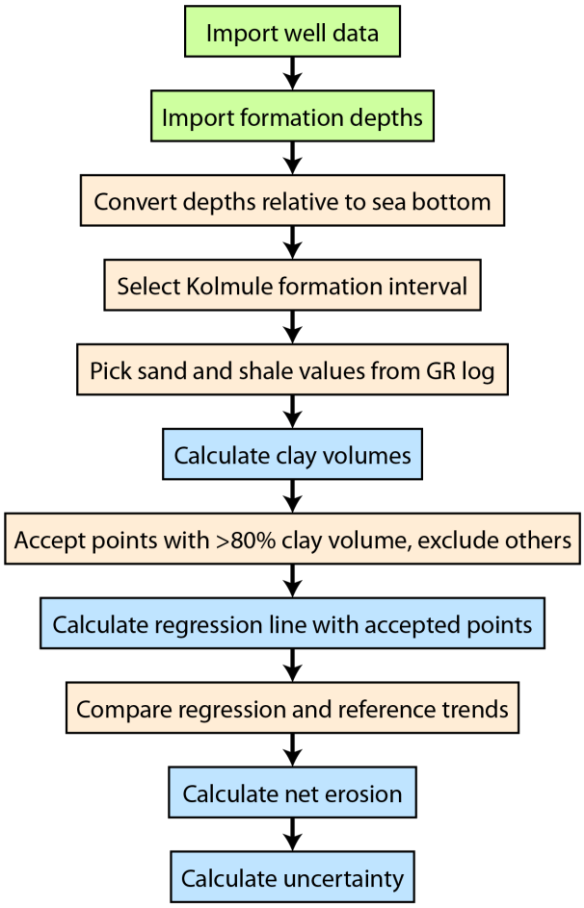

Figure 3.9. Workflow outlining steps taken for processing and analysing sonic logs to estimate net erosion.

3.2. Net erosion maps

In order to display the net erosion estimates for further interpretation, two net erosion maps were created. The first net erosion map to be created encompasses the whole study area to show a general trend of net erosion. The second net erosion map is to be created by dividing the study area into seven separate regions, based on structural features and net erosion estimates. This second net erosion map was created to provide a more accurate, yet still very rough, illustration of the net erosion differences in various structural areas.

3.3. Seismic interpretation and linking net erosion to geology

One of the main objectives of this report is to relate net erosion estimates to the geology in the Barents Sea. This was carried out by interpretation of eight seismic lines which tied all

the well estimates together. The main focus of interpretation and linking net erosion estimates to the geology seen in the seismic data was to interpret the regional and local uplift and erosion history of the Barents Sea, including the timing of events. This was conducted by calculating net erosion for several wells that intersect the seismic sections.

To correlate the main lithologies, a seismic well tie process was completed for all the relevant wells that intersected the seismic sections. This made it possible to distinguish the different formations and allocate geological ages.

Major and minor faults and the sea bottom were picked first. Secondly, tops of formations were picked from well top data. Other significant horizons were picked, such as erosional unconformities, deeper reflectors and other interesting reflectors that provided evidence on the depositional environment.

Once the horizon and fault picking stage was complete, interpretation continued by creating a geological model in Adobe Illustrator. This stage consisted of turning the seismic interpretation into a detailed geological model by highlighting the main facies, unconformities, faults, horizons and other interesting features, as well as colour coding the packages depending on their interpreted geological age. Each interpreted seismic section was then presented in three panels in the following format:

Top panel: A clean seismic section with no interpretations, showing only seismic data and well locations.

Middle panel: An interpreted seismic section. This contains the same as the first panel; however it also includes all the interpretations carried out in Petrel such as important horizons, faults and unconformities.

Bottom panel: A geological model. This model is created in Adobe Illustrator and contains all the interpretations from the second panel, along with colour coding of each of the formations and labelling of significant features for discussion.

No net erosion values were estimated for the Loppa High as the wells in this area were not suitable for processing in the same way as the other wells. Instead, seismic sections were used to estimate net erosion in this region. Lines MCG1102-005 and MCG1102-007 were selected as they both intersect the Loppa High and nearby wells with calculated net erosion

values. Horizons were selected which could be tracked over the Loppa High and to a nearby well, and the net erosion was estimated as the difference in depth of this horizon between the Loppa High and the well with a net erosion estimate.

3.4. Uplift mechanisms, erosion and their seismic signatures

The second part of seismic interpretation was to explore local examples of uplift and erosion in various structural provinces shown in the net erosion maps. One seismic example from each of the provinces was selected to illustrate the differences in seismic signatures and to interpret the mechanisms causing the local uplift events.

These zoomed in examples were taken from the seismic super-tie lines. The selection and interpretation criteria were similar to the regional interpretations, although focused more on the local uplift and erosion events and the seismic signatures the erosional surfaces have in different areas.

Chapter 4: Results

4.1. Net erosion estimates from P-wave velocity variations

Net erosion values for all eleven wells have been calculated using the methodology described in Chapter 3. A plot for each of the 11 wells was created, each showing the reference trend, the calculated linear regression line and the interval length for the points used. The complete set of processed well logs can be found in the appendices section.

An example of a processed well log is shown below, Figure 4.1. From this, a net erosion average was calculated, as well as an uncertainty value. After the wells were processed and analysed, the resulting regression trends for the Kolmule intervals from each of the wells were plotted together, as well as the reference trend, Figure 4.2. The resulting net erosion estimates for each of the wells as well as their respective uncertainty values are summarised below, Table 4.1. These results are also displayed in a plot with error bars, Figure 4.3.

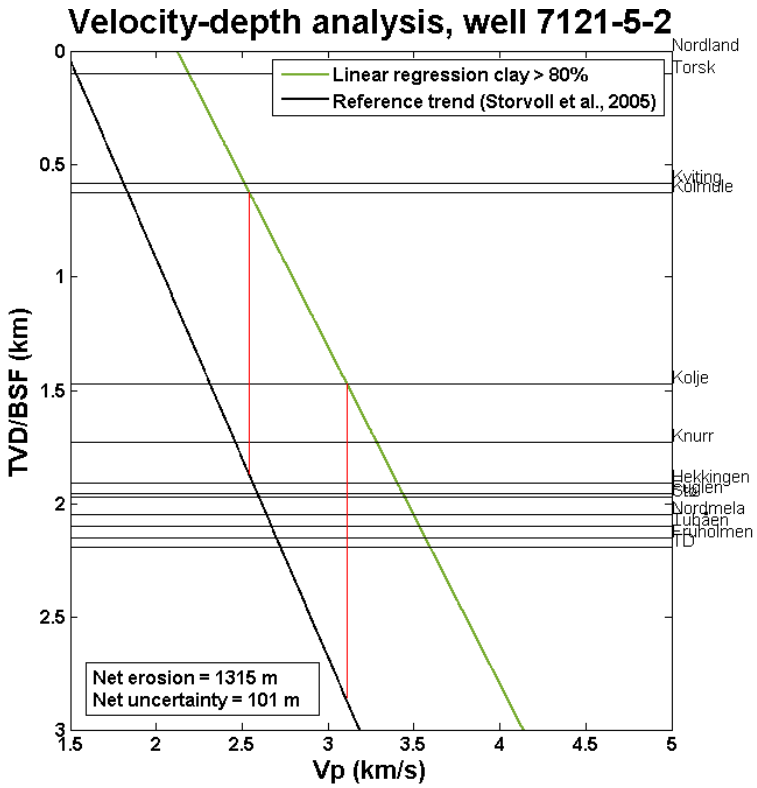

Figure 4.1. Example of velocity-depth analysis plotting for well 7121/5-2. Calculated regression line (green), reference trend (black) and minimum and maximum net erosion estimates (red) for the Kolmule interval. Similar plots were made for all 11 Barents Sea wells that were studied.

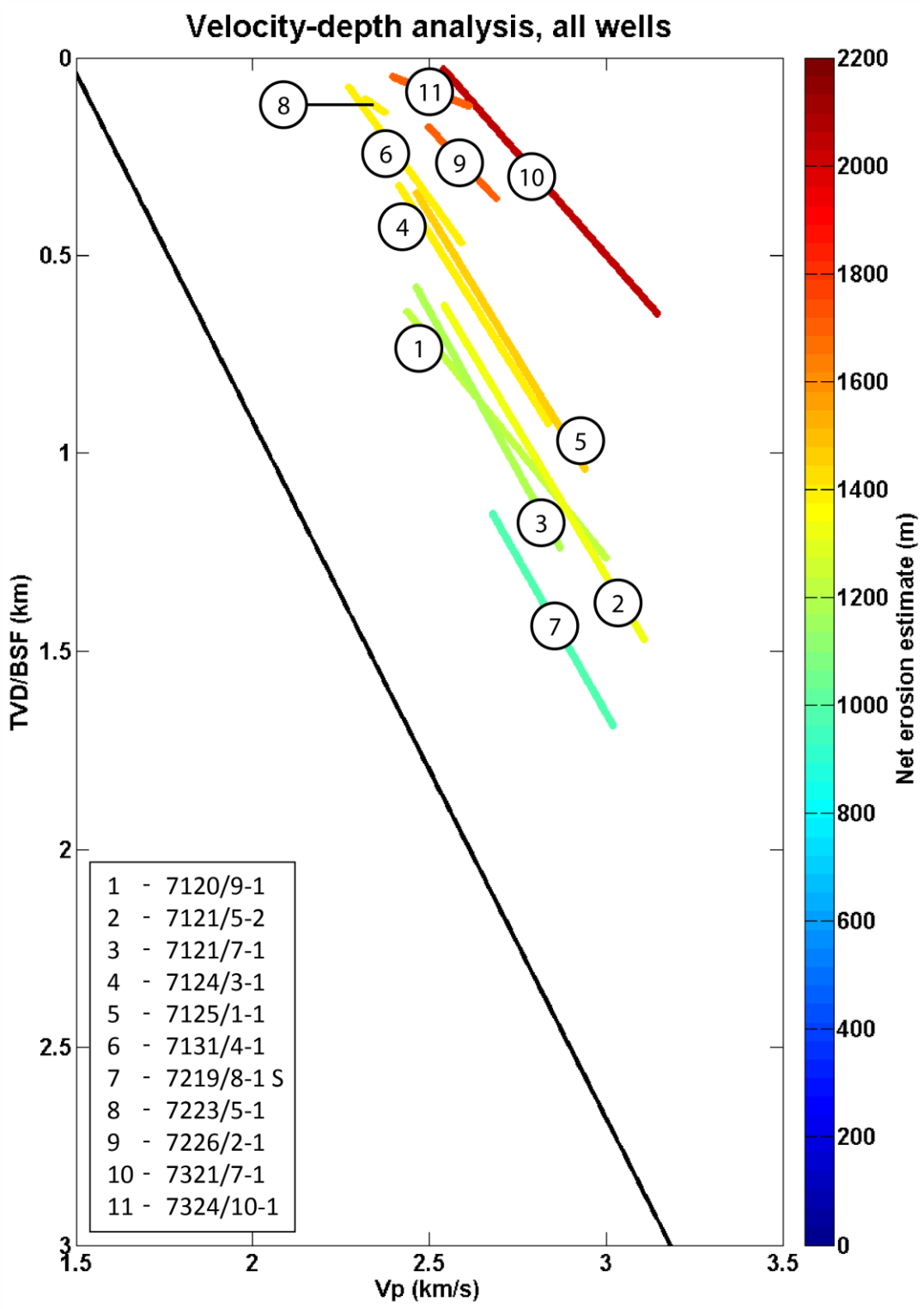

Figure 4.2. Results of the velocity-depth analysis of 11 wells in the Barents Sea. The black line represents the reference trend calculated by Storvoll et al., 2005. Coloured lines show the regression trends calculated for Kolmule intervals for each of the wells, with their colours representing the magnitude of net erosion.

Table 4.1. Net erosion estimates and uncertainty values for 11 Barents Sea wells.

Number	Well ID	Uplift (m)	Uncertainty (m)
1	7120/9-1	1226	± 328
2	7121/5-2	1315	± 201
3	7121/7-1	1182	± 148
4	7124/3-1	1389	± 233
5	7125/1-1	1454	± 223
6	7131/4-1	1406	± 309
7	7219/8-1 S	979	± 153
8	7223/5-1	1398	± 558
9	7226/2-1	1692	± 491
10	7321/7-1	2053	± 531
11	7324/10-1	1715	± 793

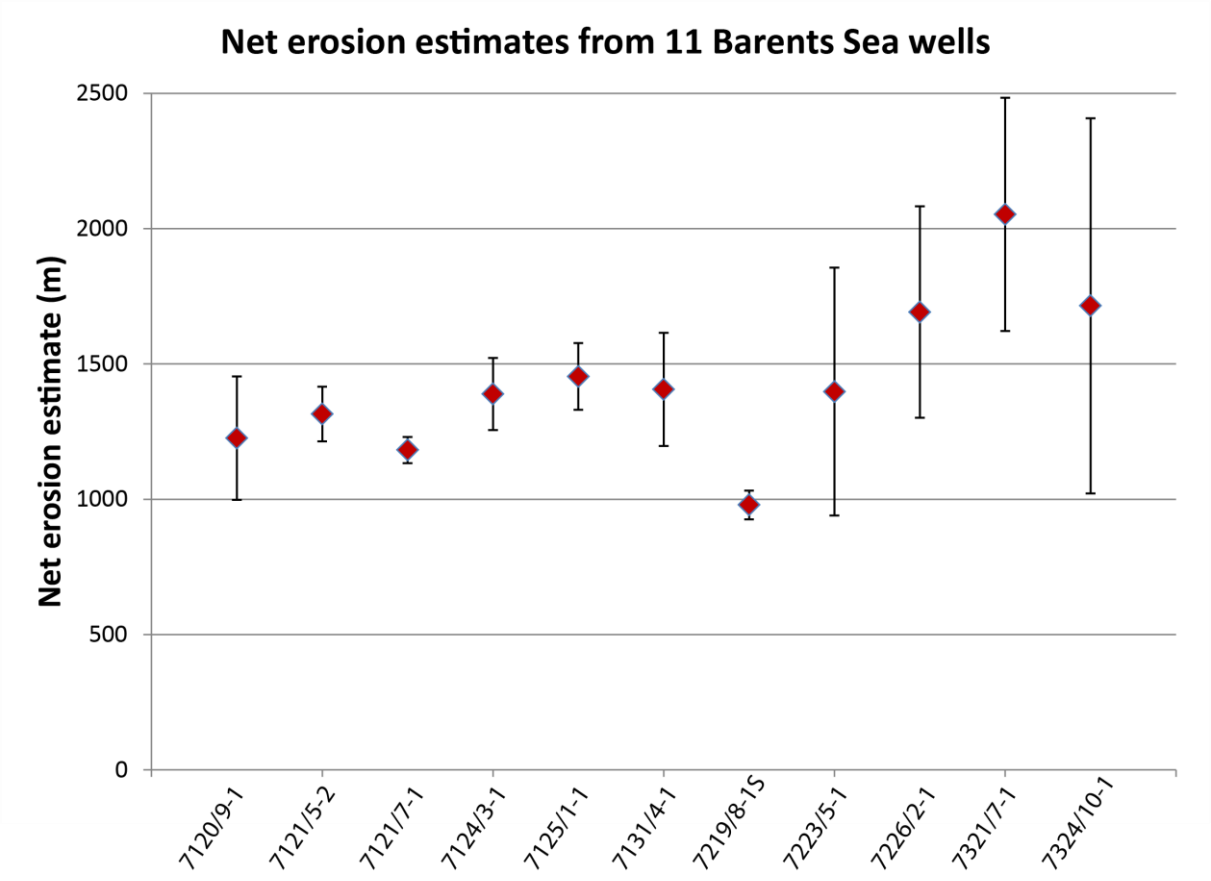

Figure 4.3. Net erosion estimates plotted for 11 Barents Sea wells. Uncertainty values are indicated by the error bars.

4.2. Net erosion maps

Net erosion estimates have been calculated using well logs, and calculated values have been plotted on a map view of the Barents Sea, Figure 4.4. The well IDs, net erosion estimates and uncertainties are annotated next to each of the wells.

Two net erosion maps have been produced using Petrel. The first shows a net erosion map created using all data points from the calculated wells, Figure 4.5. The second shows seven separate erosion maps overlayed on a structural map of the western Barents Sea, Figure 4.6. Each of the seven regions has been divided up to show areas of similar net erosion estimates and structural features.

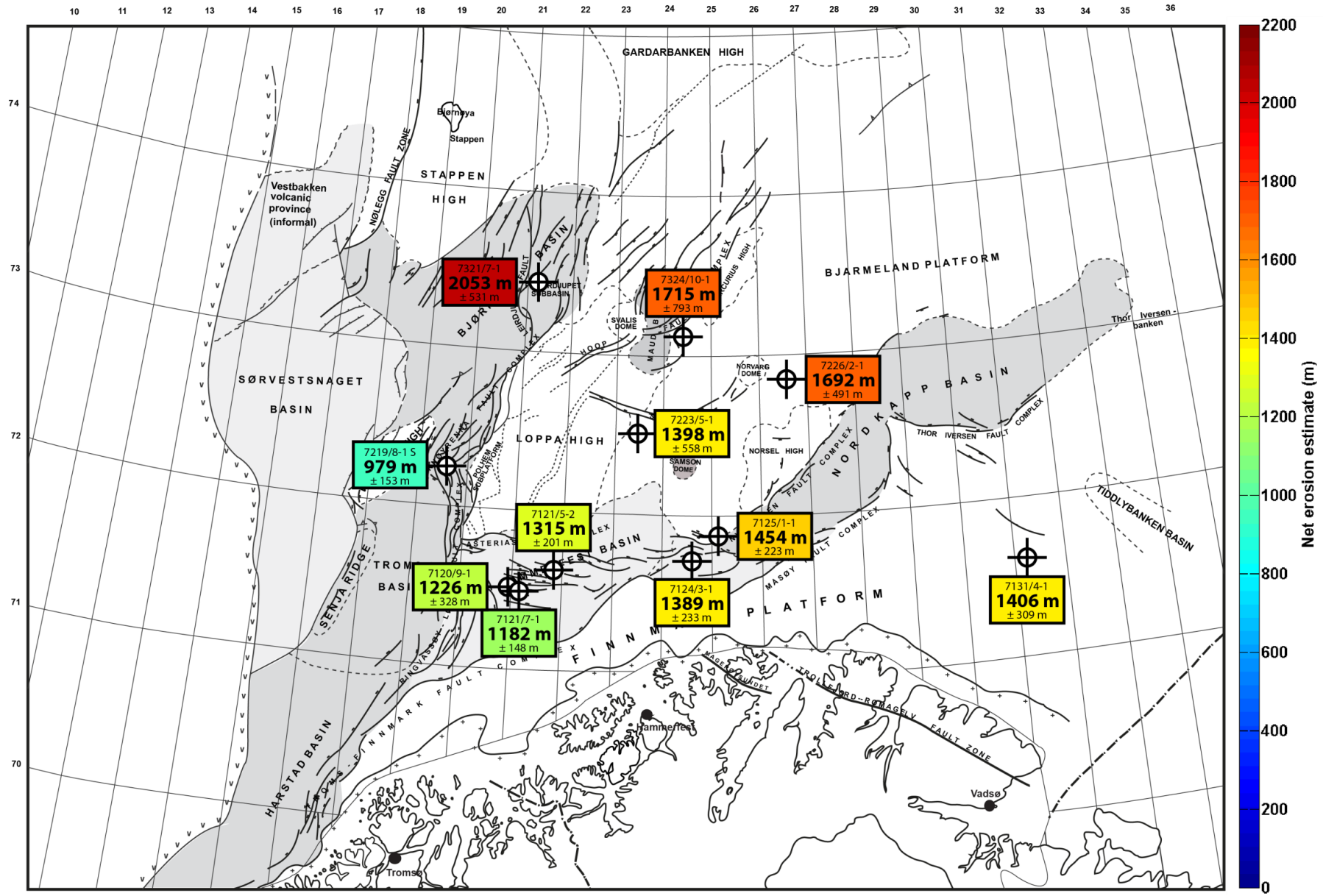

Figure 4.4. Net erosion estimates calculated from well logs, plotted on their respective locations. Well names, uplift estimates and uncertainties are annotated and the text boxes are colour coded to their net erosion estimates. A general increase of net erosion values is observed to the north and north east. Modified from NPD (year unknown).

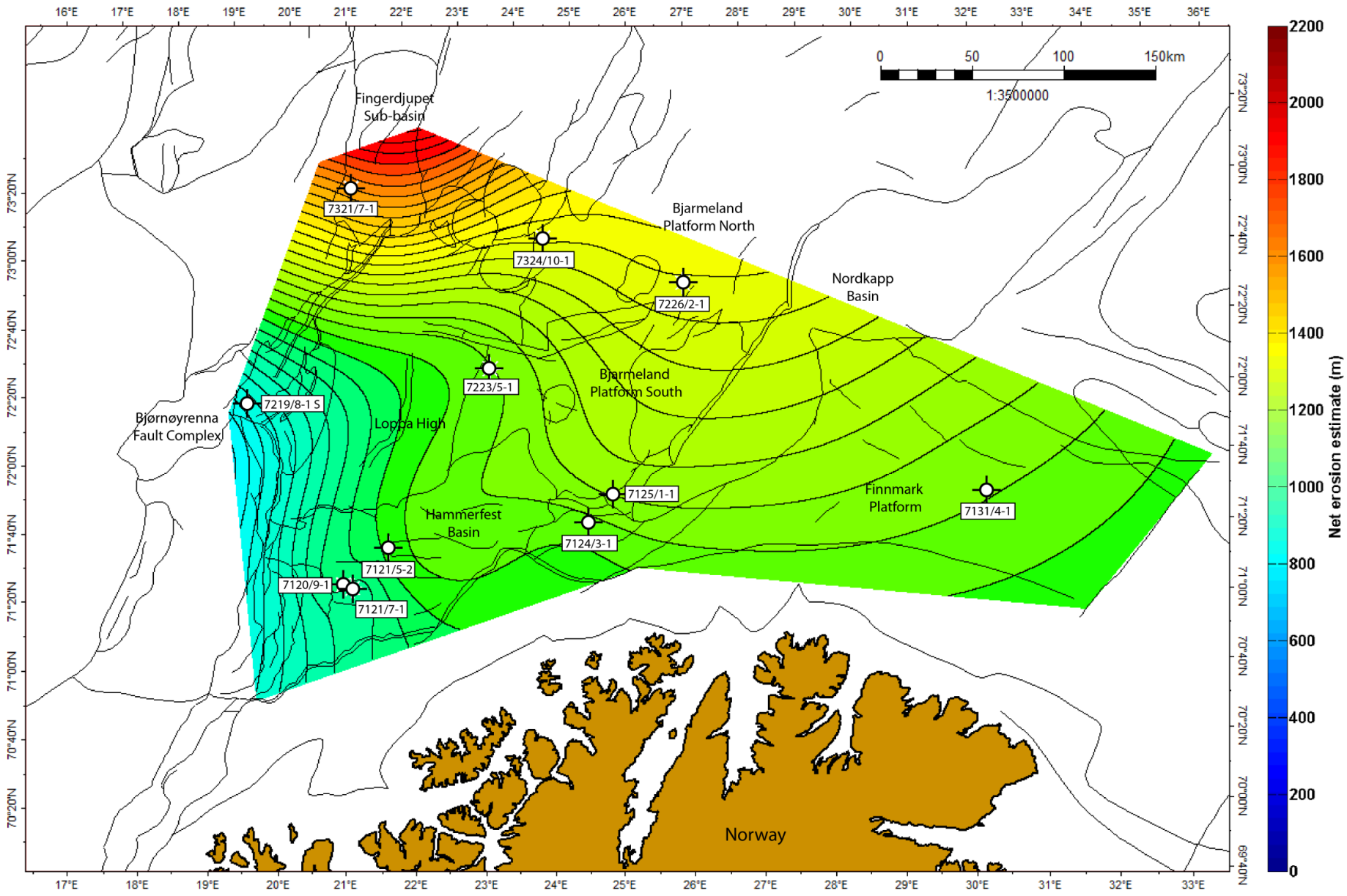

Figure 4.5. Net erosion map created with Petrel. A general trend of increasing net erosion to the north is observed and lower values of net erosion are observed in the west. Net erosion map has been extrapolated outside the extent of the data points. Data density and resolution are low.

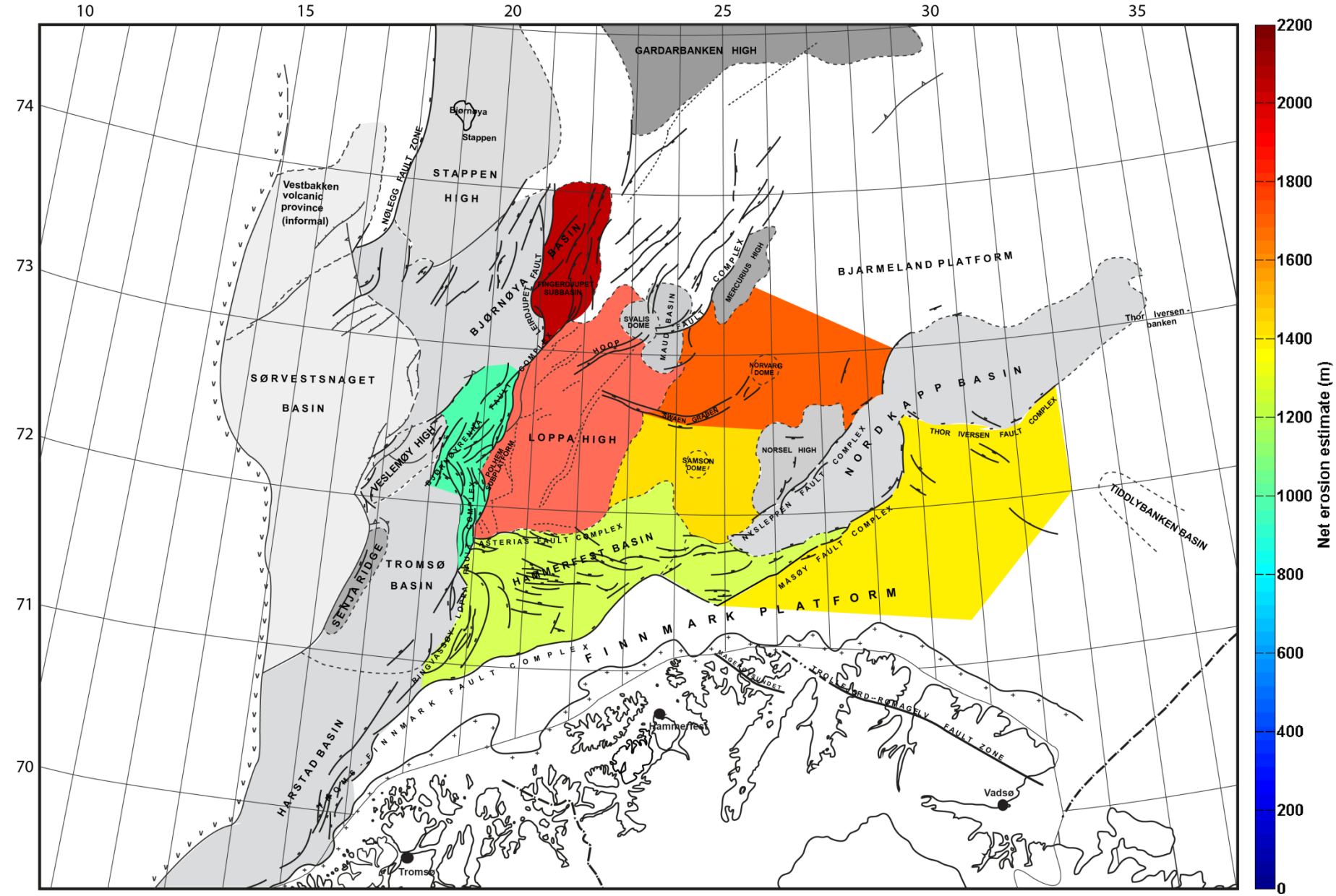

Figure 4.6. Net erosion averaged in different areas. The study area has been divided up into seven structural provinces based on structural features and net erosion estimates. Each of the provinces has been allocated an average value of the net erosion estimates calculated from sonic logs.

4.3. Interpretation and geological modelling of seismic super-tie lines

4.3.1. Regional lines

After estimating net erosion from sonic logs, three composite seismic lines were created to tie all intersecting wells together. Another line, MCG1102-025, was also selected to tie the three lines together. These four lines were interpreted in Petrel following the methodology stated in Chapter 3.

Information from well tops was used to assign an age to each of the seismic packages. Major erosional unconformities were highlighted and uplift estimates were added to each of the sections in their respective locations. Seismic facies have been labelled A-F and erosional unconformities annotated. These figures are displayed below, Figure 4.7 through to Figure 4.10.

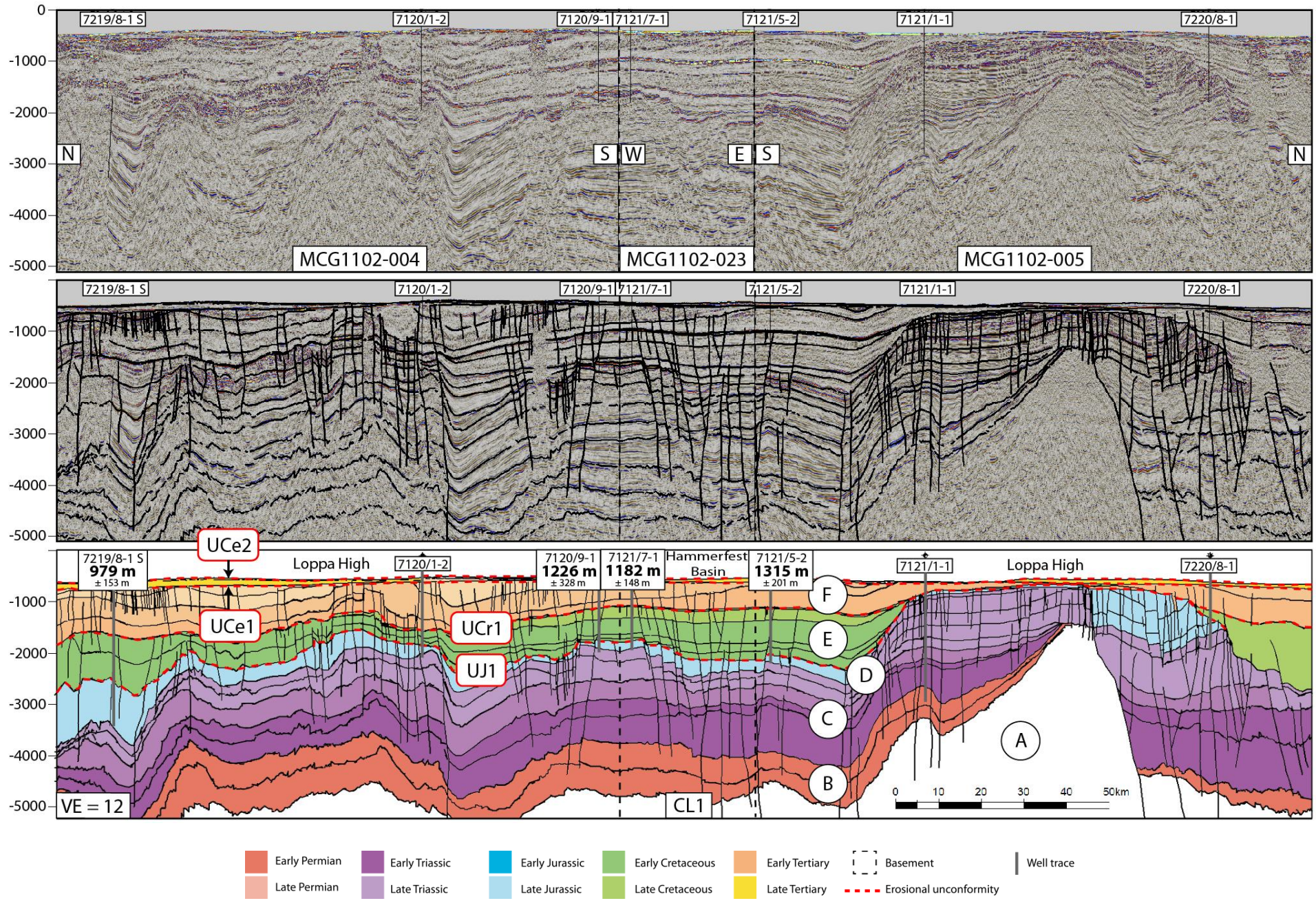

Figure 4.7. Interpretation and geological model of seismic line CL1. Refer to Figure 3.1 for line location. Y-axis is TWT in ms.

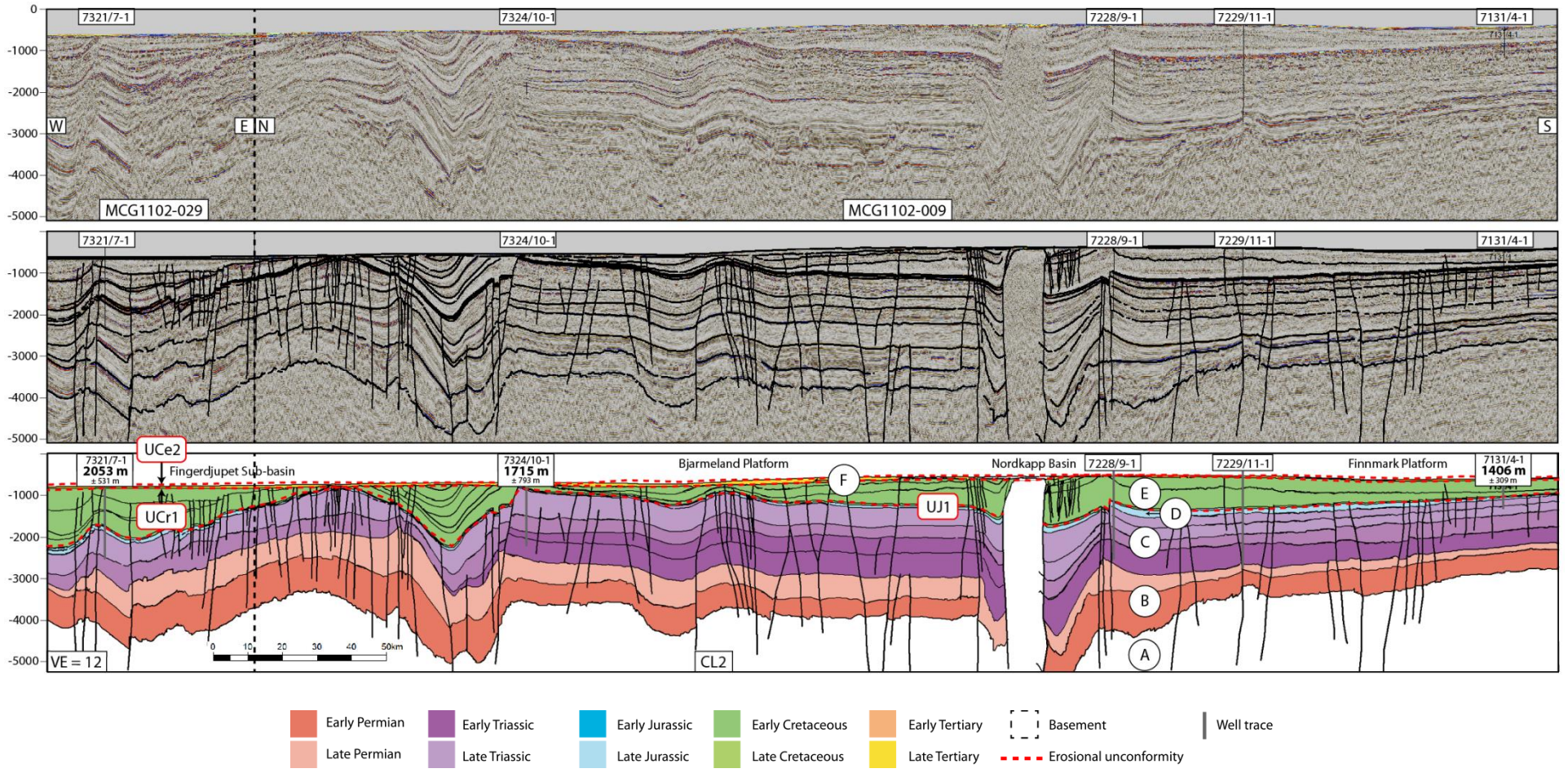

Figure 4.8. Interpretation and geological model of seismic line CL2. Refer to Figure 3.1 for line location. Y-axis is TWT in ms.

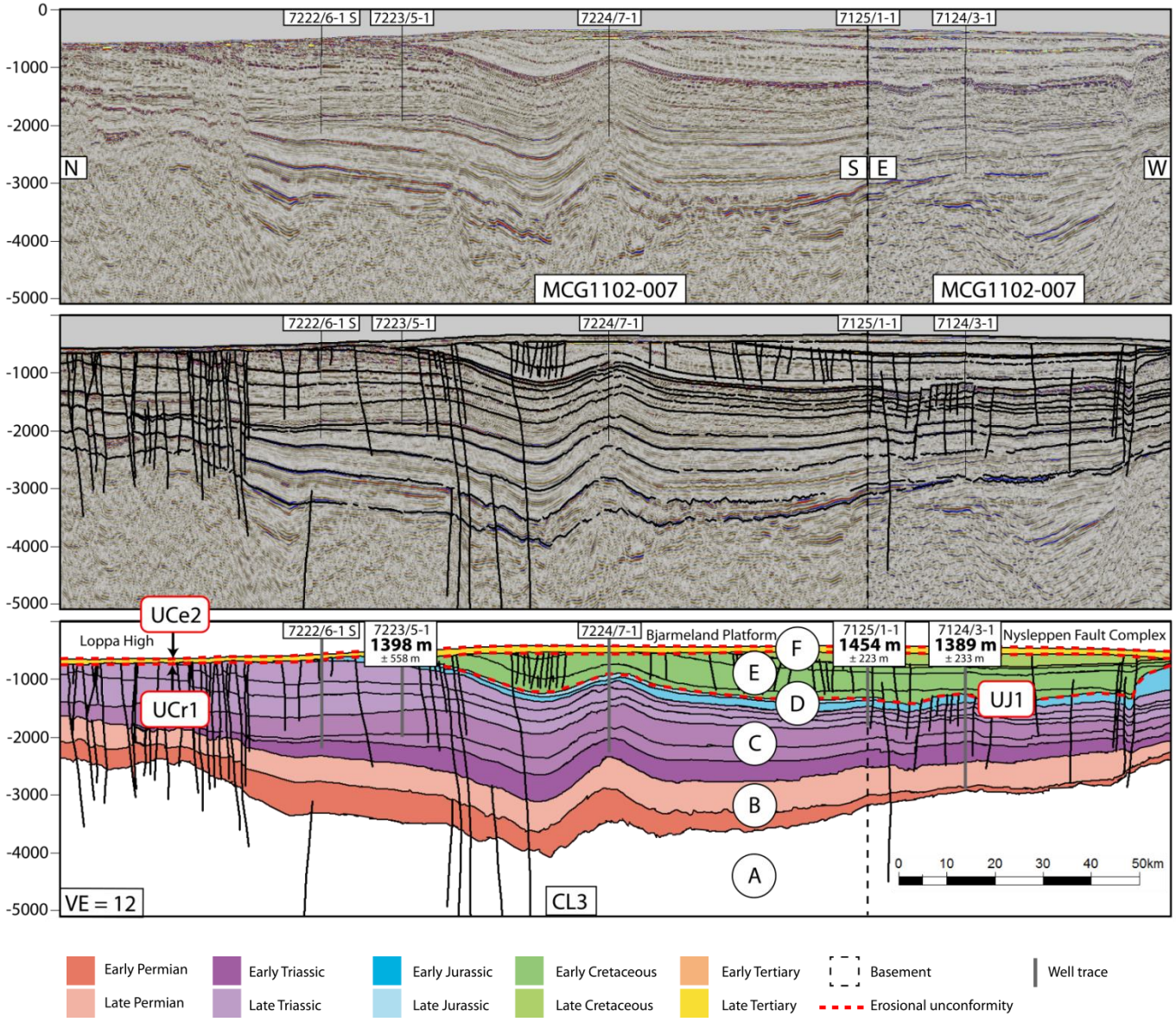

Figure 4.9. Interpretation and geological model of seismic line CL3. Refer to Figure 3.1 for line location. Y-axis is TWT in ms.

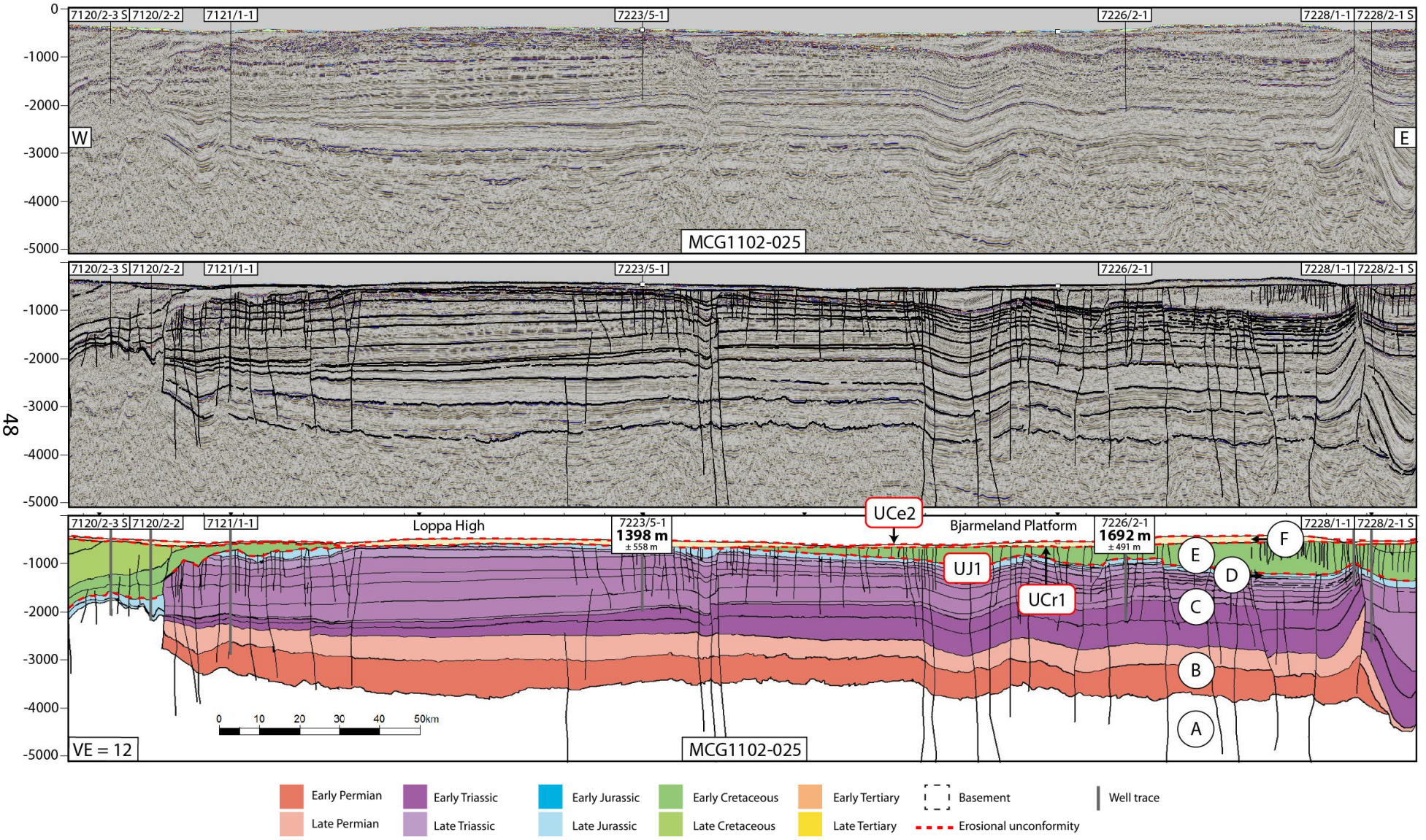

Figure 4.10. Interpretation and geological model of seismic line MCG1102-025. Refer to Figure 3.1 for line location. Y-axis is TWT in ms.

Chapter 5: Discussion of results

5.1. P-wave velocity variations from well logs

5.1.1. Data quality, estimates and assumptions

Net erosion estimates were calculated from P-wave velocity variations as described earlier. Well selection was more challenging than first expected, as many wells were unsuitable for analysis. Some sonic logs were incomplete, or the sonic log was started from a point below the formation of interest. Others contained poor gamma ray data, making the clay volume calculations unreliable. Many wells with significant net erosion had no Kolmule data as the formation had been entirely eroded away and some had short intervals of the Kolmule formation and data was too sparse.

As seen in Table 4.1, net erosion estimates range from 979 – 2053 m, with uncertainties ranging from ± 148 – 793 m. As the study area is quite large, it is not unexpected to find such variance between net erosion estimates. Net erosion estimates of wells in close proximity to one another are reliable and well within the calculated error. Wells 7120/9-1 and 7121/7-1 in the Hammerfest Basin have net erosion estimates of 1226 ± 328 m and 1182 ± 148 m respectively, with a separation distance of approximately 5 km. Another well lying in the Hammerfest Basin, well 7121/5-2, is estimated to have a net erosion of 1315 ± 201 m; also within the uncertainty range.

Three assumptions were made during well log analysis in order to simplify the process. Firstly, the assumed linear velocity-depth trend is not valid for longer or deeper well intervals. Areas which are severely uplifted and eroded are likely to have a different thermal history than areas that have experienced less uplift and erosion. Therefore it is likely that the chemical and mechanical compaction processes would have affected the areas differently, and a linear velocity-depth trend wouldn't be suitable. Secondly, properties of shales would vary significantly across the Barents Sea and North Sea. These have not been accounted for and homogeneous shales have been assumed for all Barents Sea and reference trend wells. Thirdly, thermal histories have been assumed to be the same across all areas of the Barents Sea and North Sea. Variations in thermal histories are likely to exist, which have not been accounted for.

5.1.2. Uncertainty

Uncertainty in the net erosion estimations has been attributed to several sources. Thermal history has been assumed to be the same for all regions, however due to the size of the study area, significant differences in thermal histories are likely to exist. Poor gamma ray data has led to challenges in choosing minimum and maximum gamma ray values for clay content calculations giving rise to uncertainties in clay volumes, such as the example from well 7321/7-1 shown in Figure 5.1.

Velocity data for the Kolmule formation appear to be a poor representation of the velocity-depth trend of the whole well in some cases, such as the example from well 7223/5-1 shown in Figure 5.2. In this example the Kolmule formation interval is very short, and the data points with calculated clay content greater than 80% produce a regression trend oblique to the reference trend, resulting in a large uncertainty. Although only Kolmule formations with a calculated clay volume greater than 80% were used to estimate net erosion, lateral differences in rock compositions are likely to exist which have not been accounted for.

Uncertainty values were generally low, however three wells had uncertainty values greater than ± 500 m. The uncertainty values calculated are likely overestimated, and could be lowered by calculating net erosion values in more wells in the vicinity of wells selected for this study. For the most part, interpretations of seismic sections agree with the net erosion estimates calculated.

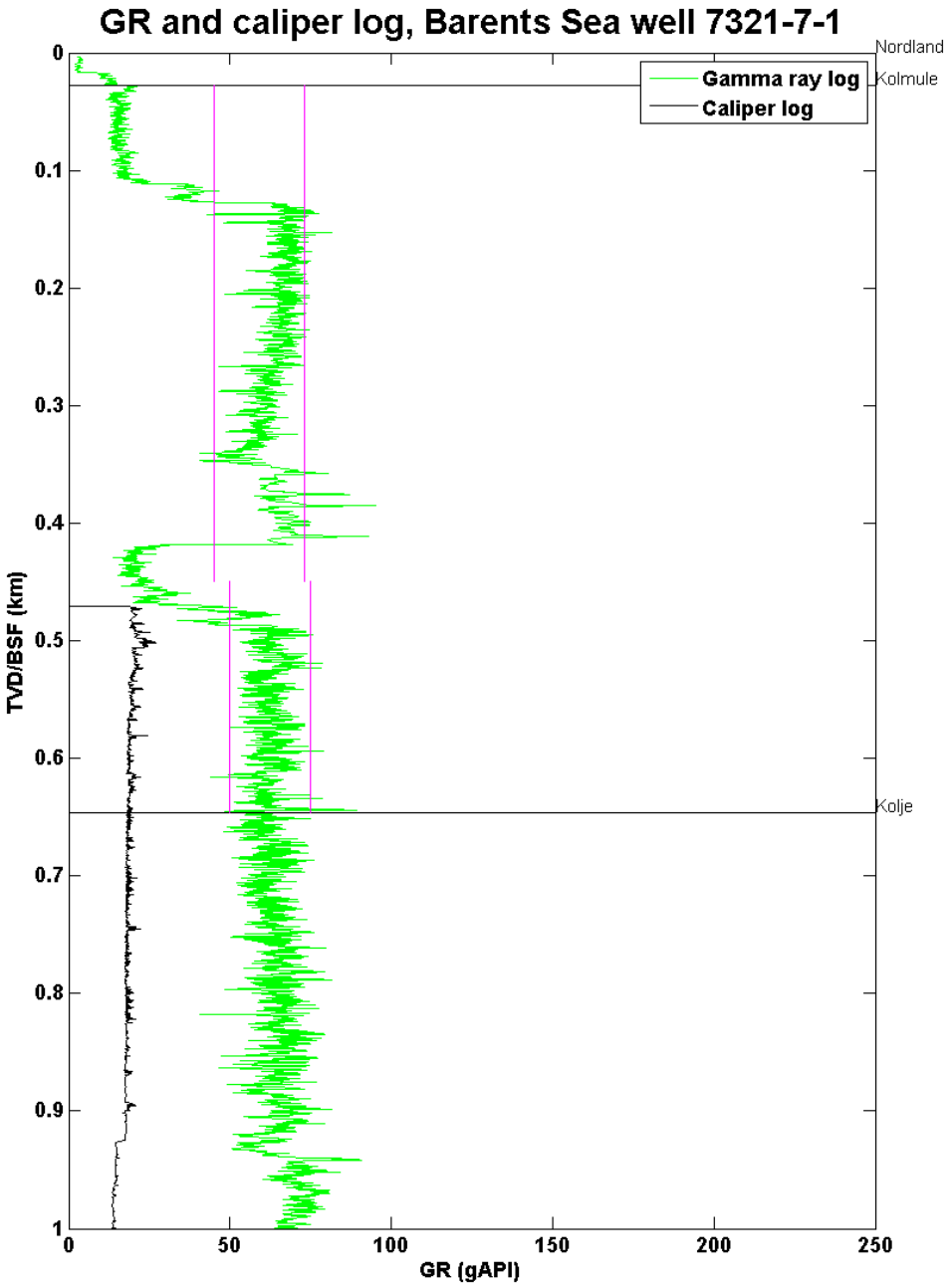

Figure 5.1. Example of poor gamma ray data. Calculation of clay content in this well has a high level of uncertainty and therefore net erosion estimations are not as accurate.

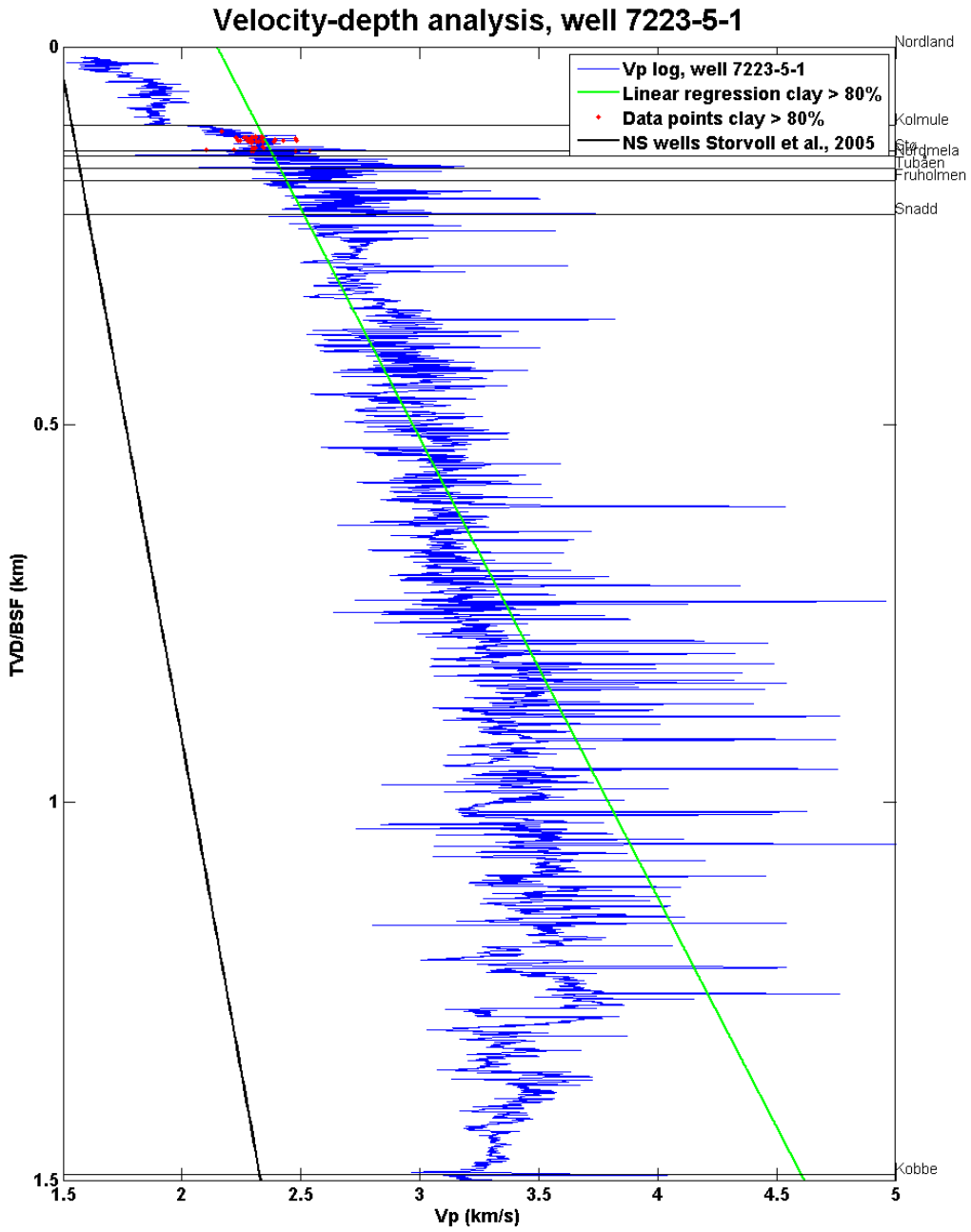

Figure 5.2. Example of poor velocity data. Regression trend calculated by using the entire well log with any clay content is expected to be a similar slope to the reference trend and with a greater uplift estimate.

5.2. Net erosion trends

Due to the low density of well data used in this study, total coverage was average; however the results were good and provided a good insight to the net erosion trends and local effects across the western Barents Sea.

A general trend of increasing net erosion towards the north and north east and decreasing net erosion to the west is observed in Figure 4.5. This surface has been created over a large area with few data points, and is useful just as a guide to the general trend of net erosion. It does not separate structural features and therefore local effects of highs and basins are not taken into account.

A second net erosion map was created after dividing the study area into seven separate structural provinces, Figure 4.6. These were divided up based on their structural properties and net erosion estimates. For example, the Bjarmeland Platform has been divided into two provinces – Bjarmeland Platform South and Bjarmeland Platform North. This is due to the large variation between net erosion estimates in the north and south. As there are no net erosion estimates for the Loppa High, estimates were made based on seismic sections and previous studies.

5.3. Net erosion estimates compared with seismic sections and interpretations

5.3.1. CL1

CL1 is a composite seismic line consisting of three seismic super-tie lines, Figure 4.7. The interpreted section in CL1 focuses on the Loppa High and Hammerfest Basin regions. Package A is interpreted as basement and packages B – F are interpreted as sedimentary packages deposited from Early Permian to Late Tertiary time.

The area in CL1 is highly faulted. A significantly large fault lies below the Loppa High in seismic line MCG1102-005, separating the Loppa High and Bjørnøyrenna Fault Complex. This is a normal fault where packages have been severely uplifted and consequentially eroded on the Loppa High side. The Hammerfest Basin area consists of thicker layers of Cretaceous and Tertiary sediments than most other regions in the western Barents Sea as a result of less erosion in this area, supported by the sonic log estimates.

The net erosion estimates along CL1 range from 979 m in the Bjørnøyrenna Fault Complex to 1315 m in the Hammerfest Basin. These estimates were calculated with relatively low uncertainty, and the close proximity of wells 7120/9-1, 7121/7-1 and 7121/5-2 with similar net erosion estimates suggest that the net erosion estimates are more consistent than the

uncertainties suggest. The Loppa High in the right hand side of the image is severely uplifted and eroded and net erosion is expected to be much higher for this part of the Loppa High than surrounding regions with less uplift. Net erosion in the Loppa High was estimated by interpretation of seismic data and literature review, discussed in section 5.4.3.

The red stippled line labelled UCe2 is interpreted as an erosional unconformity related to the widespread and severe Cenozoic uplift and erosion in the Barents Sea. This is discussed in detail in section 5.5.

5.3.2. CL2

CL2 is a composite seismic line consisting of two seismic super-tie lines, Figure 4.8. The interpreted section in CL2 focuses on the Fingerdjupet Sub-basin, Bjarmeland Platform, Nordkapp Basin and Finnmark Platform. Package A is interpreted as basement and packages B – F are interpreted as sedimentary packages deposited from Early Permian to Late Tertiary time.

The area shown in CL2 is a very long section where packages B – F are mostly gently dipping, uniform thickness beds with normal faulting. A large subsided block between the Fingerdjupet Sub-basin and Bjarmeland Platform is filled with more Cretaceous sediments than the rest of the section. Cretaceous sediments to the south are thickest in the Nordkapp Basin, and thin to the north and south into the Finnmark Platform and Bjarmeland Platform regions. Tertiary sediments, shown by package F, are very thin to non-existent throughout the whole of CL2.

Net erosion estimates range from 1406 m in the Finnmark Platform, 1715 m in the north of the Bjameland Platform and 2053 m in the Fingerdjupet Sub-basin. As the Cretaceous sediments are much closer to the sea floor than in CL1, these results are expected. However, the value of 2053 m from well 7321/7-1 has a high uncertainty of ± 531 m and appears to be less uplifted and eroded than the other two areas where erosion values are lower. This suggests that the net erosion estimate in this well is inaccurate and more wells in this area should be analysed and processed for erosion estimates.

The red stippled line labelled UCe2 is interpreted as an erosional unconformity related to the widespread and severe Cenzoic uplift and erosion in the Barents Sea. This is discussed in detail in section 5.5.

5.3.3. CL3

CL3 is a composite seismic line consisting of two seismic super-tie lines, Figure 4.9. The interpreted section in CL3 focuses on the Loppa High in the north, the Bjarmeland Platform and the Nysleppen Fault Complex in the south. Package A is interpreted as basement and packages B – F are interpreted as sedimentary packages deposited from Early Permian to Late Tertiary time.

The sedimentary packages are highly faulted and elevated in the northern area (Loppa High) and continue dipping downwards gently to the south. The Early – Late Permian sediments thin towards the south and continue thinning to the west as the line changes direction. Cretaceous sediments in the Loppa High area are completely eroded away, and appear on the margin between the Loppa High and Bjarmeland Platform and continue to thicken to up to the Nysleppen Fault Complex.

Wells 7125/1-1 and 7124/3-1 are in close proximity to each other, appear to be in similar structural settings and yield similar net erosion results of 1454 m and 1389 m, respectively. For this reason, uncertainty for these wells could be considered to be lower than the values calculated. Well 7223/5-1 is calculated to have been eroded 1398 ± 558 m. Due to this area being elevated considerably more than the other two wells on this line, it is expected to have experienced significantly greater erosional effects. This value has been calculated with a high uncertainty, due to the short interval of the Kolmule formation in the well. Therefore, the net erosion value is likely to be higher than calculated and more wells in this vicinity are suggested to be analysed to confirm this.

5.3.4. MCG1102-025

MCG1102-025 is a seismic super-tie line intersecting CL1, CL2 and CL3 and two wells with net erosion estimates. The interpreted seismic section focuses on the Loppa High in the west

and the Bjarmeland Platform in the east. The eastern most part of the Tromsø Basin is visible to the western extent of the section. Package A is interpreted as basement and packages B – F are interpreted as sedimentary packages from Early Permian to Late Tertiary Time.

The sedimentary packages B – D are dipping gradually to the east, with the Early Permian sediments thinning to the west and the Late Permian sediments thinning to the east. A large fault is observed in the easternmost part of the section. Cretaceous sediments are thinning due to erosion from east to west, and have been completely eroded away across the Loppa High.

The red stippled line labelled UCe2 is interpreted as an erosional unconformity related to the widespread and severe Cenzoic uplift and erosion in the Barents Sea. This is discussed in detail in section 5.5.

5.4. Examples of uplift and erosion in various regions

One example from seismic data of each of the seven mentioned structural provinces has been selected for more detailed interpretation on a local scale; example locations shown in Figure 5.3. This was to provide more detailed and higher resolution images of areas which have experienced both local and regional uplift and erosion.

Six examples SE1 – SE6 have been selected to illustrate and interpret the seismic signatures and effects of uplift and erosion, Figure 5.4 to Figure 5.10. These are zoomed-in sections from the MCG seismic super-tie lines. Each of the images is displayed in three panels; the top panel shows a clean, uninterpreted seismic section, the middle panel shows the seismic section with interpretations of faults, horizons and important structural features, the bottom panel shows a geological model constructed from the interpreted section.

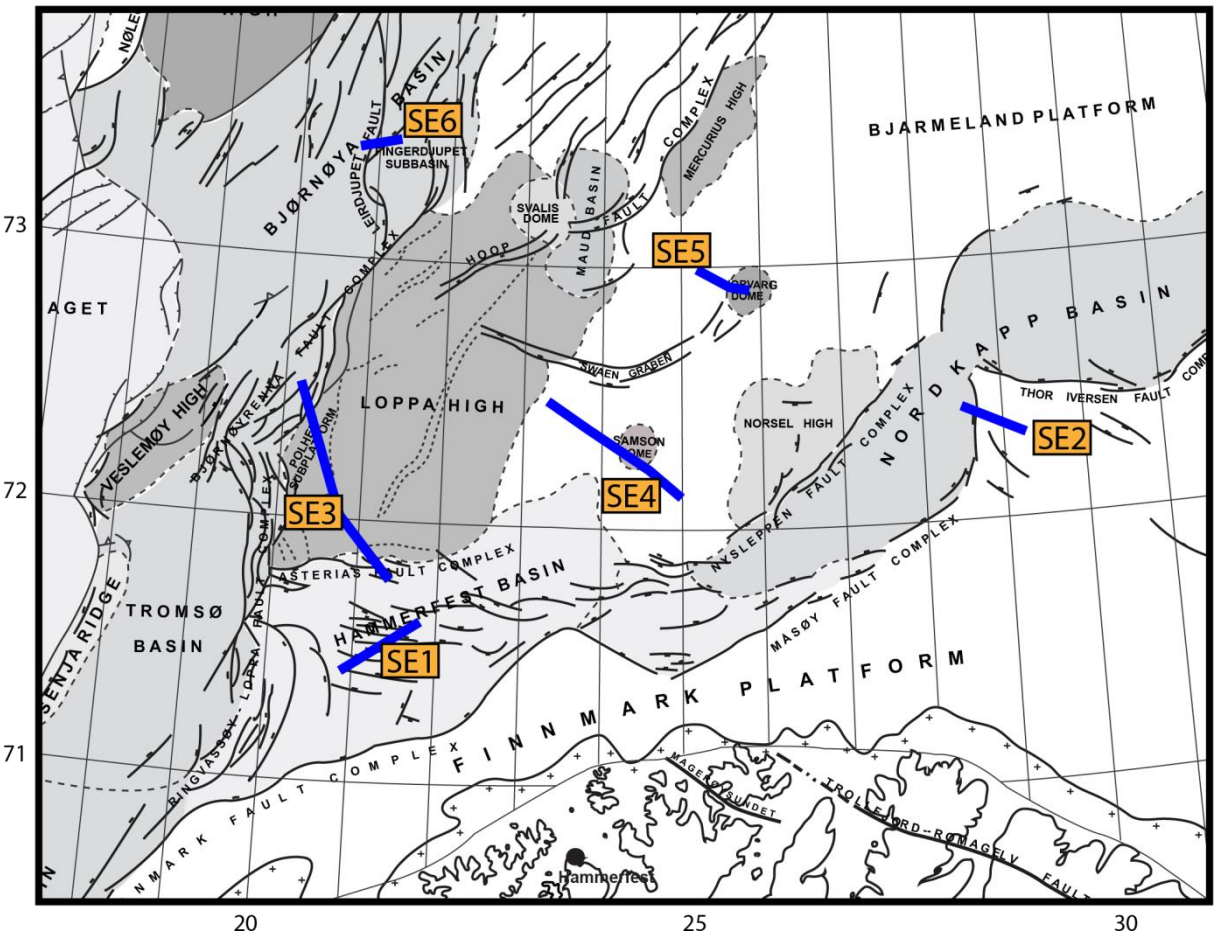

Figure 5.3. Approximate locations of seismic sections SE1 – SE6 selected for further interpretation, shown by blue lines and annotated. Major structures are marked and annotated. Modified from NPD (year unknown).

5.4.1. Hammerfest Basin

A section from MCG1102-023 has been selected, SE1, for interpretation of uplift and erosion evidence, Figure 5.4.

The Hammerfest Basin is a relatively shallow basin which may be divided into a western and eastern sub-basin, separated by the extension of the Trollfjord-Komagelv fault trend (Gabrielsen et al., 1990). Net erosion estimates have been calculated for three wells in the Hammerfest Basin region; 7120/9-1, 7121/7-1 and 7121/5-2, producing an average net erosion value of 1241 m. The uncertainty values calculated in this region are relatively low as gamma ray and P-wave velocity data quality in these wells is good.

Package D is highly faulted, with a few of these faults being reactivated after the deposition of package E. To the west, uplift is interpreted to have occurred from the faulting of package

D, shown by the white arrows. This extensional faulting could have caused the footwall blocks to be uplifted relative to the hanging wall blocks. This has likely been the cause for the thinning of package E in the western direction. This local uplift is interpreted to be caused by a rift flank uplift mechanism following extension during the development of the Hammerfest Basin.

Package F consists of Early – Late Tertiary sediments. These have been deposited onto the erosional unconformity UCr1. The geometry of the Early Tertiary sediments suggests that they are likely to have been deposited from east to west. Package F is relatively thick in the Hammerfest Basin when compared to other regions. This is supported by the net erosion estimates being lower in this region than in others. UCe1 marks the erosional unconformity between the Early and Late Tertiary sediments. The erosional surface truncates the oblique horizons of the Early Tertiary sediments, highlighted by the blue ellipse.

The Late Tertiary sediments in package F are very thin. This is likely due to the regional Cenozoic uplift and erosion that has taken place in the Barents Sea, discussed in section 5.5.

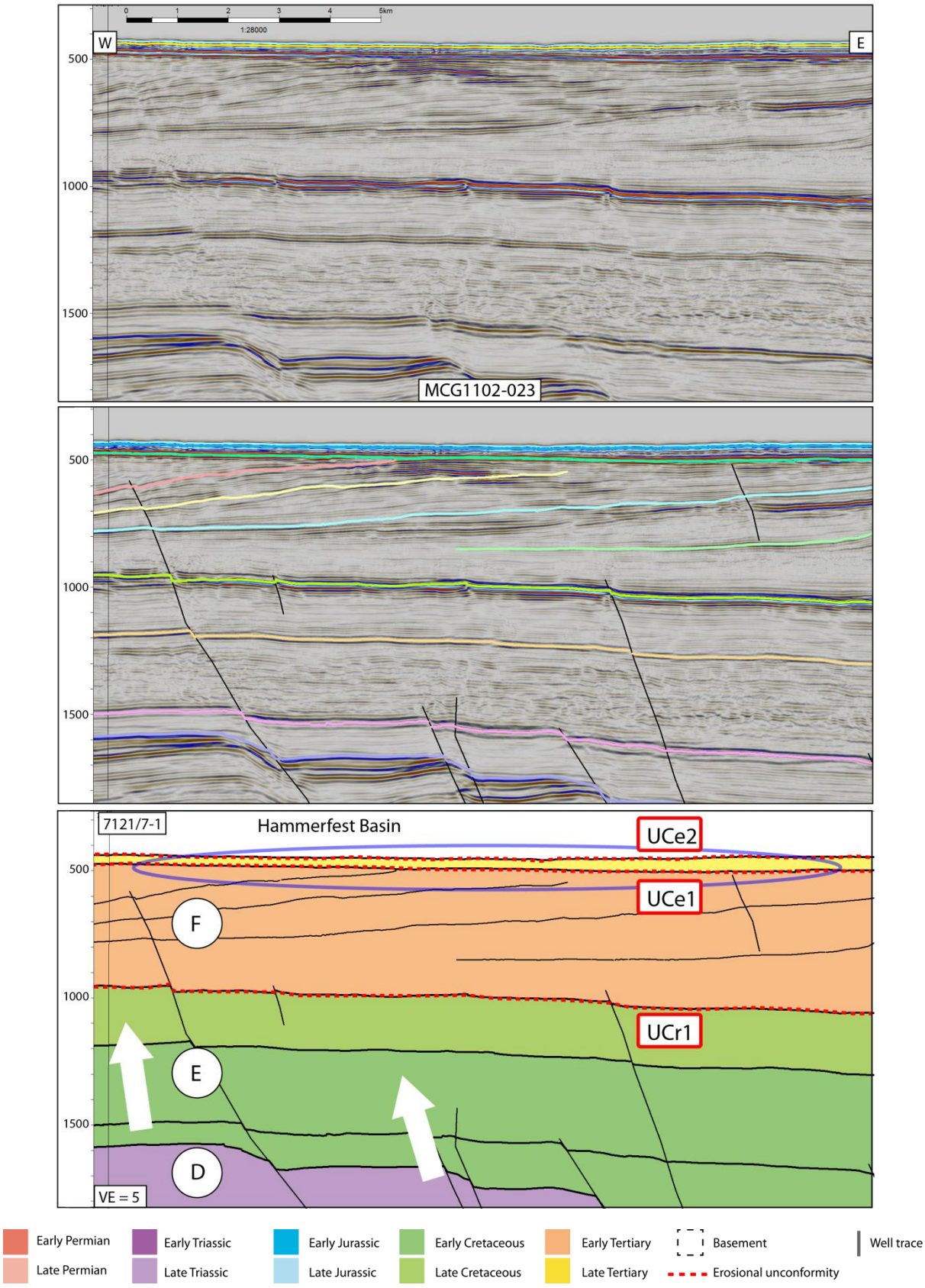

Figure 5.4. Interpreted section SE1 from seismic line MCG1102-023. Packages, structural features, erosional unconformities and movement directions are highlighted and annotated. Y-axis is in TWT (ms) and the vertical exaggeration is 5. Refer to Figure 5.3 for location.

5.4.2. Finnmark Platform

A section from seismic line MCG1102-009 has been selected, SE2, for interpretation of uplift and erosion evidence, Figure 5.5.

The Finnmark Platform is a large platform region bound to the south by mainland Norway and to the north by the Nordkapp Basin and Hammerfest Basin. One well in the Finnmark Platform, 7131/4-1, has been selected for P-wave velocity analysis, with net erosion estimated to be 1406 m. Data quality for this well is good, and a long Kolmule interval of approximately 400 m has produced a reliable trend with an uncertainty of 209 m.

On this line a fault system has developed following the deposition of the Jurassic sediments in package D. The fault system occurs on the margin separating the Finnmark Platform and Nordkapp Basin. The faulting is likely due to extension and footwall uplift is interpreted as the mechanism causing the local uplift.

Following the faulting of packages C and D, deposition of Cretaceous sediments began, package E. The small scale faulting observed above the fault system suggests movement in the fault system continued following the deposition of package E. This has led to doming uplift of package E to the western side of the section. This is indicated by the large white arrow. Erosion of this locally uplifted area is greater than the surrounding Cretaceous sediments that lie relatively lower.

ECr1, indicated by the stippled red line, marks the erosional unconformity between Cretaceous and Tertiary sediments. The seismic horizons to the west and east of the uplifted dome are truncated by this unconformity, suggesting erosion took place after the deposition and uplifting of the Cretaceous sediments in package E.

The erosion was followed by deposition of Tertiary sediments in package F. The package is of uniform thickness and very thin. The stippled red line marked as UCe2 is interpreted as an erosional unconformity due to uplift and erosion caused by a regional uplift mechanism, discussed in section 5.5.

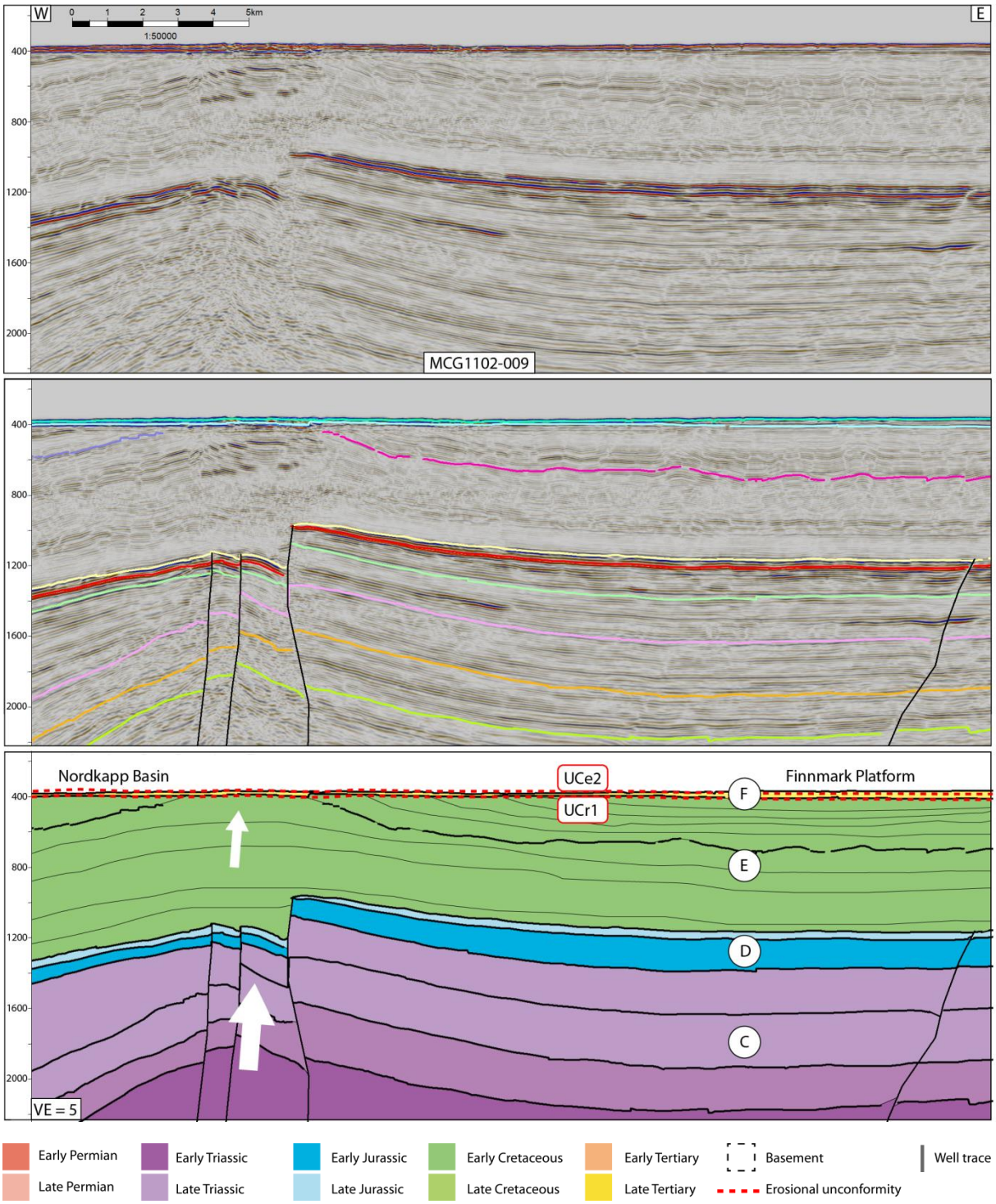

Figure 5.5. Interpreted section SE2 from seismic line MCG1102-009. Packages, structural features, erosional unconformities and movement directions are highlighted and annotated. Y-axis is in TWT (ms) and the vertical exaggeration is 5. Refer to Figure 5.3 for location.

5.4.3. Loppa High

A section from seismic line MCG1102-005 has been selected, SE3, for interpretation of uplift and erosion evidence, Figure 5.7.

The Loppa High is situated north of the Hammerfest Basin and southeast of the Bjørnøya Basin. It consists of an eastern platform and a crestal western and northwestern margin (Gabrielsen et al., 1990). No wells were suitable for net erosion estimations on the Loppa High due to the lack of Kolmule formation sediments.

Uplift for the Loppa High has been estimated from horizon depth analysis in seismic line MCG1102-005. The method is illustrated in Figure 5.6. A common and reliable reflector separating Middle and Late Triassic sediments was selected to measure the difference between the Hammerfest Basin and Loppa High. Well 7121/5-1 in the Hammerfest basin has been estimated to have been eroded 1315 m net. The same reflector is elevated approximately 500 ms TWT in the Loppa High. Using an approximate velocity of 2500 m/s from the sonic log in well 7121/1-1, a difference in elevation is calculated to be approximately 300 m, giving the Loppa High a net erosion estimate of approximately 1800 - 2000 m.

On this line a large normal fault can be seen which has resulted in the basement coming quite close to the sea bottom, highlighted by the black arrow. This has pushed all the sedimentary layers up, and extreme local uplift and erosion has taken place. The major pulse of this local uplift likely followed the deposition of Late Triassic sediments. Several more pulses are likely to have followed as the thinning of Jurassic and Cretaceous sediments from south to north suggests. The local uplift and erosion observed in the Loppa High is likely to have been due to a combination of initial rift flank uplift during the formation of the Barents Sea, followed by tectonism.

Early Tertiary sediments are seen to this from south to north on the Loppa High, suggesting another later pulse. The stippled red line labelled UCe2 is an erosional unconformity due to regional uplift and erosion, discussed in section 5.5.

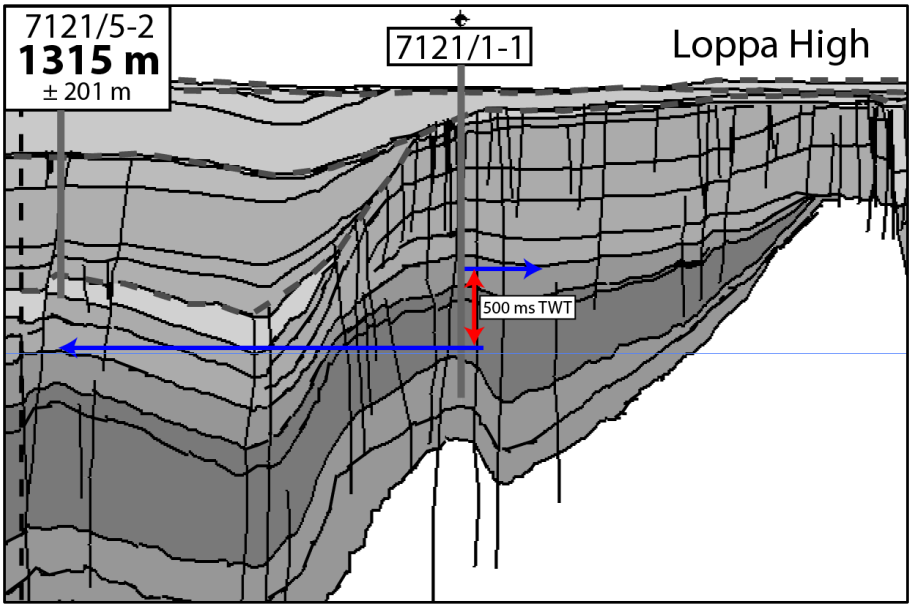

Figure 5.6. Estimating net erosion by measuring the vertical difference between similar horizons. Horizon selected is the boundary between Middle and Late Triassic sediments, change in depth highlighted by the blue and red lines.

5.4.4. Bjørnøyrenna Fault Complex

A section from seismic line MCG1102-005 has been selected, SE3, for interpretation of uplift and erosion evidence, Figure 5.7.

The Bjørnøyrenna Fault Complex defines the boundary between the Loppa High and the Bjørnøya Basin. One well in this region, 7219/8-1 S, has been used to estimate net erosion, yielding a value of 979 ± 153 m.

On this line packages B, C and D form highly faulted blocks of slightly increasing thickness to the north. These are normal faults likely due to extensional movement during the development of the Loppa High. The Cretaceous unit labelled package E is thinning from north to south, suggesting uplift due to the development of the Loppa High occurred during the time of deposition.

The thinning of Tertiary packages from north to south suggests another pulse of local uplift related to the development of the Loppa High occurred during their deposition. The red stippled line labelled UCe2 is interpreted as the erosional unconformity related to the regional Cenozoic uplift and erosion, discussed in section 5.5.

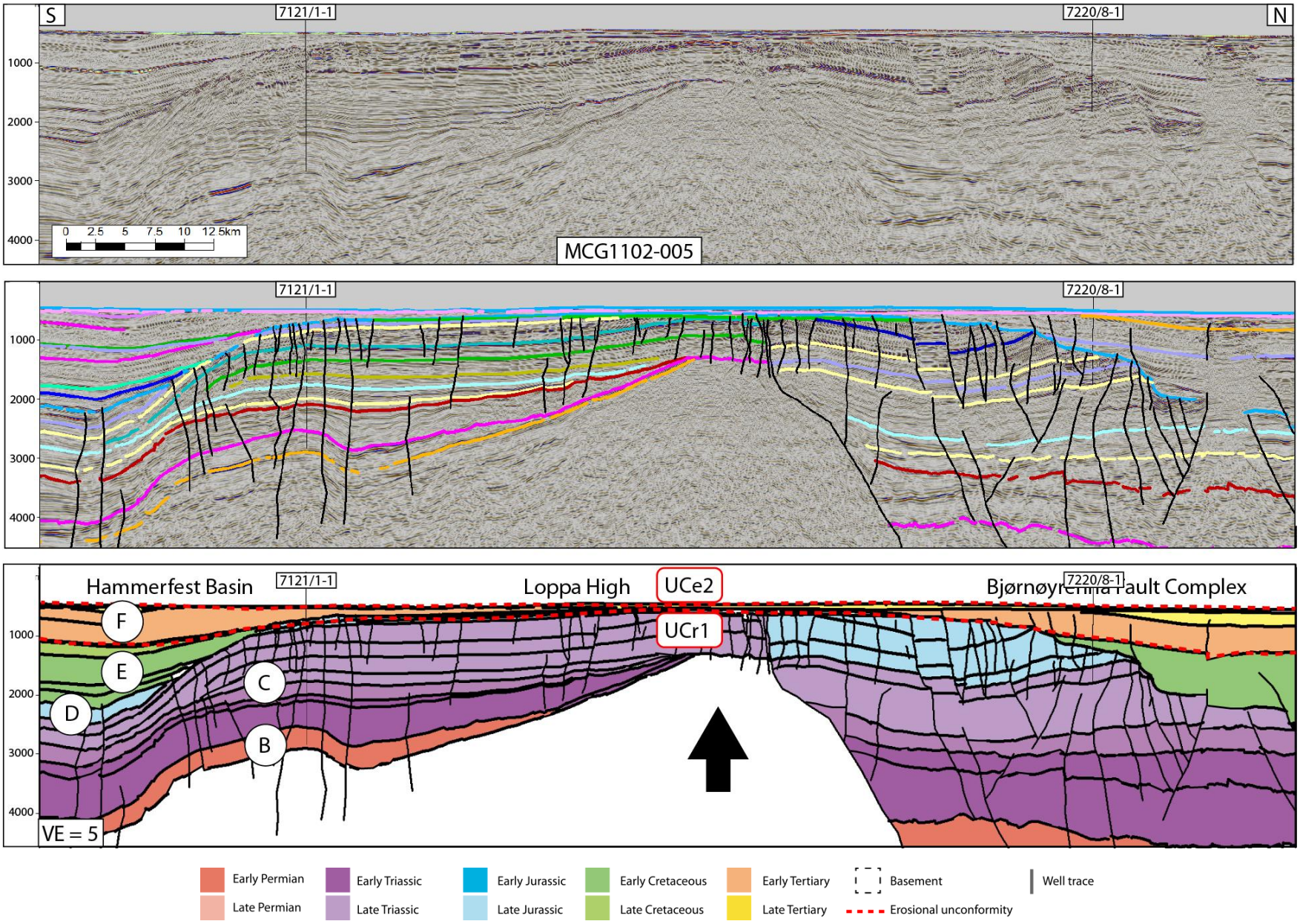

Figure 5.7. Interpreted section SE3 from seismic line MCG1102-005. Packages, structural features, erosional unconformities and movement directions are highlighted and annotated. Y-axis is in TWT (ms) and the vertical exaggeration is 5. Refer to Figure 5.3 for location.

5.4.5. Bjarmeland Platform South

A section from seismic line MCG1102-007 has been selected, SE4, for interpretation of uplift and erosion evidence, Figure 5.8.

The southern part of the Bjarmeland Platform represents the stable area between the Loppa High to the north east, the Hammerfest Basin to the south and the Nordkapp basin to the south east. Two wells from the Bjarmeland Platform, 7223/5-1 and 7125/1-1, and one well from the neighbouring Nysleppen Fault Complex, 7124/3-1, have been used to estimate net erosion in the southern part of the Bjarmeland Platform, producing an average net erosion value of 1413 m.

Uniform strata form packages B – E, creating a gentle upward slope of layers in the northwest direction, into the Loppa High. This movement has likely occurred after Cretaceous time, suggested by the erosional unconformity UCr1 truncating the tilted layers of Cretaceous sediments.

The locally uplifted area in the middle of the section is the Samson Dome, shown by the white arrow. The formation of this has led to greater erosional effects on the uplifted Cretaceous sediments in package E. Erosional truncations of this package are highlighted by the blue ellipse. The Samson Dome is interpreted as having been formed due to salt tectonics, activated by local compressional forces.

The red stippled line labelled UCe2 indicates the erosional unconformity caused by the regional Cenozoic uplift and erosion of the Barents Sea, discussed in section 5.5.

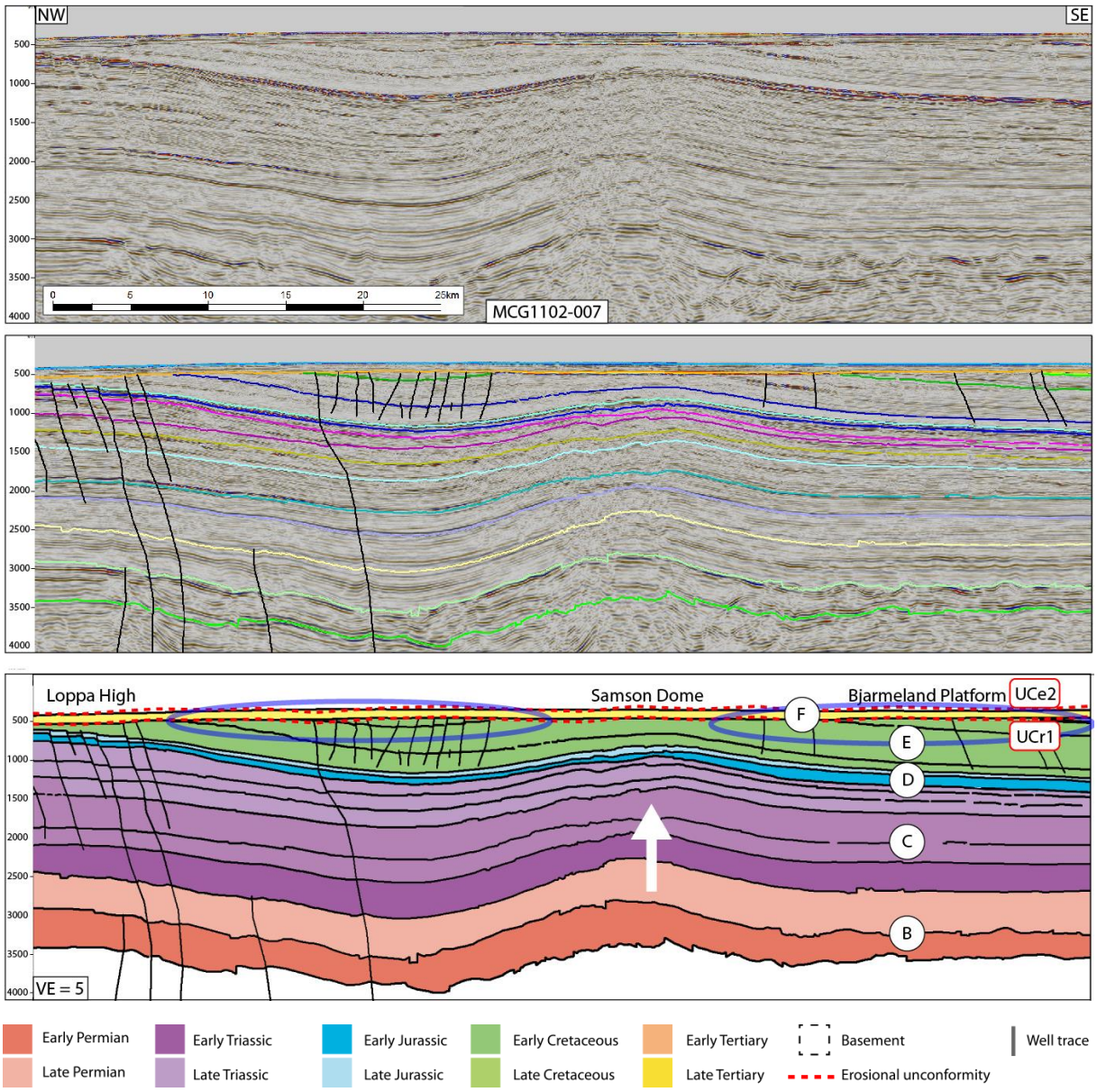

Figure 5.8. Interpreted section SE4 from seismic line MCG1102-007. Packages, structural features, erosional unconformities and movement directions are highlighted and annotated. Y-axis is in TWT (ms) and the vertical exaggeration is 5. Refer to Figure 5.3 for location.

5.4.6. Bjarmeland Platform North

A section from seismic line MCG1102-007 has been selected, SE5, for interpretation of uplift and erosion evidence, Figure 5.9.

The northern part of the Bjarmeland Platform represents the stable area between the Loppa High to the west and the Nordkapp Basin to the south east. Two wells from the northern

part of the Bjarmeland Platform have been used to estimate net erosion, producing an average net erosion value of 1703 m.

Packages C – E have uniform thickness and are locally uplifted in the east forming the Norvarg Dome. A radial fault pattern forms the faulted structures that are observed in packages C and D, likely to have formed during the development of the Norvarg Dome. Local uplift is observed in this dome area, with even smaller scale uplift being observed in the uplifted fault blocks. The development of the Norvarg Dome is interpreted to have been caused by salt tectonics activated by extensional forces.

Erosional truncations are observed on erosional unconformity UCr1, highlighted by the blue ellipse. A thin layer of Late Tertiary sediments is bound by UCr1 below and UCe2 above. UCe2 is interpreted as the erosional unconformity related to the regional uplift and erosion of the Barents Sea, discussed in section 5.5.

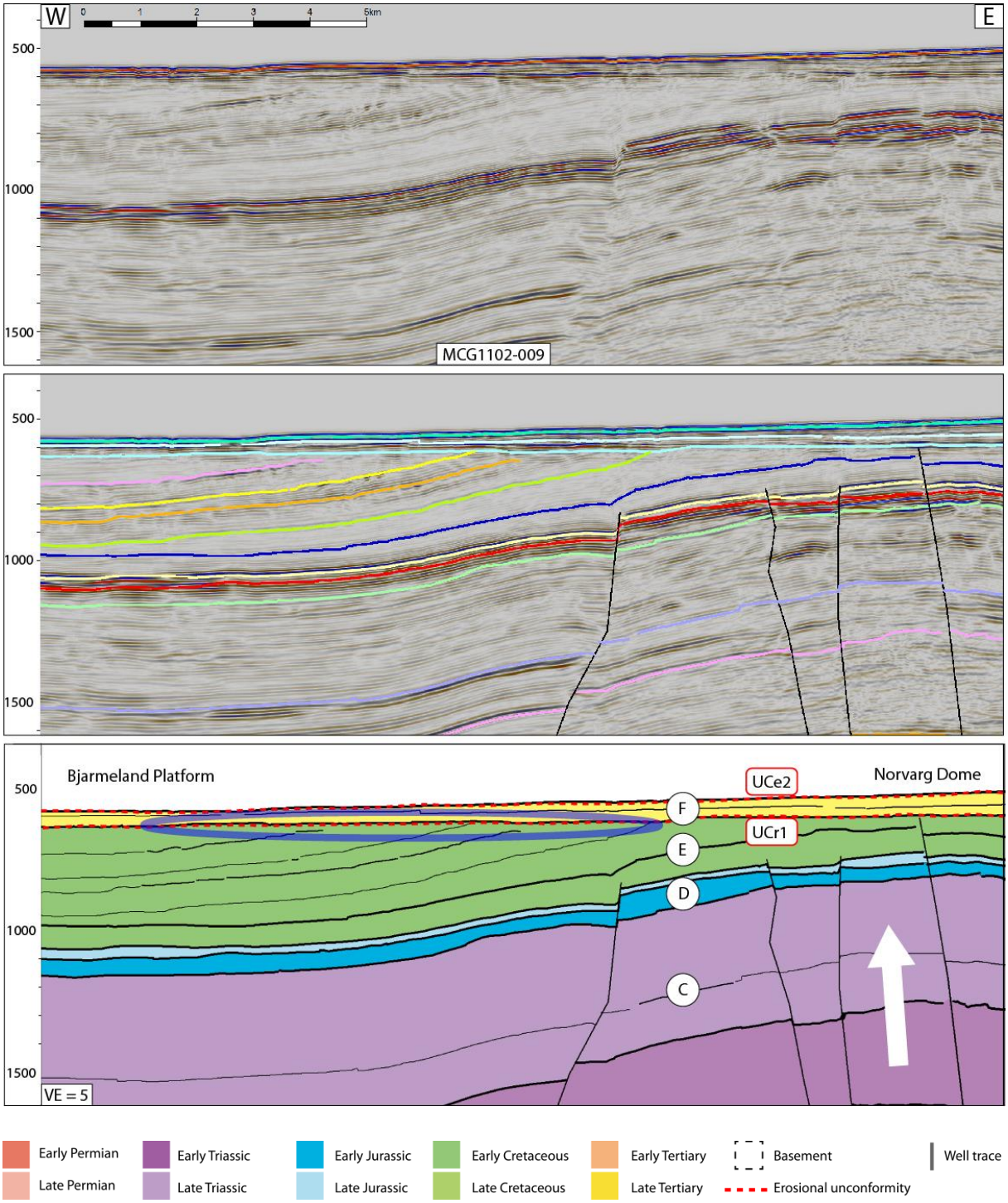

Figure 5.9. Interpreted section SE5 from seismic line MCG1102-009. Packages, structural features, erosional unconformities and movement directions are highlighted and annotated. Y-axis is in TWT (ms) and the vertical exaggeration is 5. Refer to Figure 5.3 for location.

5.4.7. Fingerdjupet Sub-basin

A section from seismic line MCG1102-029 has been selected, SE6, for interpretation of uplift and erosion evidence, Figure 5.10.

The Fingerdjupet Sub-basin is a shallow, north easterly part of the Bjørnøya Basin. It is bound to the south by the Loppa High and to the east by the Bjarmeland Platform. One well in this area has been selected for analysis, well 7321/7-1, with net erosion calculated to be 2053 m. Data quality for this well is average, and uncertainty in this value is high.

The example shows packages C – E as uniform thickness strata, rising up in the middle on the margin between the Fingerdjupet Sub-basin and the Bjørnøya Basin, indicated by the black arrow. This local uplift and erosion is likely to have occurred after the deposition of Cretaceous sediments in package E. This movement has given rise to the radial fault pattern in the middle of the section. Erosional truncations highlighted by the blue ellipses on either side of the uplifted zone form the erosional unconformity, UCr1. This is interpreted as uplift in two stages; the first caused by basin margin uplift due to an isostatic response to extensional forces, followed by inversion in response to compressional forces, the latter is highlighted by the stippled white ellipse.

A thin layer of Tertiary sediments lies on top of UCr1 and is bound by erosional unconformity UCe2. This is likely related to the regional Cenozoic uplift and erosion observed across most of the Barents Sea, discussed in section 5.5.

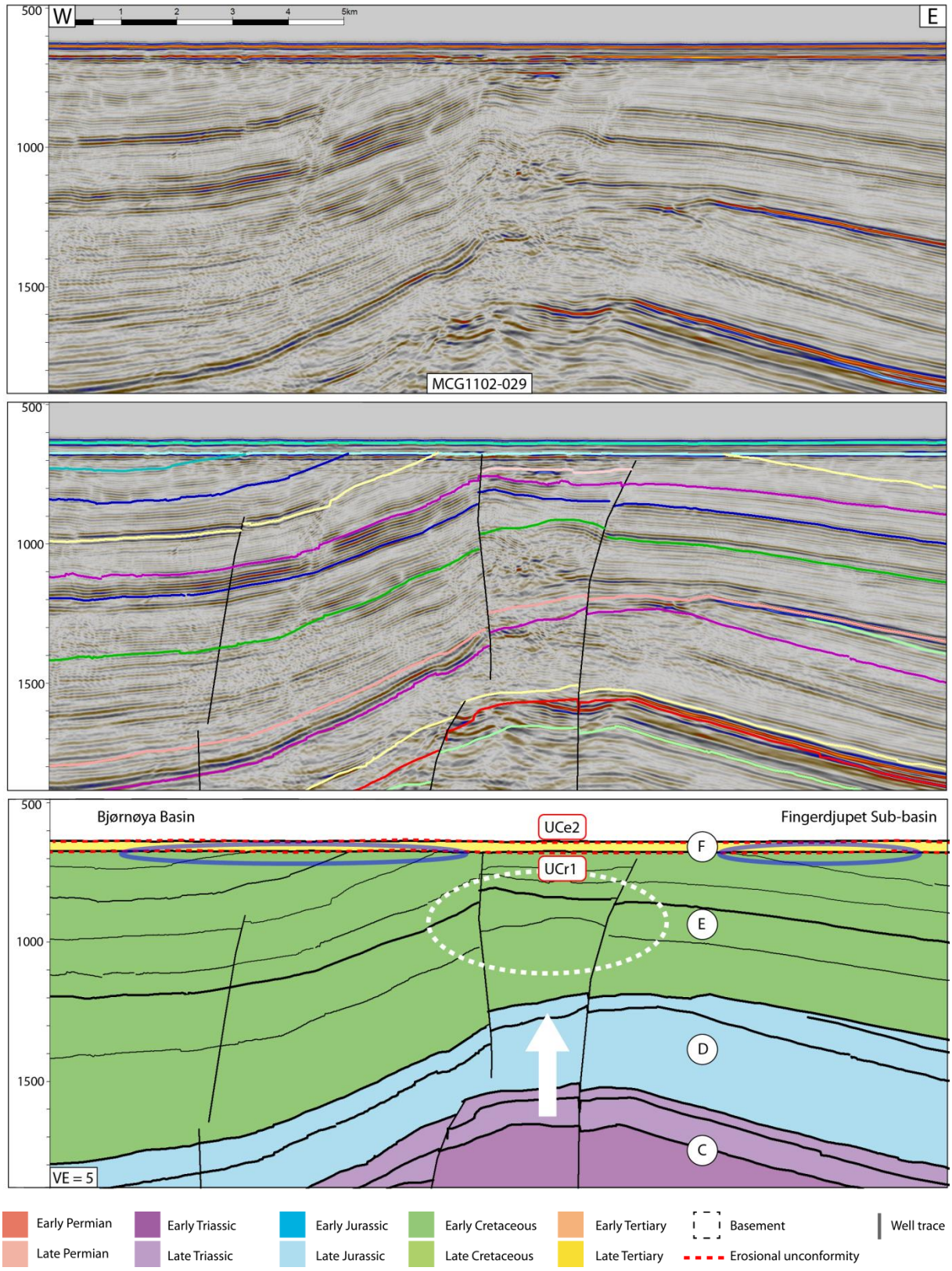

Figure 5.10. Interpreted section SE6 from seismic line MCG1102-029. Packages, structural features, erosional unconformities and movement directions are highlighted and annotated. Y-axis is in TWT (ms) and the vertical exaggeration is 5. Refer to Figure 5.3 for location.

5.5. Regional uplift and erosion mechanisms in the Barents Sea

The first model of uplift and erosion in the Barents Sea was formulated by Nansen (1904). This model showed the Barents Sea had experienced Tertiary uplift of approximately 500 m. Since then, several studies have been conducted to quantify the magnitude and explain the cause(s) of the extensive uplift and erosion observed in the western Barents Sea (Dimakis et al., 1998).

Glacial erosion and subsequent isostatic rebound has been suggested as the mechanism causing uplift and erosion, however a study by Dimakis et al. (1998), suggests that glacial erosion and isostatic uplift alone only account for one-half to two-thirds of the total erosion observed here. A thermal mechanism is suggested as the cause of the uplift and erosion to constitute the remainder of erosional effects as it is capable of explaining uplift over an area as large as the Barents Sea.

A study conducted by Riis and Fjeldskaar (1992) suggests that the uplift observed in the Barents Sea is related to two events: (1) mountain building in Central South Norway and along the trend Lofoten-Bjørnøya-Svalbard due to Palaeocene to Oligocene tectonic phases; and (2) glaciation in the Late Pliocene and Pleistocene, also related to plateau uplift of large areas. Their study results suggest that the compensating isostatic uplift accounts for approximately 70% of total erosion, and therefore another mechanism must be the cause. A migration of phase boundaries in the lithosphere is suggested. This implies an increase in surface pressure by sedimentation can cause the upward migration of the phase boundary, resulting in uplift due to a decrease in pressure by erosion.

A regional uplift mechanism has been suggested as the cause of severe and extensive Cenozoic erosion in examples SE1 – SE6. This has led to the removal of the majority of Cenozoic sediments in the western Barents Sea, as well as Cretaceous, Jurassic and Triassic sediments in some areas such as the Loppa High. Due to significantly high values of net erosion calculated from P-wave velocity variations and analysis of seismic horizon depth variations in several seismic lines in this study, it is clear that the Barents Sea is affected by severe regional uplift and erosion. From the results in this project and previous studies, this is suggested to be due to a tectonic mechanism occurring in several phases during Cenozoic time, followed by severe glacial erosion and isostatic rebound.

5.6. Comparison of net erosion estimates with published studies

Several previous studies have been carried out to quantify the uplift and erosion observed in the Barents Sea, however large discrepancies have existed between studies depending on techniques being used. Examples of the differences between studies is illustrated below, Figure 5.11. This image shows net erosion maps from various studies using vitrinite reflectance, pyrolysis T-max, opal A – opal CT and shale compaction. The lower right plot illustrates the discrepancies between the studies, with difference in estimates as high as 500 m in parts. This significant variation creates great risk for exploration as it is challenging to accurately predict the effects on source rock maturation, reservoir properties and migration of hydrocarbons.

A study conducted by Dimakis et al. (1998) estimated the net erosion in the western Barents Sea by combining several studies utilising geochemical, vitrinite reflectance, shale compaction, seismic velocity and opal A – opal CT methods, Figure 5.12. This shows an increasing amount of erosion to the north at low latitudes and west at higher latitudes. The erosion is lowest in the south west of the western Barents Sea.

A more recent study by Henriksen et al. (2011) has been carried out using a combination of geological and geophysical data and a regional net erosion map has been constructed, Figure 5.13. This illustrates net erosion values between 0 and 3000+ m, and a general trend of increasing net erosion to the north of the study area. Again, the highest erosion values are located to the north and east.

Exhumation maps from three different data sets including an average from a recent study (Baig et al., 2016) are shown below, Figure 5.14. These maps have been created from sonic logs, seismic shot gathers, vitrinite reflectance and by arithmetic averaging of the three methods. These four maps are very similar in exhumation magnitudes and general trends. The results estimated from the various methods in their study agree with the net erosion results calculated from this study.

Other published studies on the topic, (Dore and Jensen, 1996, Storvoll et al., 2005), also show an increase in uplift and erosion to the north and east of the western Barents Sea. It is clear that new technologies, better quality data, new processing techniques and more

surveys allow for more reliable interpretations and calculations with regard to uplift and erosion. This results in ongoing demand for research on this topic.

The results in this project show a trend very similar to the previously mentioned studies – more uplift and erosion in the north and north east, with less erosion observed to the west and south west. Although discrepancies exist, they are relatively low and restricting data to include only shaly parts of the Kolmule formation has improved consistency.

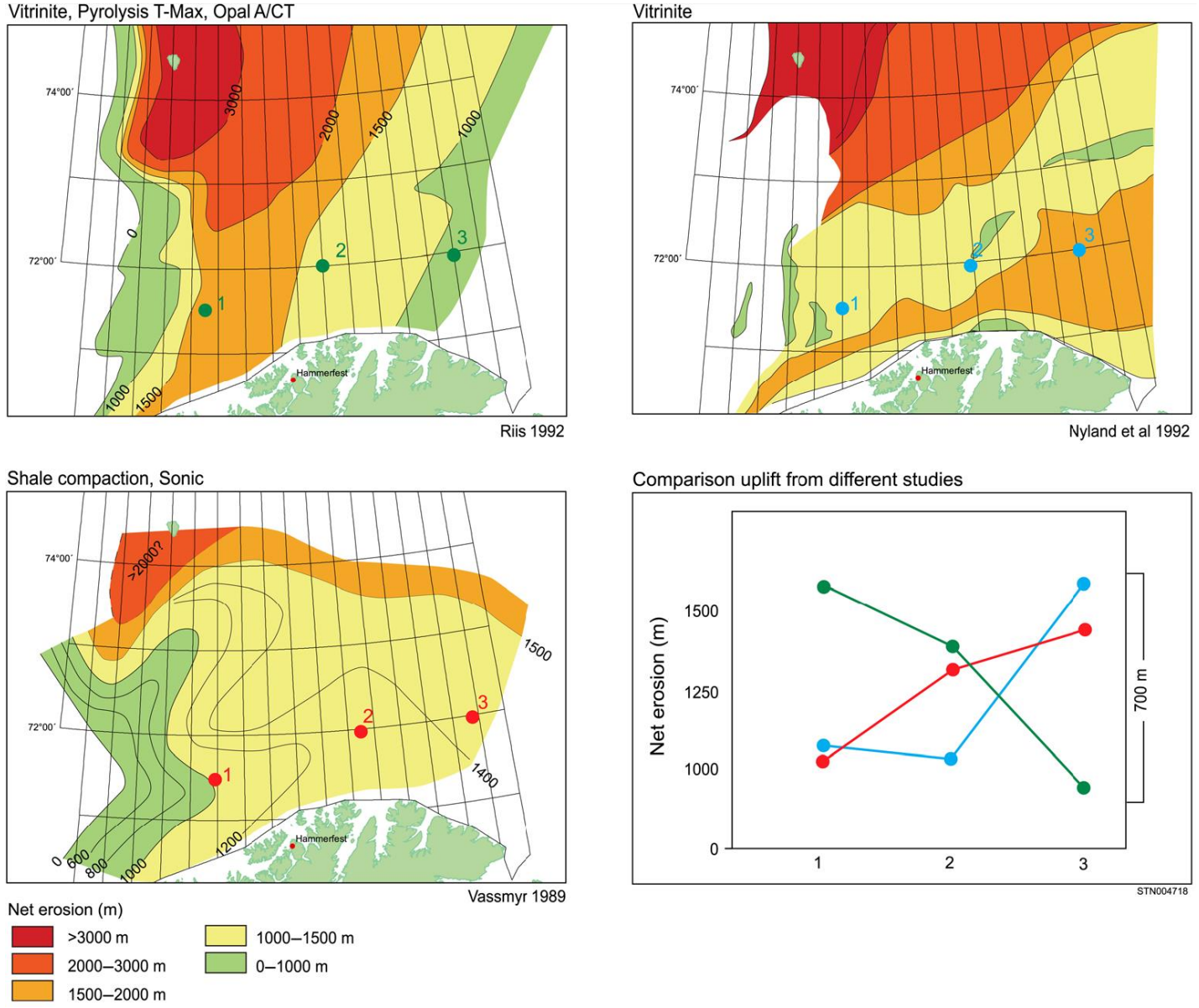

Figure 5.11. Uplift maps from previous studies, illustrating the differences in net erosion estimates. There is a general trend between the three studies of increasing uplift to the north and east, however discrepancies of up to 500 – 600 m still exist. Modified from Henriksen et al. (2011).

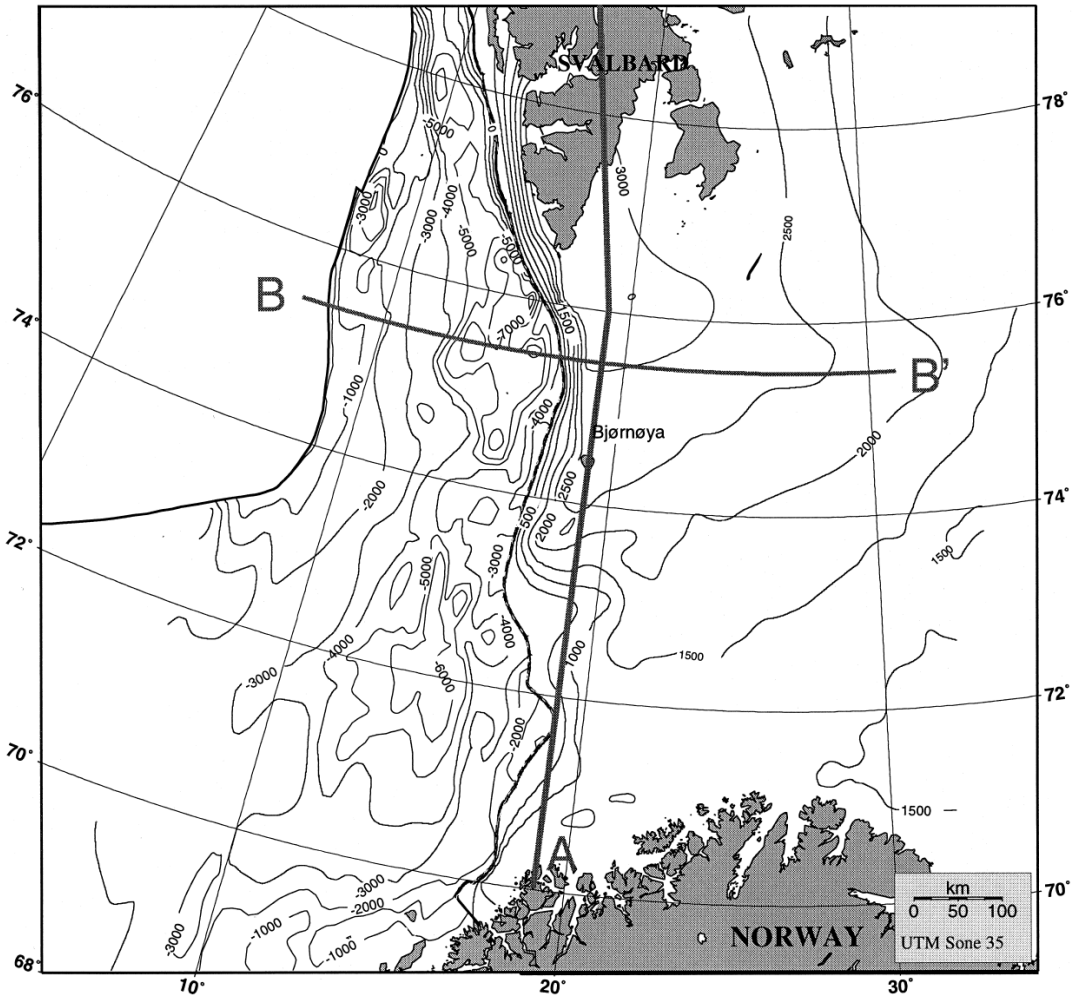

Figure 5.12. Erosion map for the western Barents Sea, erosion estimates shown by the positive integers to the east of the continental margin. Results are from a combination of previous studies using geochemical, vitrinite reflectance, shale compaction, opal A – opal CT and seismic velocity methods. From Dimakis et al. (1998).

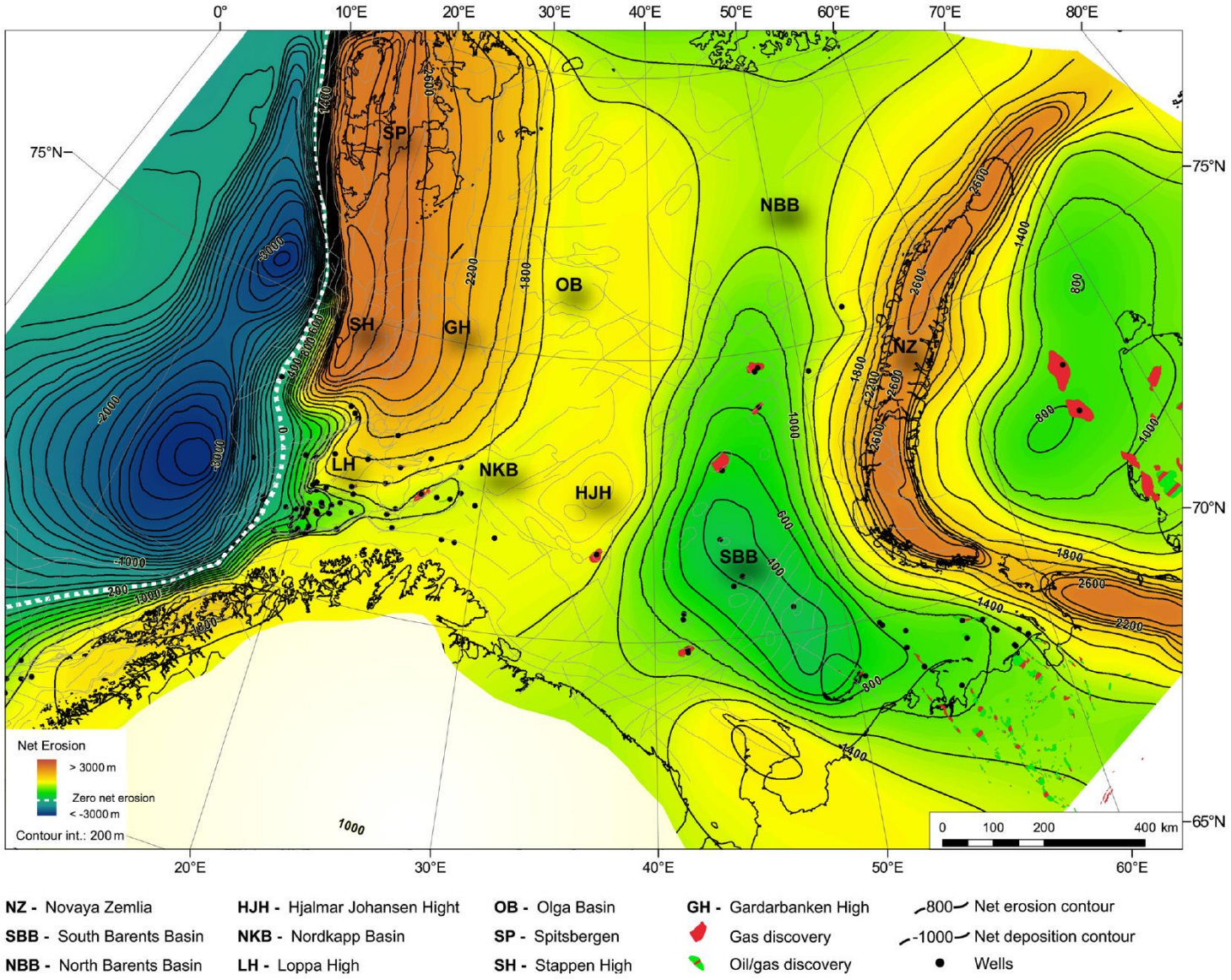

Figure 5.13. Regional net erosion map of the Greater Barents Sea illustrating the variations in net erosion values. The study area is indicated by the red box. A general trend of increasing net erosion northwards is seen in the study area, and net erosion values range from 0 – 3000+ m throughout the entire Greater Barents Sea region. From Henriksen et al. (2011).

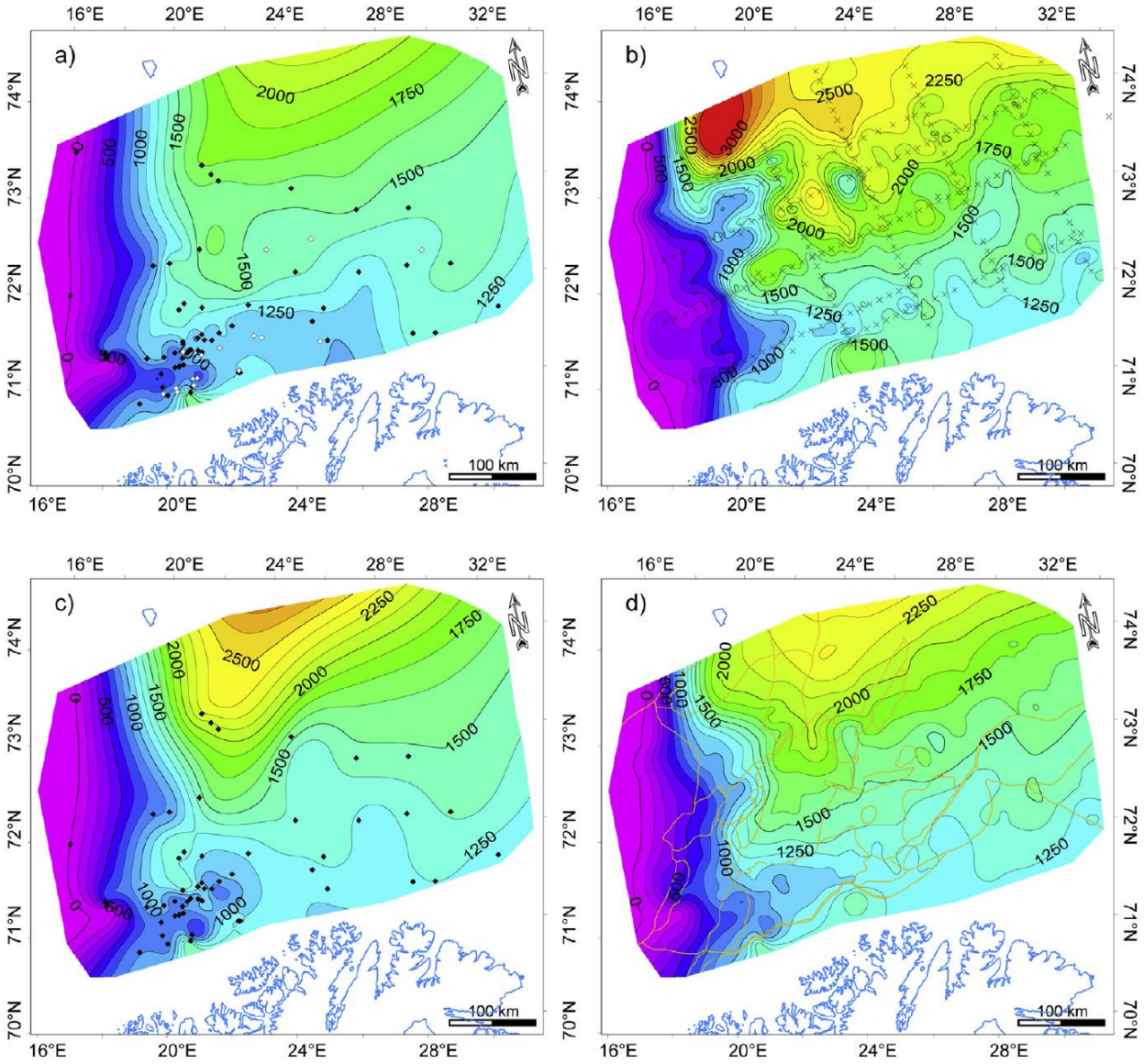

Figure 5.14. Net exhumation maps calculated using different techniques; a) sonic logs, b) seismic shot gathers, c) vitrinite reflectance and d) arithmetic average map of the three datasets. From Baig et al. (2016).

5.7. Suggestions for further work

In this section several suggestions for further work will be made. The aims of these suggestions are to improve confidence in results, lower uncertainties and increase resolution and data coverage. Suggestions for further work are as follows:

- **Analyse different formations**. In this study, only the Kolmule formation was used due to its widespread distribution, age, clay content and available velocity data in wells. Analysis of other formations is suggested to explore the effects of analysing different lithologies and to increase the resolution of net erosion maps by adding more data points.
- **Analyse sandstones**. Shaly formations were used in this study, however including sandstones and comparing results from both sandstone and shale calculations would allow more estimates to be made in areas where shaly formations are absent.
- **Develop a new reference trend**. A reference trend from Storvoll et al., 2005 was used in this study. Developing a new reference trend using the same methodology herein would increase comparability between the reference trend and regression trends, in turn reducing uncertainty.
- **Account for porosity**. Pore size, distribution and geometry all have an effect on P-wave velocities in rocks. As these effects have not been considered in this study, looking into the effects of pore properties could reduce uncertainties and lead to different net erosion estimates.
- **Study thermal regimes in various regions in the western Barents Sea**. As mentioned earlier, the transition from mechanical to chemical compaction is temperature dependent. Investigating the thermal history of each area estimated for net erosion could improve results.
- **Investigate the accuracy of these results and previous studies**. Creating difference maps between studies could provide useful information on which techniques are most useful and accurate in estimating net erosion.

Chapter 6: Summary and conclusions

The purpose of this report was to develop a work flow for calculating net erosion by analysis of P-wave velocity variations, carry out these calculations in the western Barents Sea, compare these results with seismic data, comment on the validity of the results and comment on the implications of the results for petroleum prospectivity. In order to do this, sonic logs from 11 wells have been analysed and several MCG super-tie seismic lines have been interpreted.

Net erosion estimates have been made, Table 4.1, and the results show that net erosion in the central and south west part of the study area has been uplifted and eroded 1000 – 1500 m, whereas the north and north eastern areas have been uplift and eroded 1500 – 2000 m. These results have been plotted, Figure 4.4, and a net erosion map has been made, Figure 4.5. From these maps, it is clear there is a trend of increasing uplift and erosion to the north and north east, and little to no uplift and erosion in the west and south west. These significantly high net erosion estimates across the majority of the western Barents Sea indicate one or more regional uplift and erosion episodes has occurred, supporting the results of several previous studies. Due to the low resolution of these erosion maps and the lack of detail separating the different tectonic features, net erosion estimates from each structural province have been averaged and the average values have been attributed to each province, Figure 4.6.

Uncertainty in net erosion estimates has varied significantly between wells, Table 4.1 and Figure 4.3. More consistent net erosion estimates occur to the west and south west of the study area with uncertainties ranging from ± 153 – 328 m. More inconsistent results were found in the north and north east, with uncertainties ranging from ± 491 – 793 m. These larger uncertainties have been attributed to poor gamma ray logs, poor sonic logs, short Kolmule formation intervals or variations in thermal histories. Areas with greater uncertainty present a greater risk for exploration as implications for source rock maturation, reservoir properties and migration of hydrocarbons are not as clear.

Results calculated from sonic logs were then compared with MCG super-tie lines in the western Barents Sea. The validity of results has been commented on from interpreted seismic sections. Net erosion estimates have been found to agree with interpretations made

from seismic data. Regional erosional unconformities in the interpreted seismic data support previous studies' suggestions of one or more regional Cenozoic uplift and erosion events in the western Barents Sea. The total net erosion value has been attributed to be the sum of the interpreted local and regional uplift and erosion events. Through interpretation of seismic data and literature review, the regional Cenozoic uplift event has been suggested to be due to several phases of tectonic uplift during Cenozoic time, followed by severe glacial erosion and isostatic rebound.

Uplift and erosion can have large implications for petroleum prospectivity. These can be positive effects such as redeposition of sediments and more mature than expected source rocks, but can also have negative effects on source rock maturation, reservoir properties and migration of hydrocarbons. Being able to consistently estimate net erosion plays a large part in predicting these effects. Processing and analysing of sonic logs has been shown to be a robust method in estimating net erosion in the western Barents Sea. New data, processing techniques and discoveries make this an ongoing and interesting topic both from a geological perspective and a petroleum exploration perspective.

Chapter 7: References

ALLEN, P. A. & ALLEN, J. R. 1990. *Basin Analysis: Principles and Applications,* Oxford, UK, Blackwell Publishing.

BAIG, I., FALEIDE, J. I., JAHREN, J. & MONDOL, N. H. 2016. Cenozoic exhumation on the southwestern Barents Shelf: Estimates and uncertainties constrained from compaction and thermal maturity analyses. *Marine and Petroleum Geology,* 73**,** 105-230.

CANNON, S. 2016. *Petrolphysics: A Practical Guide,* West Sussex, John Wiley & Sons, Ltd.

CLOETINGH, S., GRADSTEIN, F. M., KOOI, H., GRANT, A. C. & KAMINSKI, M. 1990. Plate reorganization: a cause of rapid late Neogene subsidence and sedimentation around the North Atlantic. *Geological Society,* 147**,** 495-506.

DIMAKIS, P., BRAATHEN, B. I., FALEIDE, J. I., ELVERHØI, A. & GUDLAUGSSON, S. T. 1998. Cenozoic erosion and the preglacial uplift of the Svalbard-Barents Sea region. *Tectonophysics,* 300**,** 311-327.

DORE, A. G. 1992. The Base Tertiary surface of southern Norway and the northern North Sea. *Post-Cretaceous Uplift and Sedimentation along the Western Fennoscandian Shield.* Nor. Geol. Tidsskr.

DORE, A. G. & JENSEN, L. N. 1996. The impact of late Cenozoic uplift and erosion on hydrocarbon exploration: offshore Norway and some other uplifted basins. *Global and Planetary Change,* 12**,** 415-436.

ENGLAND, P. & MOLNAR, P. 1990. Surface uplift, uplift of rocks, and exhumation of rocks. *Geology,* 18**,** 4.

FALEIDE, J. I., BJØRLYKKE, K. & GABRIELSEN, R. H. 2010. Geology of the Norwegian continental shelf. *In:* BJØRLYKKE, K. (ed.) *Petroleum Geoscience.* Springer-Verlag Berlin Heidelberg.

FALEIDE, J. I., GUDLAUGSSON, S. T. & JACQUART, G. 1984. Evolution of the western Barents Sea. *Marine and Petroleum Geology,* 1.

FALEIDE, J. I., SOLHEIM, A., FIEDLER, A., HJELSTUEN, B. O., ANDERSEN, E. S. & VANNESTE, K. 1996. Late Cenozoic evolution of the western Barents Sea-Svalbard continental margin. *Global and Planetary Change,* 12**,** 53-74.

FALEIDE, J. I., TSIKALAS, F., BREIVIK, A. J., MJELDE, R., RITZMANN, O., ENGEN, Ø., WILSON, J. & ELDHOLM, O. 2008. Structure and evolution of the continental margin off Norway and the Barents Sea. *Episodes,* 31**,** 82-91.

FOSSEN, H. 2010. *Structural Geology,* Cambridge, Cambridge University Press.

GABRIELSEN, R. H., FÆRSETH, R. B., JENSEN, L. N., KALHEIM, J. E. & RIIS, F. 1990. *NPD-Bulletin No 6*, Norwegian Petroleum Directorate.

GALLAGHER, K. 2012. Uplift, denudation, and their causes and constraints over geological timescales. *Principles of Geologic Analysis,* 10**,** 30.

GHAZI, S. A. 1992. Cenozoic uplift in the Stord Basin area and its consequences for exploration. *Nor. Geol. Tidsskr.,* 72.

HANSEN, S. 1996. Quantification of net uplift and erosion on the Norwegian Shelf south of 66 degrees N from sonic transit times of shale. *Norsk Geologisk Tidsskrift,* 76**,** 245-252.

HARLAND, W. B. 1969. Mantle changes beneath the Barents Sea. *Trans N.Y. Acad. Sci.,* 31**,** 25-41.

HARLAND, W. B. 1973. Tectonic evolution of the Barents Shelf and related plates. *Arctic geology,* 19**,** 599-608.

HENRIKSEN, E., BJØRNSETH, H. M., HALS, T. K., HEIDE, T., KIRYUKHINA, T., KLØVJAN, O. S., LARSSEN, G. B., RYSETH, A. E., RØNNING, K., SOLLID, K. & STOUPAKOVA, A. 2011. Uplift and erosion of the greater Barents Sea: impact on prospectivity and petroleum systems. *Arctic Petroleum Geology.* London: The Geological Society of London.

HERMANRUD, C., WENSAAS, L., TEIGE, G. M. G., BOLAS, H. M. N., HANSEN, S. & VIK, E. 1998. Shale porosities from well logs on Haltenbanken (offshore mid-Norway) show no influence of overpressuring. *In:* LAW, B. E., ULMISHEK, G. F. & SLAVIN, V. I. (eds.) *Abnormal pressures in hydrocarbon environments: AAPG Bulletin.*

HJELSTUEN, B. O., ELVERHØI, A. & FALEIDE, J. I. 1996. Cenozoic erosion and sediment yield in the drainage area of the Storfjorden fan. *Impact of glaciations on basin evolution; data and models from the Norwegian margin and adjacent areas*, 95-117.

JAPSEN, P. 2000. Investigation of multi-phase erosion using reconstructed shale trends based on sonic data. *Global and Planetary Change,* 24**,** 189-210.

JENSEN, L. N., RIIS, F. & BOYD, R. Post-Cretaceous uplift and sedimentation along the western Fennoscandian Shield. *In:* JENSE, L. N., RIIS, F. & BOYD, R., eds. Proceedings of the 7th TSGS Conference, 1990 Stavanger. Norsk Geologisk Tidsskrift.

JENSEN, L. N. & SCHMIDT, B. J. 1993. Neogene uplift and erosion offshore south Norway: magnitude and consequences for hydrocarbon exploration in the Farsun Basin. *Generation, Accumulation and Production of Europe's Hydrocarbons, III.* Berlin: Springer.

LABERG, J. S., ANDREASSEN, K. & VORREN, T. O. 2012. Late Cenozoic erosion of the high-latitude southwestern Barents Sea shelf revisited. *GSA Bulletin,* 124**,** 77-88.

NANSEN, F. 1904. The bathymetric features of the North Polar seas, with a discussion of the continental shelves and previous oscillations of the shore-line. *In:* NANSEN, F. (ed.) *The Norwegian North Polar Expeditions 1893-1896.* Christiania: Jacob Dubwad.

NPD. 2014. *The 2014 NPD lithostratigraphic charts* [Online]. Norway: NPD. Available: http://www.npd.no/Global/Engelsk/2-Topics/Geology/Lithostratigraphy/BH-OD1409003.pdf 2016].

NPD 2016. Wellbore statistics. *In:* DIRECTORATE, N. P. (ed.). Norway.

REEMST, P., CLOETINGH, S. & FANAVOLL, S. 1994. Tectonostratigraphic modelling of Cenozoic uplift and erosion in the south-western Barents Sea. *Marine and Petroleum Geology,* 11**,** 12.

RIDER, M. 2000. *The geological interpretation of well logs,* Scotland, Rider-French Consulting Ltd.

RIIS, F. & FJELDSKAAR, W. 1992. On the magnitude of the Late Tertiary and Quaternary erosion and its significance for the uplift of Scandinavia and the Barents Sea. *Structural and Tectonic Modelling and its Application to Petroleum Geology.* Amsterdam: Elsevier.

RIIS, F. & JENSEN, L. N. 1992. Introduction: Measuring uplift and erosion - proposal for a terminology. *Norsk Geologisk Tidsskrift,* 72**,** 223-228.

ROEDER, D. 2012. Convergent margins and orogenic belts. *Principles of Geological Analysis.* Elsevier B.V.

ROHRMAN, M., VAN DER BEEK, P. A., VAN DER HILST, R. D. & REEMST, P. 2002. Timing and mechanisms of North Atlantic Cenozoic uplift: evidence for mantle upwelling. *Exhumation of the North Atlantic Margin: Timing, Mechanisms and Implications for Petroleum Exploration,* 196**,** 27-43.

RØNNEVIK, H. C., BESCOR, B. & JACOBSEN, H. P. 1982. Structural and stratigraphic evolution of the Barents Sea. *Petroleum Geologists,* 8**,** 431-440.

SMELROR, M., PETROV, O. V., LARSSEN, G. B. & WERNER, S. 2009. *Geological history of the Barents Sea,* Trondheim, Norges geologiske undersøkelse.

STORVOLL, V., BJØRLYKKE, K. & MONDOL, N. H. 2005. Velocity-depth trends in Mesozoic and Cenozoic sediments from the Norwegian Shelf. *AAPG Bulletin,* 89**,** 359-381.

TEIGE, G. M. G., HERMANRUD, C., WENSAAS, L. & BOLAS, H. M. N. 1999. The lack of relationship between overpressure and porosity in North Sea and Haltenbanken shales. *Marine and Petroleum Geology,* 16**,** 321-335.

TORSKE, T. 1972. Tertiary oblique uplift of western Fennoscandia; crustal warping in connection with rifting and break-up of the Laurasian continent. *Nor. Geol. Unders.,* 273**,** 43-48.

VÅGNES, E. & AMUNDSEN, H. E. F. 1993. Late Cenozoic uplift and volcanism on Spitsbergen, caused by mantle convection. *Geology,* 21**,** 251-254.

WILLETT, S. D., SLINGERLAND, R. & HOVIUS, N. 2001. Uplift, shortening, and steady state topography in active mountain belts. *American Journal of Science,* 301**,** 455-485.

Appendices

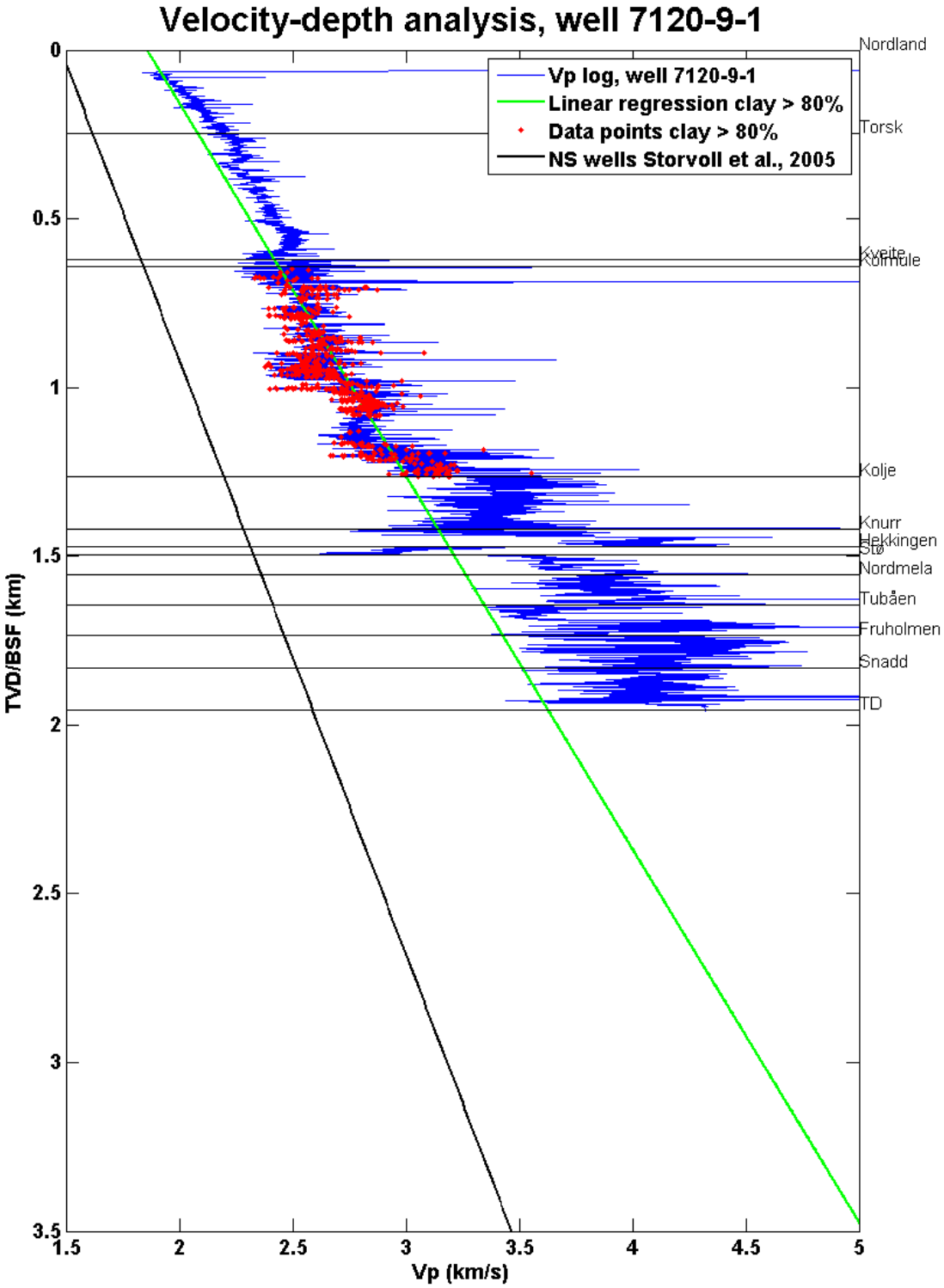
Velocity-depth analysis, well 7120-9-1
Vp log, well 7120-9-1
Linear regression clay > 80%
Data points clay > 80%
NS wells Storvoll et al., 2005
Nordland
Torsk
Kveite
Kolmule
Kolje
Knurr
Hekkingen
Stø
Nordmela
Tubåen
Fruholmen
Snadd
TD
TVD/BSF (km)
Vp (km/s)
0
0.5
1
1.5
2
2.5
3
3.5
1.5
2
2.5
3
3.5
4
4.5
5

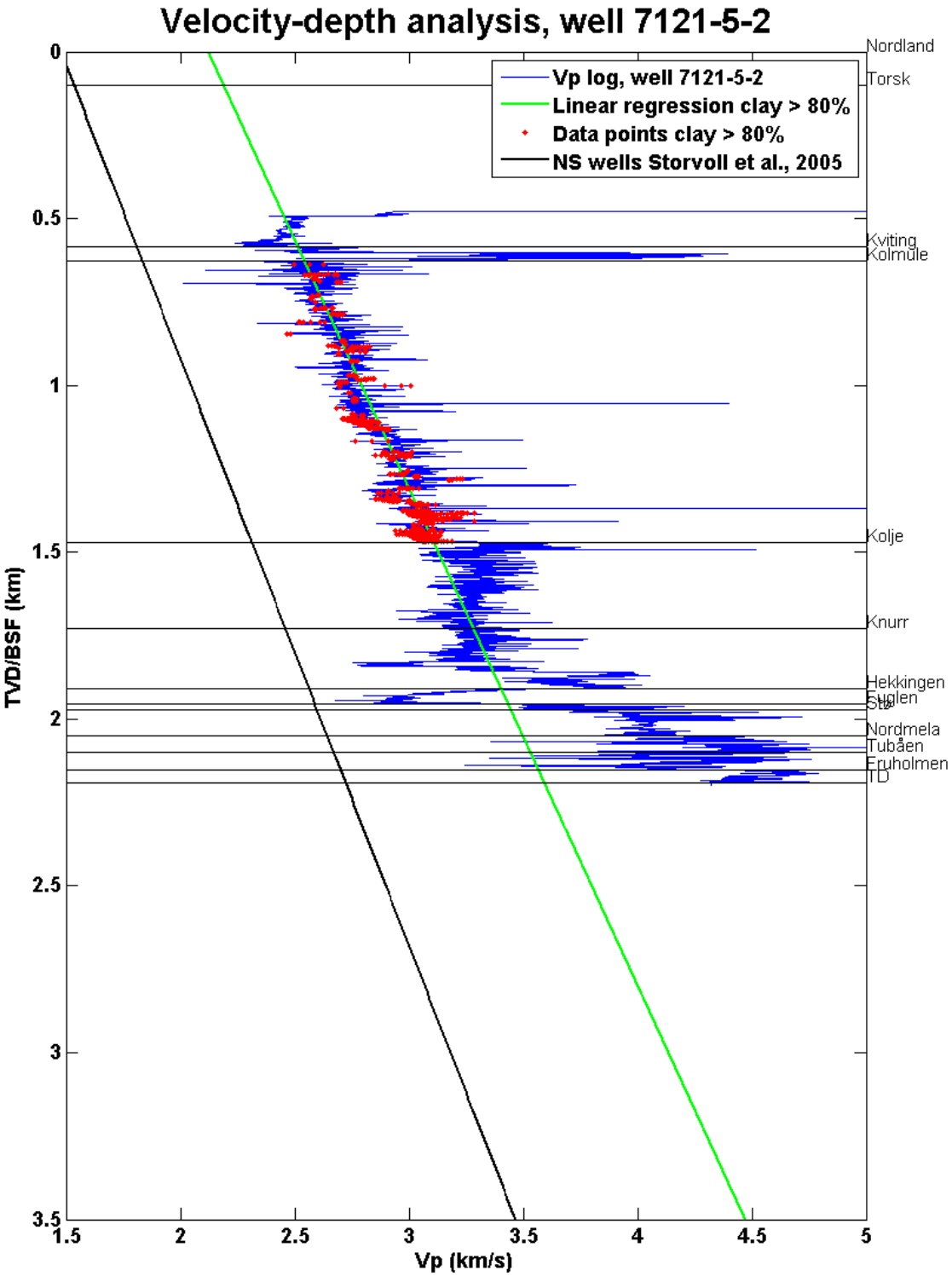
Velocity-depth analysis, well 7121-5-2
Vp log, well 7121-5-2
Linear regression clay > 80%
Data points clay > 80%
NS wells Storvoll et al., 2005
TVD/BSF (km)
Vp (km/s)
0
0.5
1
1.5
2
2.5
3
3.5
1.5
2
2.5
3
3.5
4
4.5
5
Nordland
Torsk
Kviting
Kolmule
Kolje
Knurr
Hekkingen
Fuglen
Stø
Nordmela
Tubåen
Fruholmen
TD

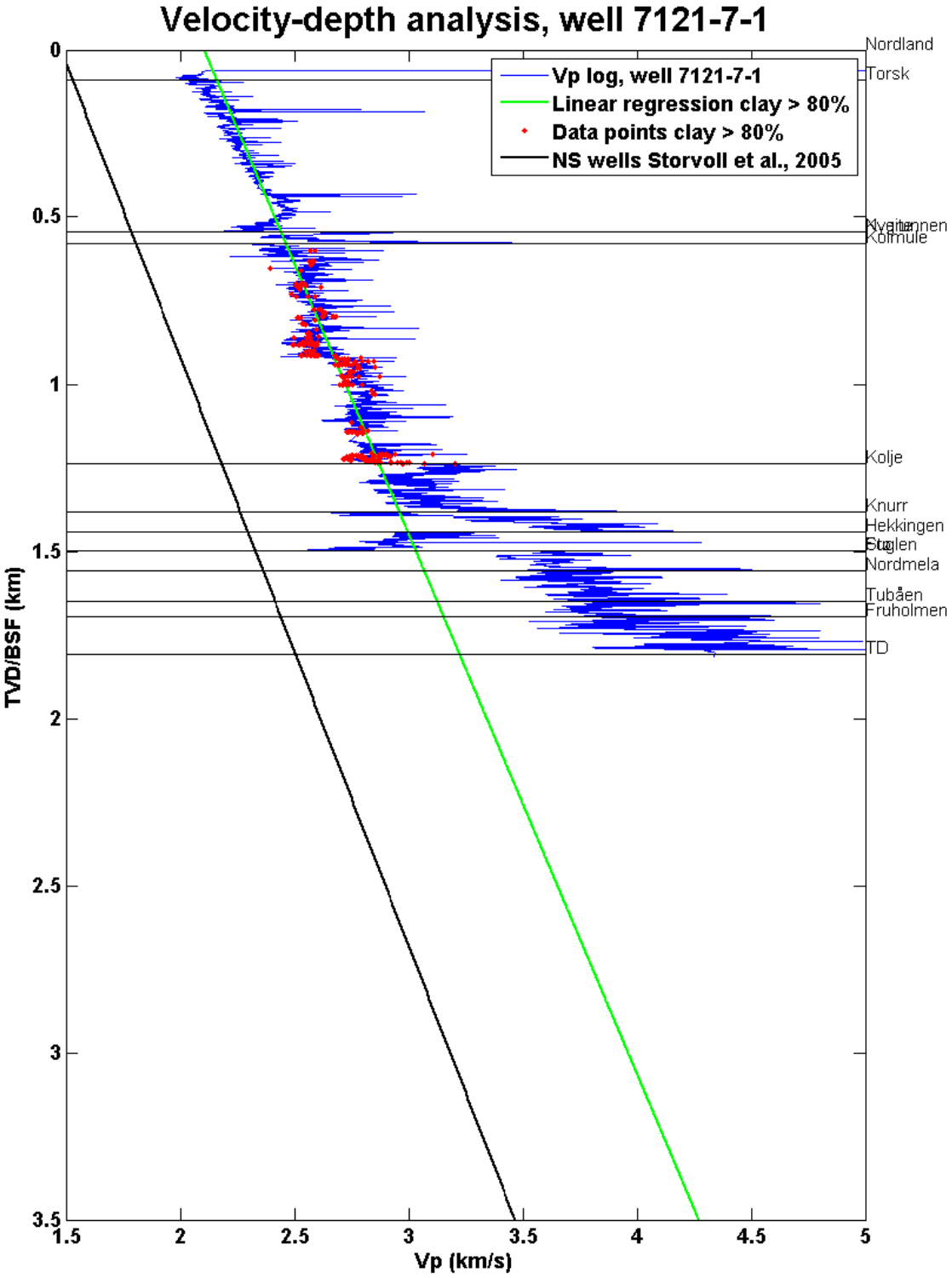
Velocity-depth analysis, well 7121-7-1
Vp log, well 7121-7-1
Linear regression clay > 80%
Data points clay > 80%
NS wells Storvoll et al., 2005
Nordland
Torsk
Kolmule
Kolje
Knurr
Hekkingen
Nordmela
Tubåen
Fruholmen
TD
TVD/BSF (km)
Vp (km/s)
0
0.5
1
1.5
2
2.5
3
3.5
1.5
2
2.5
3
3.5
4
4.5
5

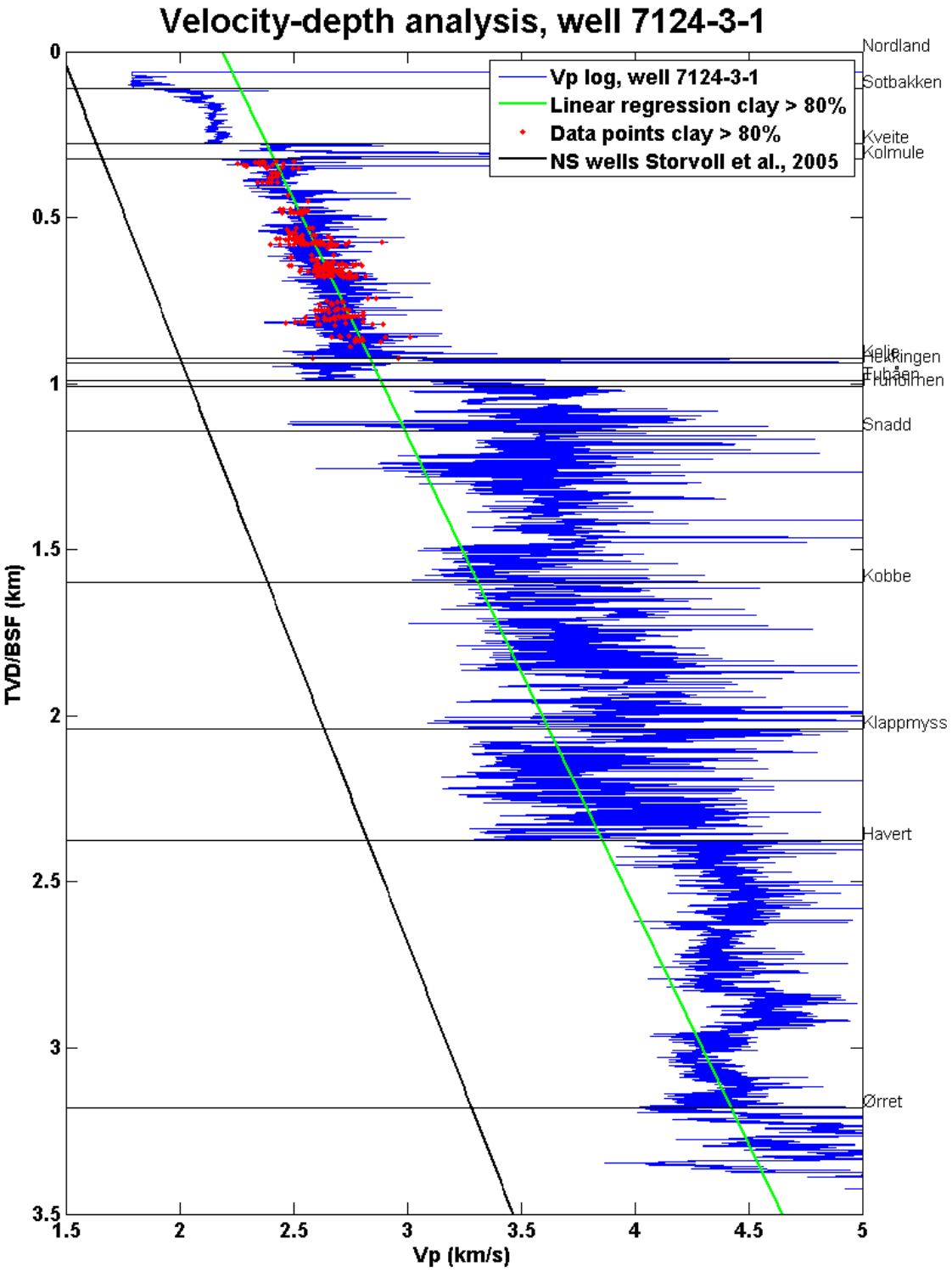
Velocity-depth analysis, well 7124-3-1
Vp log, well 7124-3-1
Linear regression clay > 80%
Data points clay > 80%
NS wells Storvoll et al., 2005
Nordland
Sotbakken
Kveite
Kolmule
Kolje
Hekkingen
Fuglen
Fruholmen
Snadd
Kobbe
Klappmyss
Havert
Ørret
TVD/BSF (km)
Vp (km/s)
0
0.5
1
1.5
2
2.5
3
3.5
1.5
2
2.5
3
3.5
4
4.5
5

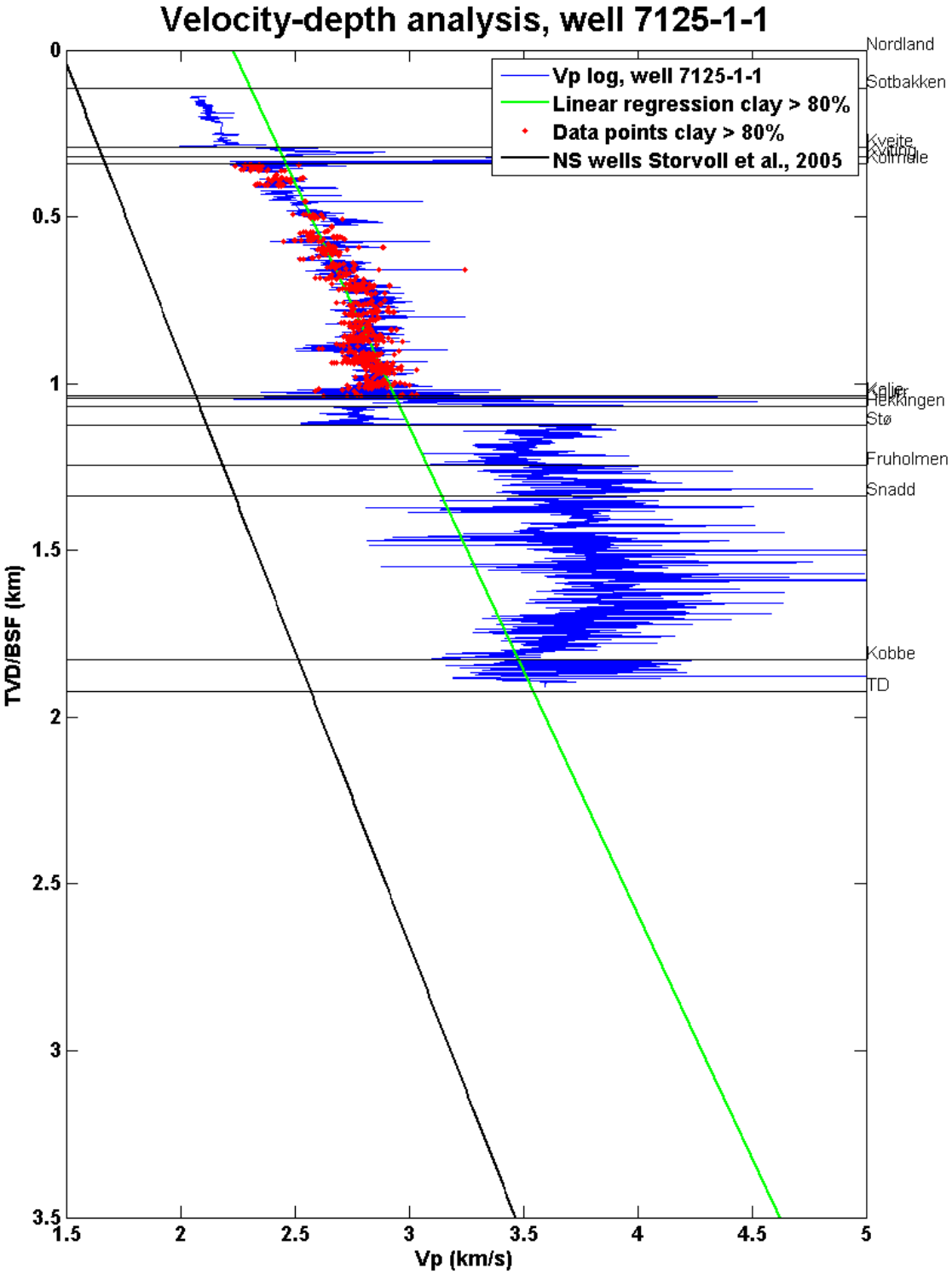
Velocity-depth analysis, well 7125-1-1
Vp log, well 7125-1-1
Linear regression clay > 80%
Data points clay > 80%
NS wells Storvoll et al., 2005
Nordland
Sotbakken
Kveite
Kolmule
Kolje
Hekkingen
Stø
Fruholmen
Snadd
Kobbe
TD
TVD/BSF (km)
Vp (km/s)
0
0.5
1
1.5
2
2.5
3
3.5
1.5
2
2.5
3
3.5
4
4.5
5

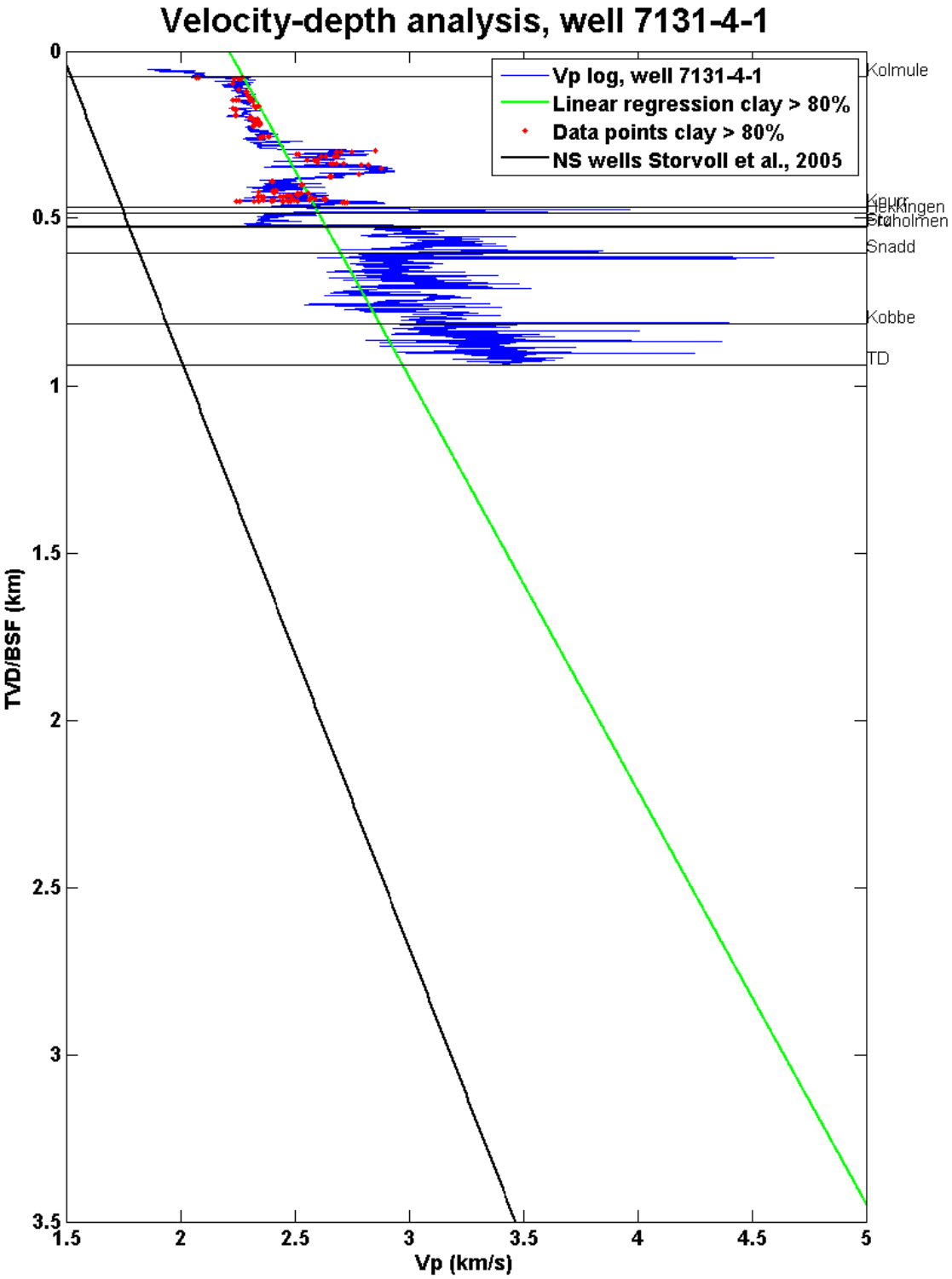
Velocity-depth analysis, well 7131-4-1
Vp log, well 7131-4-1
Linear regression clay > 80%
Data points clay > 80%
NS wells Storvoll et al., 2005
Kolmule
Kyrr
Hekkingen
Stø
Fuglholmen
Snadd
Kobbe
TD
TVD/BSF (km)
Vp (km/s)
0
0.5
1
1.5
2
2.5
3
3.5
1.5
2
2.5
3
3.5
4
4.5
5

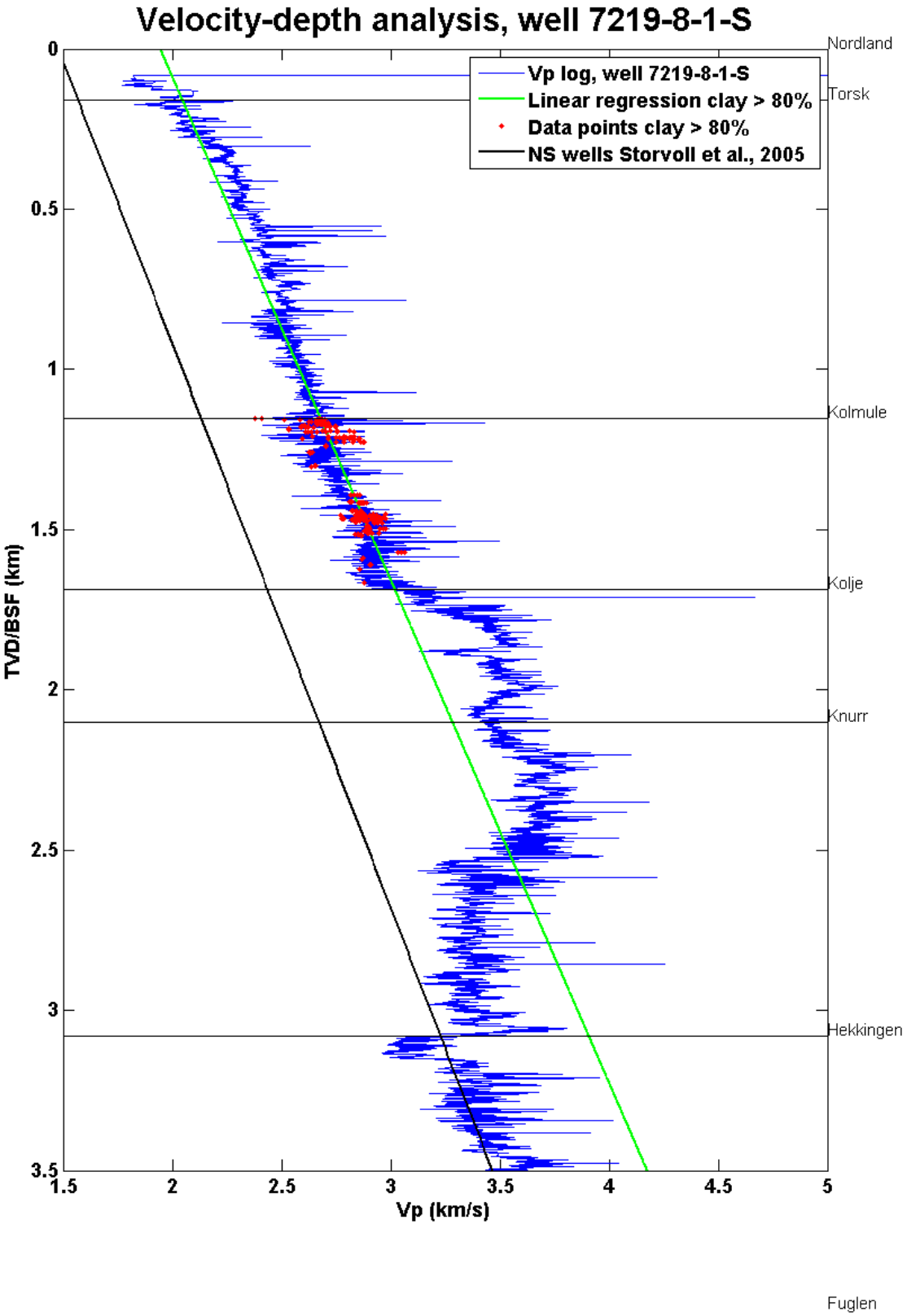
Velocity-depth analysis, well 7219-8-1-S
Vp log, well 7219-8-1-S
Linear regression clay > 80%
Data points clay > 80%
NS wells Storvoll et al., 2005
TVD/BSF (km)
Vp (km/s)
0
0.5
1
1.5
2
2.5
3
3.5
1.5
2
2.5
3
3.5
4
4.5
5
Nordland
Torsk
Kolmule
Kolje
Knurr
Hekkingen
Fuglen

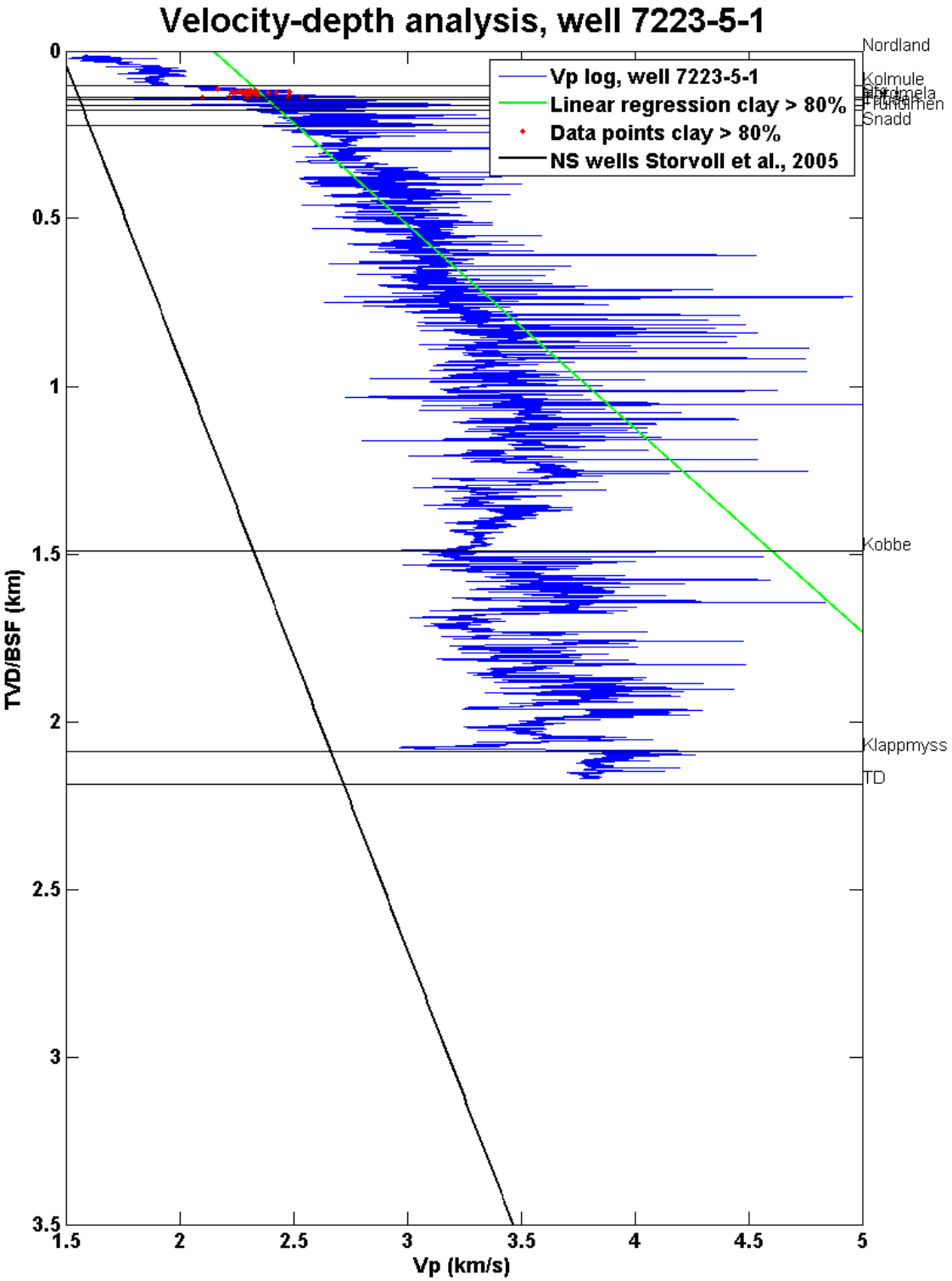
Velocity-depth analysis, well 7223-5-1
Vp log, well 7223-5-1
Linear regression clay > 80%
Data points clay > 80%
NS wells Storvoll et al., 2005
Nordland
Kolmule
Snadd
Kobbe
Klappmyss
TD
TVD/BSF (km)
Vp (km/s)
0
0.5
1
1.5
2
2.5
3
3.5
1.5
2
2.5
3
3.5
4
4.5
5

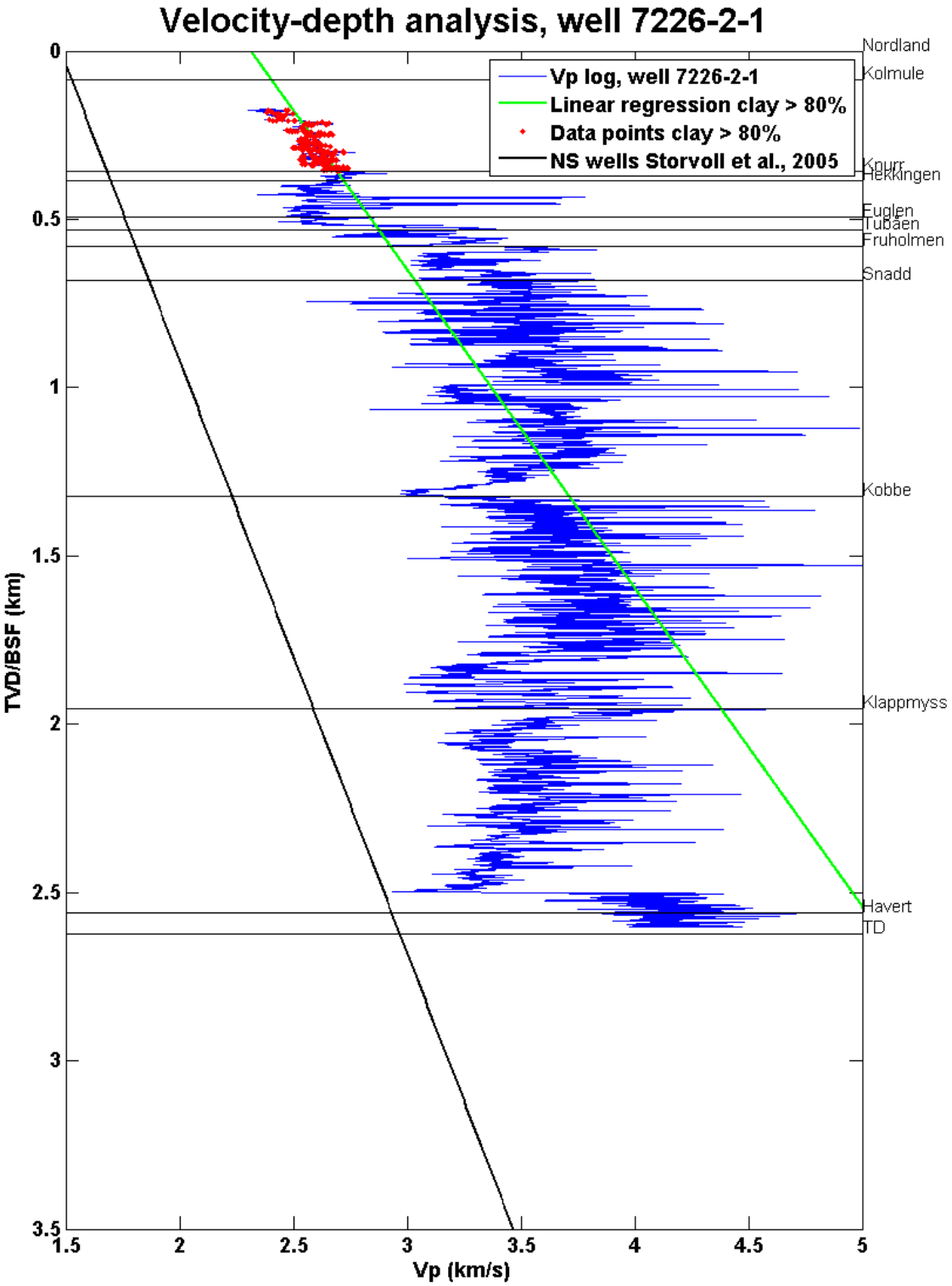
Velocity-depth analysis, well 7226-2-1
Vp log, well 7226-2-1
Linear regression clay > 80%
Data points clay > 80%
NS wells Storvoll et al., 2005
Nordland
Kolmule
Knurr
Hekkingen
Fuglen
Tubåen
Fruholmen
Snadd
Kobbe
Klappmyss
Havert
TD
TVD/BSF (km)
Vp (km/s)
0
0.5
1
1.5
2
2.5
3
3.5
1.5
2
2.5
3
3.5
4
4.5
5

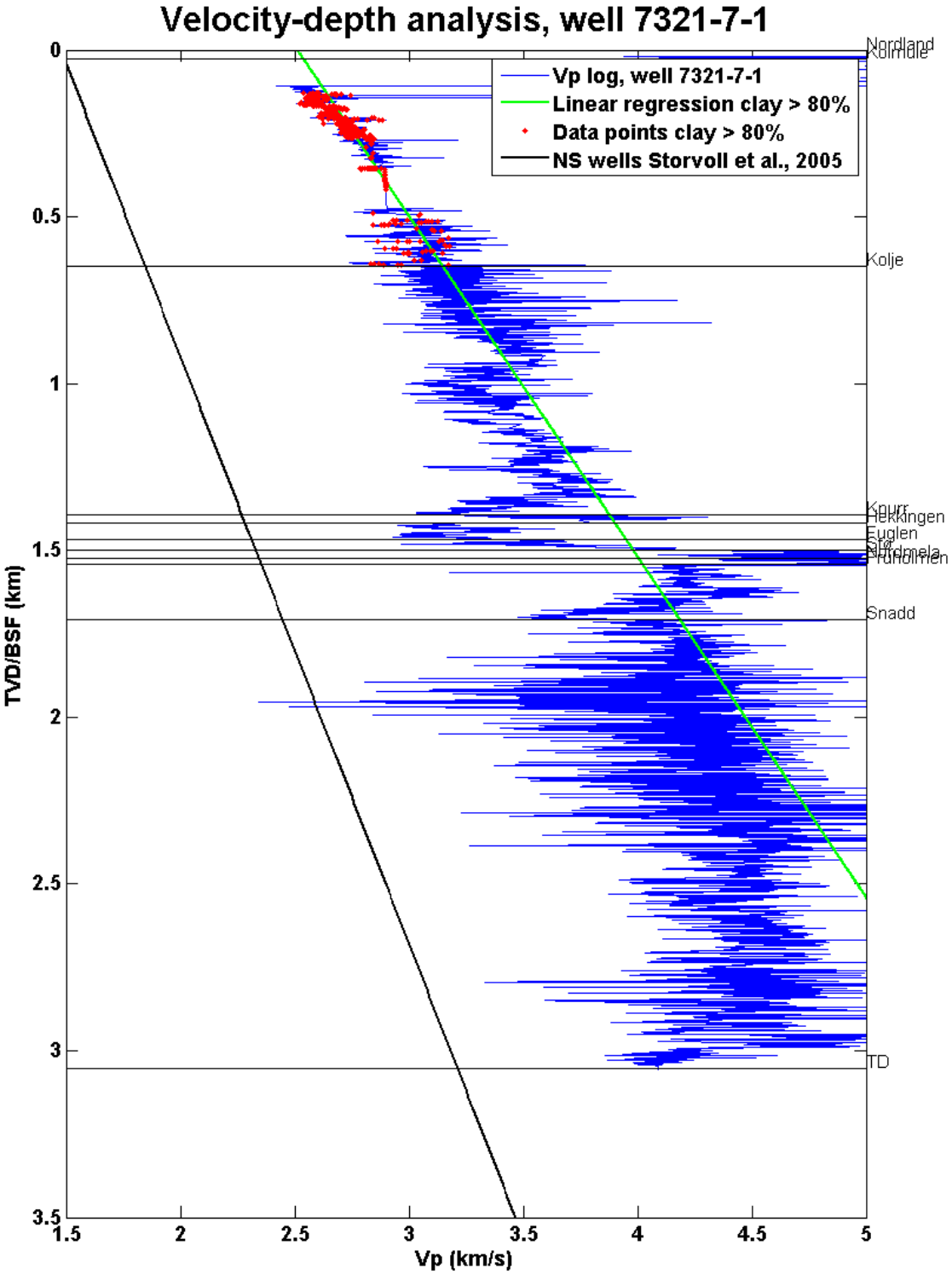
Velocity-depth analysis, well 7321-7-1
Vp log, well 7321-7-1
Linear regression clay > 80%
Data points clay > 80%
NS wells Storvoll et al., 2005
Nordland
Kolmule
Kolje
Kyrr
Hekkingen
Fuglen
Snadd
TD
TVD/BSF (km)
Vp (km/s)
0
0.5
1
1.5
2
2.5
3
3.5
1.5
2
2.5
3
3.5
4
4.5
5

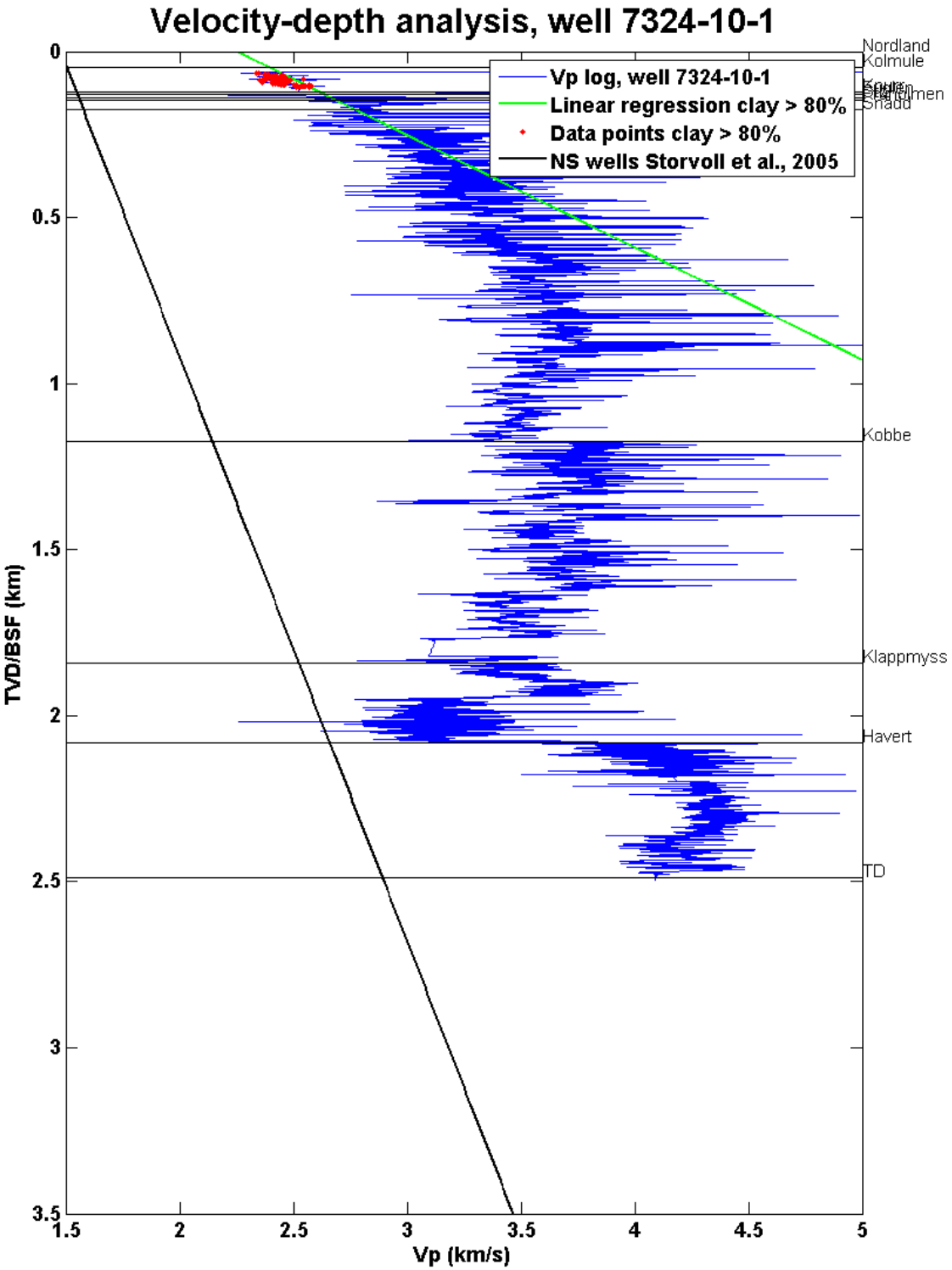
Velocity-depth analysis, well 7324-10-1
Vp log, well 7324-10-1
Linear regression clay > 80%
Data points clay > 80%
NS wells Storvoll et al., 2005
Nordland
Kolmule
Kobbe
Klappmyss
Havert
TD
TVD/BSF (km)
Vp (km/s)
0
0.5
1
1.5
2
2.5
3
3.5
1.5
2
2.5
3
3.5
4
4.5
5